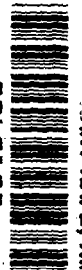


NASA Contractor Report 3234

NASA
CR
3234
c.1

LOAN COPY: RETURN TO
AFWL TECHNICAL LIBRARY
KIRTLAND AFB, NM

EO12900



Development of Panel Methods for Subsonic Analysis and Design

D. R. Bristow

CONTRACT NAS1-15369
FEBRUARY 1980





NASA Contractor Report 3234

Development of Panel Methods for Subsonic Analysis and Design

D. R. Bristow
McDonnell Douglas Corporation
St. Louis, Missouri

Prepared for
Langley Research Center
under Contract NAS1-15369



National Aeronautics
and Space Administration

**Scientific and Technical
Information Office**

1980

TABLE OF CONTENTS

<u>Section</u>	<u>Page</u>
SUMMARY	1
SYMBOLS	2
INTRODUCTION	6
AIRFOIL MIXED ANALYSIS-DESIGN METHOD	7
Analysis-Only Solution Method	10
First-Order Inverse	21
Prediction Accuracy of Analysis Solutions	33
Example Design Solutions	34
Recommendations and User Guidelines	42
KUTTA CONDITION FOR FINITE TRAILING EDGE THICKNESS	43
THREE-DIMENSIONAL POTENTIAL FLOW METHOD	48
Geometry Panel Modeling	50
Singularity Distributions on a Panel	56
Doublet Strength at Panel Edges	57
Boundary Condition Satisfaction	63
Velocity and Pressure Calculation	64
Example Solution	65
FIRST-ORDER EXPANSION APPROACH FOR THICK WING-FUSELAGES	65
Low Cost Method for Analyzing Geometry Perturbations	69
Finite Wing Design	74
CONCLUSIONS	76
REFERENCES	77

LIST OF ILLUSTRATIONS AND TABLES

<u>Figure</u>		<u>Page</u>
1	Illustration of a Mixed Analysis-Design Problem . . .	8
2	Menu of Surface Singularity Panel Methods	9
3	Multi-Element Airfoil Panelling Nomenclature . . .	11
4	Simulation of Wind Tunnel Wall Interference	11
5	Control Points at a Sharp Corner and/or Trailing Edge	12
6	Singularity Density Distributions on a Panel . . .	13
7	Coordinate System of Panel i	15
8	Division of an Airfoil Element into Regions	22
9	Transformation of a Design Region Between Successive Iteration Cycles	24
10	Two-Element Airfoil Analysis Solution	36
11	Two-Element Airfoil Design Solution	36
12	Design of a Constant Pressure Geometry	37
13	Design to Eliminate Wind Tunnel Wall Effects . . .	38
14	Automated High Lift Design Solution	39
15	Wake Model for External Inviscid Flow Field	40
16	Airfoil-Wake Solution	41
17	Base Panel Control Equations	44
18	Symmetric Airfoils Selected for Blunt Base Analysis	45
19	GAW-1 Airfoil	45
20	Lift Prediction for Symmetric Blunt Base Airfoils .	46
21	Blunt Base Airfoil Analysis (0° Incidence)	47
22	Blunt Base Airfoil Analysis (90° Incidence)	48
23	Lift Prediction Error for GAW-1 Airfoil	49
24	A Section of a Body Surface	51

LIST OF ILLUSTRATIONS AND TABLES (Continued)

<u>Figure</u>		<u>Page</u>
25	Indexing Nomenclature for a Section of Panels . . .	52
26	Control Point Locations on a Section	54
27	Local Indexing Nomenclature and Coordinate System for a Panel	54
28	Doublet Spline Control Stations on a Section . . .	58
29	Local Indexing at a Doublet Corner Control Station.	59
30	Local Indexing at a Doublet Edge Midpoint Control Station	60
31	Doublet Discontinuity at Wake-Fuselage Inter- section	61
32	WLB-1 Wing Geometry	66
33	WLB-1 Pressure Distribution at $3.8^\circ \alpha$	67
34	WLB-1 Pressure Distribution at $8.8^\circ \alpha$	68
35	Geometry-Velocity Perturbation for an Airfoil . . .	70
36	Sample Velocity Perturbation Prediction	71
37	Design Approach for Finite Wings	75
<u>Table</u>		
I	Differences Between Analysis and Design Regions . .	22
II	Permissible Ordering of Region Types	23

SUMMARY

Two computer programs have been developed for subsonic inviscid analysis and design. The first solves arbitrary mixed analysis-design problems for multi-element airfoils in two-dimensional flow. The second calculates the pressure distribution for arbitrary lifting or nonlifting three-dimensional configurations.

In each program, inviscid flow is modelled by using distributed source-doublet (or source-vortex) singularities on configuration surface panels. The prescribed normal velocity distribution is satisfied indirectly by applying an internal perturbation potential boundary condition to the center of each panel. The method is numerically stable, and the prediction accuracy is competitive with more complex curved panel formulations.

In the two-dimensional mixed analysis-design program, the geometry of each airfoil element is divided into analysis regions of prescribed geometry and design regions of prescribed pressure. Iteration is used to predict both the shape and length of the geometry in design regions. Satisfactory convergence is usually obtained in only five iteration cycles because the inverse step uses the exact derivative matrix of velocity with respect to geometry perturbation. Example solutions illustrate applications of the mixed analysis-design feature to high lift airfoils and viscous-inviscid interactions. Also demonstrated is an improved Kutta condition model for airfoils with finite thickness trailing edges.

The three-dimensional program uses constant source and quadratic doublet distributions on arbitrary flat quadrilateral panels to induce the flow field. The method of least squares is applied to minimize doublet discontinuities at the panel edges, thereby reducing the sensitivity of the numerical solution to the paneling selected by the user.

A first-order expansion approach is defined for generating the matrix of velocity perturbations with respect to surface geometry perturbations. In the three-dimensional program, such an approach would allow the user to predict the effect of arbitrary configuration changes by the inexpensive process of multiplying a precalculated matrix by a new right-hand-side. A method of using the matrix for three-dimensional wing design is also described.

Mathematical formulations and representative solutions are presented for the computer programs.

SYMBOLS

A, B, C	Arbitrary Panels	
A_{ij}, B_{ij}, C_{ij} D_{ij}, G_{ij}	Coefficient Matrices	
$[a_{ij}]$	Rotation Matrix	
b_{ij}	Doublet Weighting Matrix, equation (78); Transformation Matrix, equation (99)	
C, c	Chord	
C_D, C_d	Drag Coefficient	
C_L, C_l	Lift Coefficient	
C_p	Pressure Coefficient	
c	Constant	
c_1, c_2, c_3	Constants, equation (23)	
c_i	Doublet Weighting Coefficients, equation (81)	
DST_p DX_p DY_p	} Region Lengths, defined by equation (58) - (60)	
(DXB, DYB)		Difference Between Calculated and Prescribed Endpoint Coordinates of a Group of Free Regions, equations (55) and (56)
d_1, d_2, d_3		Constants, equation (25)
E	Quadratic Error to be Minimized	
ETYP A ETYP B ETYP C	} Edge Type Identifier for a Section of Panels	
\vec{e}		Unit Vector
F_A, \dots, F_E		Functions Defined by equations (14) - (18)
I	Line Integral	
IGP	Index of a Group of Free Regions	

(i,j,k,l)	Indices of Points, Panels, etc.
i_{CP}	Control Point Index
(i_P, j_P)	Panel Index
i_S	Index of a Section of Panels ($1 \leq i_S \leq n_S$)
i_{SE}	Section Edge Index ($1 \leq i_{SE} \leq 4$)
(i_μ, j_μ)	Doublet Control Station Index
k	Cumulative Corner Point Index
k_P	Cumulative Panel Index
k_μ	Cumulative Doublet Control Station Index
$k_O(i_S)$	Total Number of Corner Points on Preceding Sections 1 through (i_S-1)
$k_{P_O}(i_S)$	Total Number of Panels on Preceding Sections
$k_{\mu_O}(i_S)$	Total Number of Doublet Control Stations on Preceding Sections
M	Mach Number
(m,n)	Number of Corner Points of a Section in (i,j) - Direction
NGP	Number of Groups of Free Regions on an Airfoil Element
n	Number of Points on an Airfoil Element
n_{CP}	Number of Internal Control Points for an Airfoil Element
\vec{n}	Normal Vector
P	Arbitrary Control Point
\vec{P}	Coordinate Displacement Vector from Local Origin
$PTYPE$	Identifies Airfoil Analysis and Design Region Types
p	Airfoil Region Index
q	Airfoil Element Index

R_1, R_2	Distance from a Panel Edge to Field Point, equation (10) and (11)
R_c	Chord Reynolds Number
RHS	Right-Hand-Side
S, s	Surface Distance; Length
STYPE	Identifies Type of Section
t	Thickness
u	Doublet Distribution with Discontinuities Removed
u_j	Vortex Density Array
\vec{V}, V	Velocity
v_j	Geometry Unknowns for Design Problem
W	Weighting Factor
(x, y, z)	General Flow Field Coordinate System
α	Angle of Attack of \vec{V}_∞ with Respect to x-Axis
α_1, α_2	Angle Between Field Point Vector and Panel Normal Vector, equations (12) and (13)
β	Angle Defined by equation (9)
β_i	Coefficients of Quadratic Doublet Distribution ($1 \leq i \leq 6$)
γ	Vortex Density
Δs	Length
Δs_i	Length of Panel i
$\delta \vec{R}_j$	Panel Endpoint Perturbation Vector
δSF	Length Scale Factor for Design Problems
ϵ	A Small Value (< 1)
θ	Angle with Respect to x-axis; Angle with Respect to Bisector
θ_i	Angle of Panel i with Respect to x-axis

κ_1, κ_2	Parameters for Sharp Corner, Trailing Edge Control Points, equations (2) and (3)
λ	See equation (27)
λ_x, λ_y	Lagrangian Multipliers
μ	Doublet Density
ξ, η, ζ	Panel Coordinate System; Local Coordinate System
σ	Source Density
ϕ	Potential
ϕ_S	Induced Source Potential
ϕ_V	Induced Vortex Potential

SUBSCRIPTS

A,B	Beginning, End Conditions
A,B,C	Arbitrary Panels
B	Bisector
C	Sharp Corner
CP	Control Point
D	Dependency
E	Panel Endpoint
N	Normal Component
P	Control Point; Prescribed; Panel
ref	Reference
T	Tangential Component; Total
TE	Trailing Edge
U,L	Upper, Lower
UPR, LWR	Upper, Lower
W	Wake
∞	Freestream Conditions

INTRODUCTION

The surface panel method philosophy for solving arbitrary subsonic potential flow problems involves the mating of classical potential theory with contemporary numerical techniques. Classical theory is used to reduce an arbitrary flow problem to a surface integral equation relating boundary conditions to an unknown singularity distribution. The contemporary numerical techniques are then used to calculate an approximate solution to the integral equation. This involves representing flow boundaries by surface panels on which potential flow singularities are distributed.

Whereas there is no limit to the number of different singularity distributions that can induce a given flow field, the type of singularity plays an important role in determining the success of a numerical solution method. The advantages of using the combined source-doublet distribution corresponding to the classical third identity of Green were described and demonstrated in reference 1. The combined distribution is not subject to the prediction errors associated with the application of source methods to thin, highly loaded wings or nacelles. In iterative design methods, the combined source-doublet distribution can be used to generate converged solution geometries corresponding to prescribed pressure distributions. This contrasts sharply with doublet (or vortex) methods, which are numerically unstable for leading edge design. If indirect internal perturbation potential boundary conditions are applied to constant source-quadratic doublet distributions on flat panels, the resulting prediction accuracy is typically competitive with more complex curved panel formulations.

This report describes recent developments at McDonnell Aircraft Company (MCAIR) of two and three-dimensional subsonic analysis and design methods using combined source-doublet panels to represent the inviscid flow. Formulations are presented for two potential flow computer programs. The first solves arbitrary mixed analysis-design problems in two dimensions for multi-element airfoils. The second solves three-dimensional analysis problems for wing-fuselage configurations.

The mixed analysis-design multi-element airfoil program was created by extending an earlier potential flow program that would solve all-analysis or all-design problems (reference 1). In regions selected by the user for design, the geometry corresponding to a prescribed pressure distribution is calculated by iteration. Both the shape and length of the region will converge on the geometry that most nearly corresponds to the prescribed pressures. For airfoils with thick trailing edges, a method is presented in which the predicted lift is improved by panelling the base.

The three-dimensional panel program is based on the method described in reference 1. An improvement that has been incorporated applies a spline fit technique similar to one developed by Boeing (reference 18) in order to reduce singularity discontinuities at panel edges.

An approach is discussed for generating velocity derivatives with respect to arbitrary geometry perturbations of a wing-fuselage configuration. Application of this approach to the three-dimensional panel program would enable the prediction of the effect of arbitrary configuration changes by simply multiplying a pre-calculated matrix by a new right-hand-side. Also discussed is a procedure for using the velocity derivatives to solve inviscid wing design problems.

This report presents the mathematical formulation and example solutions for the computer programs.

AIRFOIL MIXED ANALYSIS-DESIGN METHOD

A variety of two-dimensional incompressible potential flow problems can be solved by the Multi-Element Airfoil Inviscid Analysis and Design Program (Version 1), hereinafter designated "Program MAAD". Figure 1 illustrates the type of mixed analysis-design problem that can be solved. The geometry of one or more airfoil elements is divided into analysis regions of prescribed geometry and design regions of prescribed pressure distribution. It is not necessary to have regions of both type on an airfoil; therefore, analysis-only or design-only problems are permitted. For each analysis region, a normal velocity distribution is prescribed, and the tangential distribution is calculated. For each design region, desired normal and tangential velocity distributions in terms of surface distance are prescribed simultaneously, and the corresponding boundary geometry is calculated. In the typical design problem, the objective is to calculate a flow streamline of given pressure distribution. This corresponds to the prescription of zero normal velocity, with the prescribed tangential velocity distribution being generated from the pressure distribution by the application of Bernoulli's equation.

Program MAAD is an extension of an earlier two-dimensional multi-element airfoil program described in references 1 and 2. The analytical portion of the extension was accomplished as part of the MCAIR Independent Research and Development Program. Coding, check-out, and evaluation were performed as part of this contract. The significant new options are:

- (1) Arbitrary mixtures of analysis and design regions on each airfoil element,
- (2) Non-zero normal velocity boundary conditions,

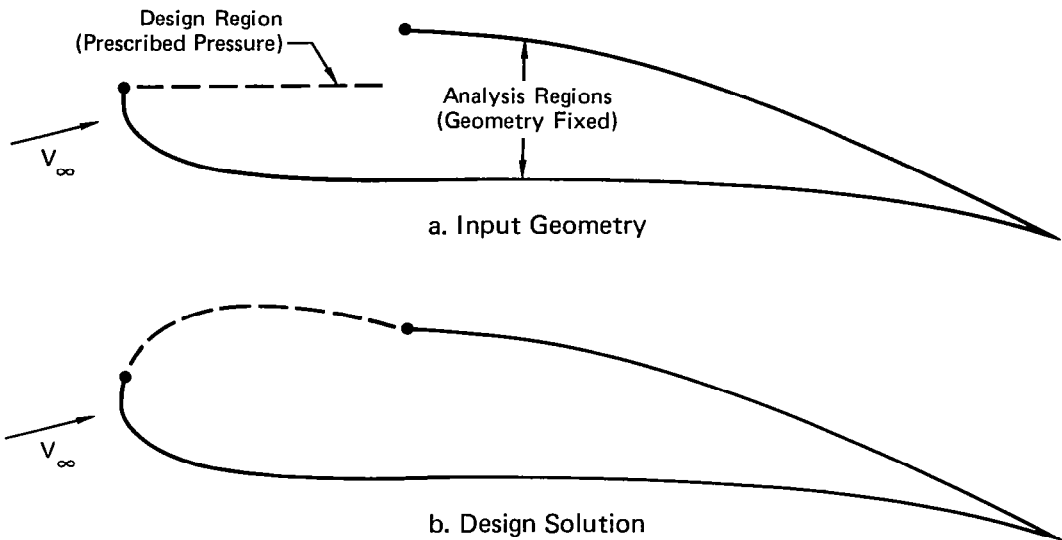


Figure 1. Illustration of a Mixed Analysis - Design Problem

- (3) Sharp corners at arbitrary points on an airfoil (such as a flap hinge line),
- (4) Arbitrary free stream velocity (including zero), and
- (5) Simulation of two-dimensional wind tunnel wall interference.

Flow fields are modelled in Program MAAD by a combined source-vortex surface panelling method. All surface panel methods are exact in the sense that the difference between the calculated and analytical incompressible potential flow solutions can be made arbitrarily small at the expense of increased computing time. However, significant differences between the various methods exist with respect to accuracy for a given number of panels, numerical sensitivity to certain boundary shapes or user generated panelling anomalies, computing efficiency, applicability to design problems, and formulation simplicity. For two-dimensional flow, nearly all the possible approaches depicted in figure 2 were evaluated at MCAIR prior to this contract. For a variety of geometries, it was consistently demonstrated that the approach selected is competitive with or superior to each of the others.

The approach is to solve for the combined source-vortex distribution associated with the classical third identity of Green (reference 3). A detailed description of the theory and discussion of the advantages of this surface singularity panel method are provided in reference 1 and will be summarized only briefly here. The reason for selecting combined source-vortex

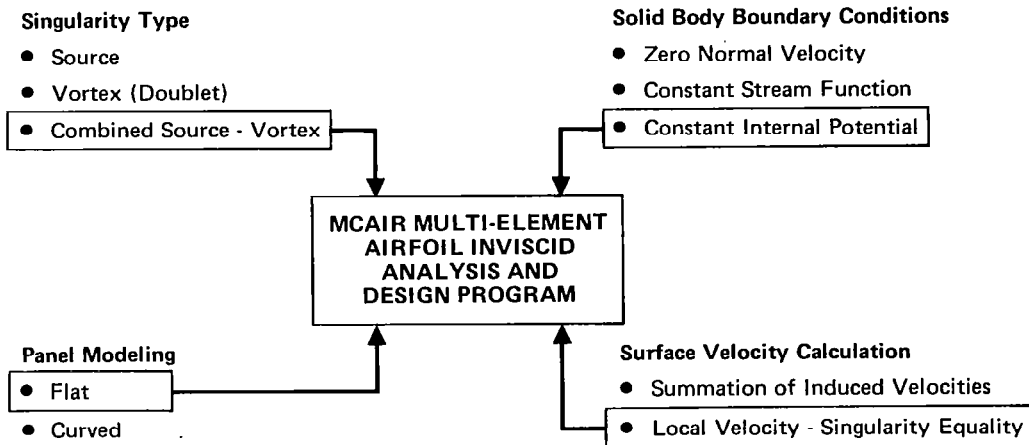


Figure 2. Menu of Surface Singularity Panel Methods
Incompressible, Potential Flow

distributions is to eliminate the numerical instabilities associated with: (1) the application of source-only panel methods to the analysis of thin, highly loaded geometries and (2) the design of leading edge regions by vortex-only methods. The use of indirect internal perturbation potential boundary conditions, flat surface panels, and the local singularity-velocity relationships of Green's identity lead to an efficient, straightforward panel method. Furthermore, the subsequent prediction accuracy is typically competitive with more complex higher order (curved panel) formulations (references 4 and 5). It is noteworthy that the first use of indirect internal potential boundary conditions was by Morino (reference 6).

In Program MAAD, the vortex distribution is linear on each panel. The program has an option for either piecewise constant or linear source distributions. In almost all cases, the type of source distribution selected has no appreciable effect on the solution.

Mixed analysis-design and design-only problems are solved by iteration. The user must provide a starting geometry for each design region in order to initialize the calculations. As illustrated in figure 1, continuity with an adjacent analysis region is not required at the aft end of a design region starting geometry. Before any aerodynamic calculations are performed, the program automatically satisfies continuity requirements by generating the least possible stretching and shape perturbation of the panelled design region starting geometry. Then the combined source-vortex representation is used to calculate an analysis-only solution. Next, a first-order inverse method is applied to predict the design region geometry modification that will minimize the difference between the prescribed and the calculated tangential velocity distributions. The inverse method satisfies normal

velocity boundary conditions and geometric continuity as first-order constraints. Finally, the predicted geometry modification is applied in order to provide the starting geometry for the next iteration cycle.

This section presents the detailed mathematical formulation for (1) the analysis-only method and (2) the first-order inverse method for design regions. It is assumed that the reader is familiar with surface singularity theory. Reference 1 provides adequate background. The approach used in the first-order inverse method was created in 1973 (reference 7). Numerical examples demonstrating the capabilities of Program MAAD follow the formulation presentation.

Analysis-Only Solution Method

Given one or more airfoil elements with prescribed normal velocity (Neumann) boundary conditions, the objective is to calculate the tangential surface velocity distribution in incompressible potential flow. The solution process consists of the following five steps:

- (1) Establish a panelled surface geometry.
- (2) Calculate the source distribution based on the local surface slope with respect to the free stream direction.
- (3) Calculate source and vortex potential influence coefficients.
- (4) Set up and solve the system of linear equations relating boundary conditions to unknown vortex strengths.
- (5) Calculate the tangential velocity distribution from the solution vortex strengths.

These steps are described in detail below.

The geometry panelling nomenclature is defined by figure 3. Each airfoil element is identified by index q ($1 \leq q \leq q_T$). The geometry of an element is defined by n surface points input in clockwise order. The trailing edge is defined by points 1 and n . Normally, these two points coincide to form a closed panelled geometry. Although it is not recommended, a gap between points 1 and n is permitted. Completely enclosed flows are allowed. For example, consider the wind tunnel test section of figure 4. The rectangular enclosure is treated as an airfoil element. The only difference is that the input points of an enclosing boundary are ordered counterclockwise. The velocity components at the midpoint of any panel i on any element q are designated VT_i and VN_i . It is noted that positive VN_i is directed toward the real fluid side of a panel. On the other side of a panel,

the flow is imaginary. In accordance with Green's third identity, the imaginary flow is selected to be uniform with velocity \vec{V}_∞ . The length of panel i is defined as Δs_i , and the angle with respect to the x -axis is θ_i .

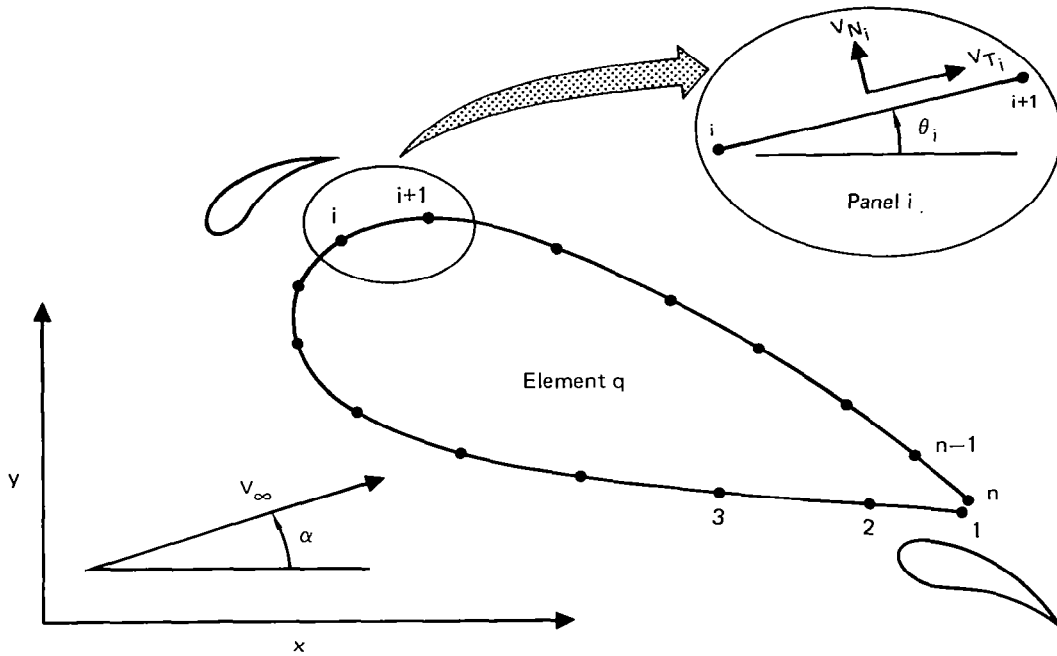


Figure 3. Multi-Element Airfoil Panelling Nomenclature

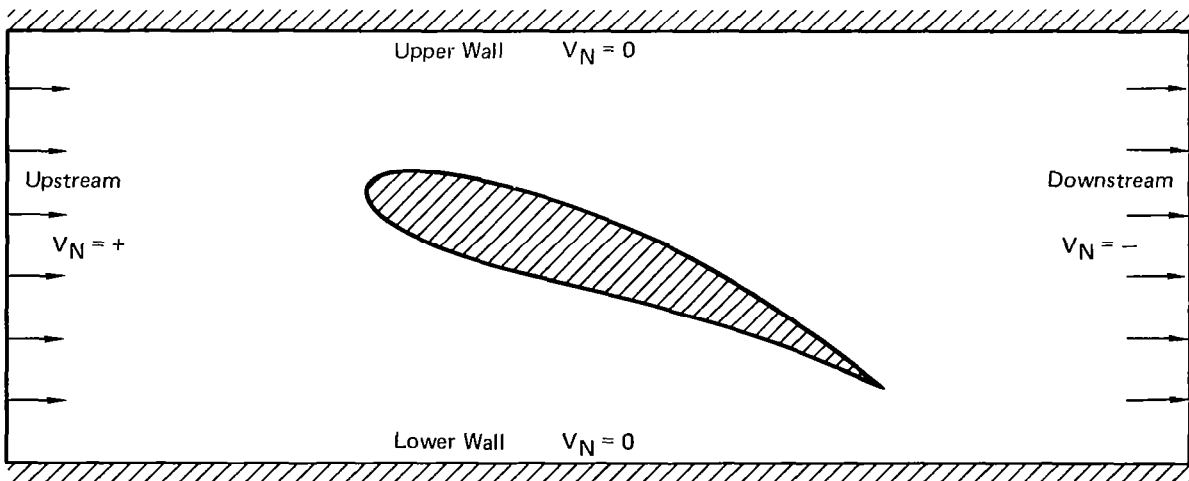


Figure 4. Simulation of Wind Tunnel Wall Interference

There is one boundary condition control point at the mid-point of each panel. The control point is slightly withdrawn to the imaginary flow (internal) side of the panel in order to avoid a discontinuity in potential at the exact panel surface. At each sharp corner, an additional internal control point is inserted (figure 5) to control the discontinuity in vortex density that is theoretically expected at a surface slope discontinuity. Here a sharp corner refers to the intersection of two panels at a point where the user designates that the actual airfoil surface slope is discontinuous. At a trailing edge, two Kutta condition control points are inserted in the actual flow to control the circulation (figure 5). It is not necessary for a trailing edge to be a sharp corner. Therefore, a smooth geometry such as an ellipse can be modelled. Definitions for the terms depicted in figure 5 follow:

$$\vec{e}_C \equiv \frac{\vec{n}_A + \vec{n}_B}{|\vec{n}_A + \vec{n}_B|} \quad (1)$$

$$\Delta s_C \equiv \frac{\kappa_1}{2} (\Delta s_A + \Delta s_B) \quad (2)$$

$$\Delta s_{TE} \equiv \frac{\kappa_2}{2} (\Delta s_A + \Delta s_B) \quad (3)$$

where Δs_A and Δs_B are the lengths of panels A and B, and where κ_1 and κ_2 are input values much smaller than 1. The recommended values are $\kappa_1 = 0.01$ and $\kappa_2 = 0.02$. The value for ϵ (figure 5) has been arbitrarily selected to be 1/2 radian in Program MAAD.

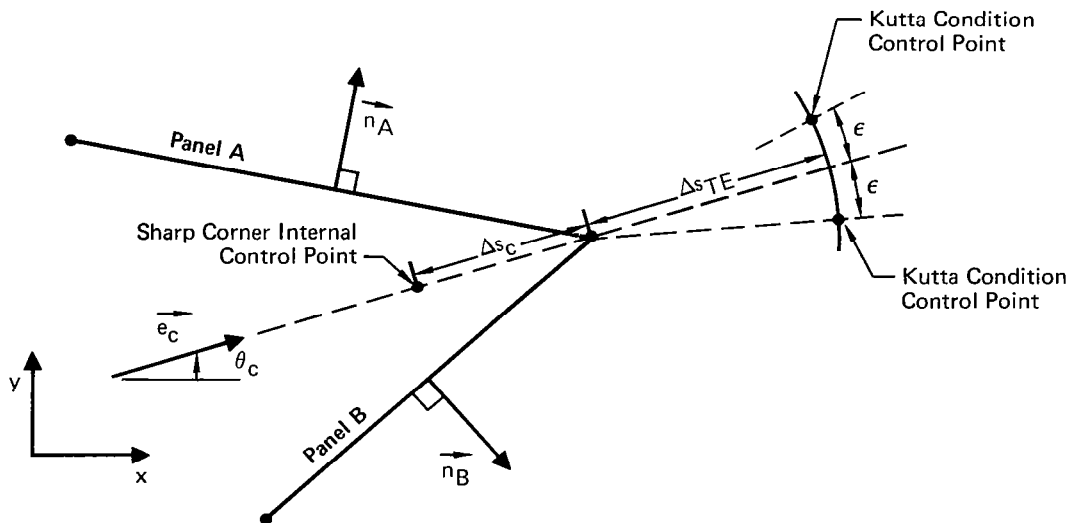
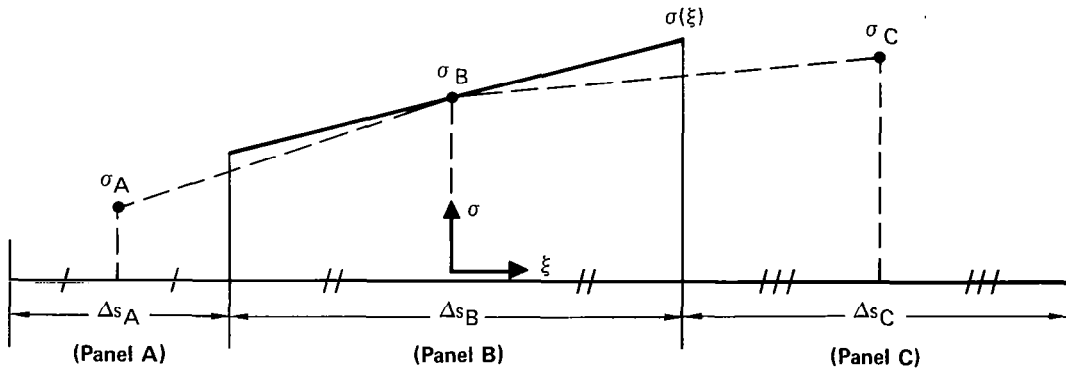


Figure 5. Control Points at a Sharp Corner and/or Trailing Edge

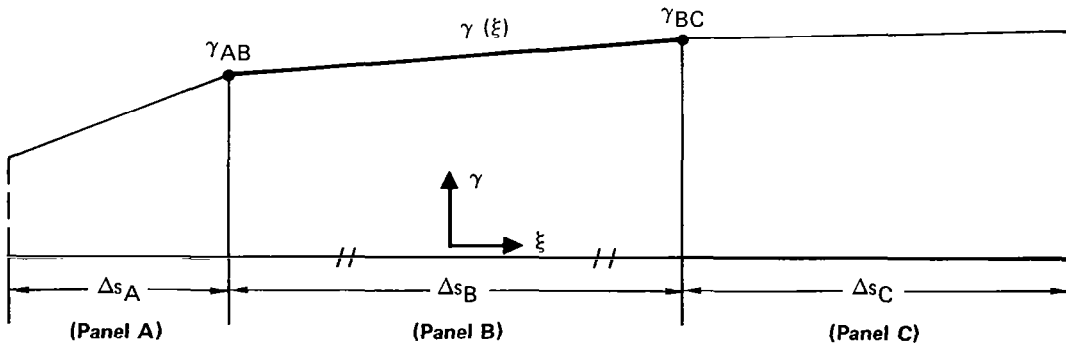
Figure 6 illustrates the linear source and vortex distributions on the panel designated B, adjacent to panels A and C. Here the ξ -axis measures surface distance, so that panels A and C can be assumed to have been rotated to coincide with the plane of panel B. The source function $\sigma(\xi)$, which passes through σ_B , is a close linear curve fit to the source density at the three panel midpoints (σ_A , σ_B , σ_C). The linear vortex function $\gamma(\xi)$ is determined by the vortex density at the endpoints of panel B (γ_{AB} , γ_{BC}).

$$\sigma(\xi) = \sigma_B + 2\xi \frac{\left(\frac{\Delta s_B + \Delta s_C}{\Delta s_A + \Delta s_B}\right)(\sigma_B - \sigma_A) + \left(\frac{\Delta s_A + \Delta s_B}{\Delta s_B + \Delta s_C}\right)(\sigma_C - \sigma_B)}{\Delta s_A + 2\Delta s_B + \Delta s_C} \quad (4)$$

$$\gamma(\xi) = \frac{1}{2}(\gamma_{AB} + \gamma_{BC}) + \left(\frac{\gamma_{BC} - \gamma_{AB}}{\Delta s_B}\right)\xi \quad (5)$$



a. Linear Source Distribution $\sigma(\xi)$



b. Linear Vortex Distribution $\gamma(\xi)$

Figure 6. Singularity Density Distributions on a Panel

Special handling is required at sharp corners. Suppose that the intersection of panels A and B in figure 6 is designated a sharp corner by the user. Then theoretically neither the source nor vortex densities will be continuous at the intersection. To accommodate this, $\sigma(\xi)$ on panel B is selected as the linear function passing through σ_B and σ_C , instead of the function defined by equation (4). For the vortex density, γ_{AB} is assumed to be double-valued, i.e., γ_{AB}^- and γ_{AB}^+ respectively refer to the vortex density immediately to the left and right of the sharp corner. Analogous treatment is applied if the intersection of panels B and C is designated a sharp corner.

In accordance with Green's third identity, the source strength at the midpoint of each panel i on element q is immediately determined from the following equation:

$$\sigma_i = V_{N_{iP}} + V_\infty \sin(\theta_i - \alpha) \quad (6)$$

where $V_{N_{iP}}$ is the prescribed normal velocity. By combining equations (4) and (6), the source distribution over the entire multi-element airfoil system is uniquely determined.

The potential induced at each control point by the source and vortex distributions on each panel is calculated as follows. First, a (ξ, η) -coordinate system is generated for the influencing panel as illustrated in figure 7. Then the coordinates of the control point of interest are converted from the (x, y) -system to the (ξ, η) -system. Using subscript P to designate the control point location,

$$\xi_P = [x_P - \frac{1}{2}(x_i + x_{i+1})] \cos\theta_i + [y_P - \frac{1}{2}(y_i + y_{i+1})] \sin\theta_i \quad (7)$$

$$\eta_P = [y_P - \frac{1}{2}(y_i + y_{i+1})] \cos\theta_i - [x_P - \frac{1}{2}(x_i + x_{i+1})] \sin\theta_i \quad (8)$$

The following functions provide the potential at point (ξ_P, η_P) induced by unit strength and unit linear strength source and vortex distributions on the influencing panel.

Definitions:

$$\beta \equiv \begin{cases} 0 & (\eta_P \geq 0) \\ \pi & (\eta_P < 0) \end{cases} \quad (9)$$

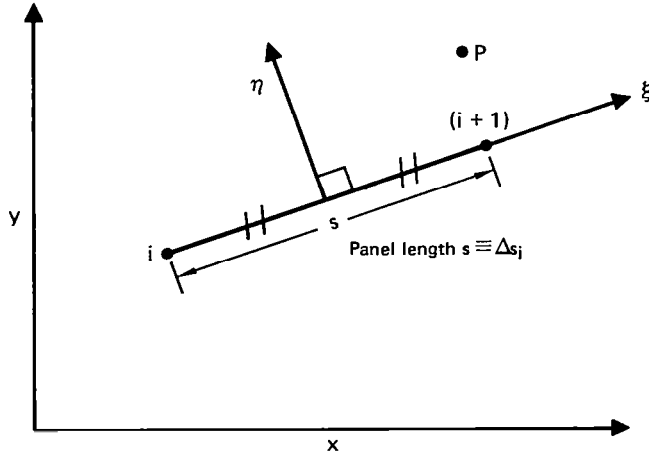


Figure 7. Coordinate System of Panel i

$$R_1^2 \equiv \left(\xi_P + \frac{s}{2}\right)^2 + \eta_P^2 \quad (10)$$

$$R_2^2 \equiv \left(\xi_P - \frac{s}{2}\right)^2 + \eta_P^2 \quad (11)$$

$$\alpha_1 \equiv \text{Tan}^{-1} \left(\frac{\xi_P + \frac{s}{2}}{\eta_P} \right) \quad (12)$$

$$\alpha_2 \equiv \text{Tan}^{-1} \left(\frac{\xi_P - \frac{s}{2}}{\eta_P} \right) \quad (13)$$

$$F_A \equiv \frac{1}{2} \ln \left(\frac{R_1^2}{R_2^2} \right) \quad (14)$$

$$F_B \equiv (\alpha_1 - \alpha_2) \quad (15)$$

$$F_C \equiv \frac{1}{4} \ln (R_1^2 R_2^2) \quad (16)$$

$$F_D \equiv \frac{1}{2} (\alpha_1 + \alpha_2) \quad (17)$$

$$F_E \equiv \left(\frac{\xi_P^2 - \eta_P^2}{s^2} \right) \quad (18)$$

Induced Potential:

Unit source $\sigma(\xi) = 1$

$$\phi_{S1} = \left(\frac{s}{2\pi}\right) \left[-1 + \left(\frac{\xi_P}{s}\right) F_A + F_C + \left(\frac{\eta_P}{s}\right) F_B\right] \quad (19)$$

Unit vortex $\gamma(\xi) = 1$

$$\phi_{V1} = \left(\frac{s}{2\pi}\right) \left[-\left(\frac{\pi}{2} + \beta\right) + \left(\frac{\xi_P}{s}\right) F_B + F_D - \left(\frac{\eta_P}{s}\right) F_A\right] \quad (20)$$

Unit Linear Source $\sigma(\xi) = \left(\frac{\xi}{s}\right)$

$$\phi_{S2} = \left(\frac{s}{2\pi}\right) \left[-\frac{1}{2} \left(\frac{\xi_P}{s}\right) + \frac{1}{2} F_A \left(F_E - \frac{1}{4}\right) + \left(\frac{\xi_P \eta_P}{s^2}\right) F_B\right] \quad (21)$$

Unit Linear Vortex $\gamma(\xi) = \left(\frac{\xi}{s}\right)$

$$\phi_{V2} = \left(\frac{s}{2\pi}\right) \left[+\frac{1}{2} \left(\frac{\eta_P}{s}\right) + \frac{1}{2} F_B \left(F_E - \frac{1}{4}\right) - \left(\frac{\xi_P \eta_P}{s^2}\right) F_A\right] \quad (22)$$

By combining equations (4) and (5) with equations (19)-(22), it is possible to determine the potential ϕ at (ξ_P, η_P) induced by the simultaneous action of all singularities on the influencing panel. To accomplish this, it is convenient to cast equation (4) in the following form:

$$\sigma(\xi) = \sigma_B + (c_1 \sigma_A + c_2 \sigma_B + c_3 \sigma_C) \left(\frac{\xi}{\Delta s_B}\right) \quad (23)$$

Here panel B of figure 6 is considered to be the influencing panel. It follows that

$$\begin{aligned} \phi = & (c_1 \phi_{S2}) \sigma_A + (\phi_{S1} + c_2 \phi_{S2}) \sigma_B + (c_3 \phi_{S2}) \sigma_C \\ & + \left(\frac{1}{2} \phi_{V1} - \phi_{V2}\right) \gamma_{AB} + \left(\frac{1}{2} \phi_{V1} + \phi_{V2}\right) \gamma_{BC} \end{aligned} \quad (24)$$

The coefficients of σ_A , σ_B , σ_C , γ_{AB} , and γ_{BC} are designated potential influence coefficients. With the exception of γ_{AB} and γ_{BC} , all the terms in equation (24) have been previously defined as functions only of V_∞ , α , and the input coordinates (x_i, y_i) . Therefore, equation (24) can be cast in the following form:

$$\phi = d_1 + d_2\gamma_{AB} + d_3\gamma_{BC} \quad (25)$$

where only γ_{AB} and γ_{BC} are unknown.

The internal boundary condition to be satisfied is that the imaginary internal flow of each airfoil element be of uniform velocity \vec{V}_∞ . This is accomplished by requiring that the internal perturbation velocity line integral between any two adjacent internal control points i_{CP} and i_{CP+1} be zero, where the control points are ordered in the direction of increasing panel index i . The line integral is defined as

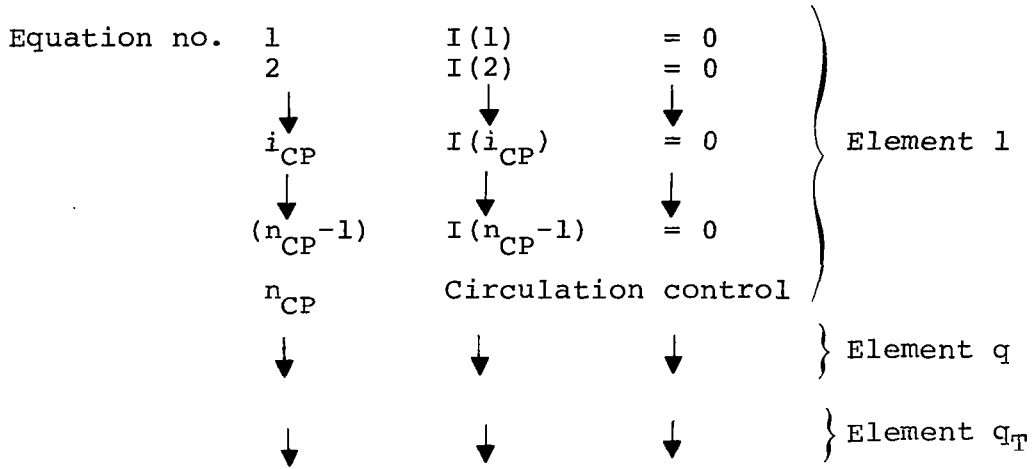
$$I(i_{CP}) \equiv \int_{i_{CP}}^{i_{CP+1}} (\vec{V} - \vec{V}_\infty) \cdot d\vec{s} \quad (26)$$

where \vec{V} is the total internal velocity and $d\vec{s}$ follows an internal path, i.e., a path in the imaginary flow. With the aid of equation (25), the contribution of all singularities on influencing panel B to line integral $I(i_{CP})$ is expressed as

$$\begin{aligned} I(i_{CP})_B = & + (d_1 + d_2\gamma_{AB} + d_3\gamma_{BC}) i_{CP+1} \\ & - (d_1 + d_2\gamma_{AB} + d_3\gamma_{BC}) i_{CP} \\ & + \lambda \frac{1}{2} (\gamma_{AB} + \gamma_{BC}) \Delta s_B \end{aligned} \quad (27)$$

where λ is equal to 0, +1, or -1, depending upon whether the internal path between control points i_{CP} and i_{CP+1} crosses the positive ξ -axis of panel B. The λ -term essentially cancels out the discontinuity in vortex-induced potential across a slit. If there are an even number of crossings, $\lambda = 0$. If there are an odd number of crossings, $\lambda = \pm 1$ if η at point i_{CP} is ≥ 0 . For simplicity, the internal path selected is the one that follows the two adjacent panels on which i_{CP} and i_{CP+1} lie. It is noted that if there are a total of n_{CP} internal control points for element q , the line integral between control points n_{CP} and 1 is not to be set to zero explicitly. This follows from the fact that any closed internal velocity line integral will be zero; therefore, there can be only $n_{CP}-1$ linearly independent internal boundary conditions per airfoil element.

It is now possible to establish the system of linear equations relating boundary condition satisfaction to the unknown vortex densities. The equations to be solved are ordered as follows:

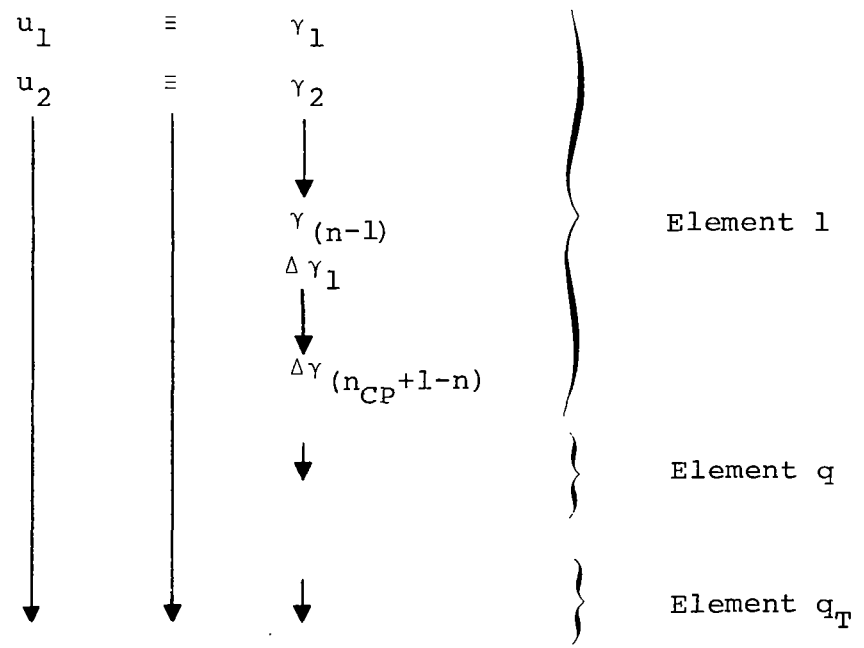


Now consider arbitrary panel j to be the influencing panel B. The unknown vortex density γ_{AB} is identified as γ_j . In the event that the intersection between panels A and B is a sharp corner,

$$\left. \begin{aligned}
 \gamma_{AB}^- &\equiv \gamma_j \\
 \gamma_{AB}^+ &\equiv \gamma_j + \Delta\gamma
 \end{aligned} \right\} \quad (28)$$

where $\Delta\gamma$ is an additional unknown. There is one unknown vortex discontinuity $\Delta\gamma$ per sharp corner.

The unknown vortex densities are set up as an array u_j , ordered as follows:



The total number of equations and unknowns are the same. That number is equal to the sum of the number of panels and sharp corners in the entire multi-element airfoil system. It remains to define the circulation control equation required for each element q .

Any one of five available circulation options can be selected for each airfoil element. The basic Kutta condition will be described fully; the other four options will be summarized. The Kutta condition is satisfied by requiring that the average velocity between the two control points in figure 5 be zero. This is accomplished in the same manner described above for two adjacent internal control points, except that the line integral between the Kutta condition control points includes the free stream contribution to velocity. The free stream contribution to the line integral between the upper and lower points is $V_{\infty} \cos \alpha (x_{UPR} - x_{LWR}) + V_{\infty} \sin \alpha (y_{UPR} - y_{LWR})$. If the angle 2ϵ between the two control points were allowed to approach zero, this Kutta condition would exactly approach the condition of zero velocity normal to the trailing edge bisector at the distance Δs_{TE} downstream. The finite value $\epsilon = 1/2$ provides a close approximation to zero normal velocity, without requiring the calculation of velocity influence coefficients.

Following are summaries of the other four circulation options:

- (1) The extrapolated bisector Kutta condition is identical to the basic condition described above, except that the angle θ_C of figure 5 is replaced by a trailing edge angle determined by extrapolation from two upper and two lower surface upstream panels. The extrapolated Kutta condition is recommended over the basic Kutta condition.
- (2) A numerical value of circulation can be prescribed, which will be set equal to the net integrated vorticity around the panelled element.
- (3) Circulation normalized by the panelled perimeter of the element can be prescribed, which is equivalent to prescribing the average vortex density. The only practical difference between this option and option (2) is for design problems, where the perimeter may not be known beforehand.
- (4) If the present analysis solution is part of an iteration cycle in a design solution and if there are any design regions on the element in question, then the prescribed midpoint tangential velocity components $V_{T_{ip}}$ can be used to fix the circulation. The corresponding circulation control equation is

$$\sum (V_{T_i} \Delta s_i) = \sum (V_{T_{ip}} \Delta s_i) \quad (29)$$

where the summation includes design regions only.

In the above options (2), (3), and (4), the Kutta condition control points are ignored.

If the entire flow is bounded by one element of counterclockwise ordering, the vorticity of that element is fixed by the condition that the total vorticity of the q_T elements must be zero. This is a consequence of the fact that the imaginary flow of the bounding (counterclockwise) element must have zero circulation in order to satisfy Green's third identity.

The system of linear equations to be solved is set up in the following form:

$$\sum_j C_{ij} u_j = RHS_i \quad (30)$$

where u_j is the array of unknown vortex strengths and RHS_i is the known right-hand-side of the i th equation. A standard matrix inverse method is used to solve the system. The matrix inverse and potential influence coefficients are stored for future use if the next analysis case involves changes in only angle of attack, circulation, and normal velocity distribution. It is noted that although any such change will alter the right-hand-side RHS_i , neither the potential influence coefficients nor matrix C_{ij} will be affected.

Corresponding to Green's third identity, the solution tangential velocity at the midpoint of panel i of element q is

$$V_{T_i} = V_\infty \cos(\theta_i - \alpha) + \frac{1}{2} [\gamma_i + \gamma_{(i+1)}] \quad (31)$$

If point i is a sharp corner, then γ_j is to be replaced by $\gamma_i + \Delta\gamma$, corresponding to equation (28). If $(i+1) = n$, then $\gamma_{(i+1)}$ is to be replaced by γ_1 .

Although prediction accuracy is usually better at panel midpoints, the velocity at panel endpoints is also calculated. In design problems, both midpoint and endpoint tangential velocity components are prescribed to provide numerical stability in the inverse step. The tangential component of velocity at point i is calculated by the formula

$$V_{T_{E_i}} = V_\infty \cos(\theta_{E_i} - \alpha) + \gamma_i \quad (32)$$

where subscript E designates a panel endpoint, i.e., point i. The angle θ_{E_i} is a weighted average of the two adjacent panel angles.

$$\theta_{E_i} = \frac{\Delta s_i \theta_{i-1} + \Delta s_{i-1} \theta_i}{\Delta s_i + \Delta s_{i-1}} \quad (33)$$

If θ_{i-1} and θ_i differ by more than π , it is necessary to adjust one of the angles by adding the proper multiple of 2π before applying equation (33). If $i = 1$ or n in equations (32) and (33), replace subscript $(i - 1)$ by $(n - 1)$ and i by 1.

The only remaining step in the analysis-only solution formulation is the calculation of pressures, forces, and moments. Under the presumption of steady state flow, Bernoulli's law is used to calculate the midpoint pressure coefficient for each panel i.

$$C_{P_i} = 1 - \frac{V_{T_i}^2 + V_{N_i}^2}{V_{ref}^2} \quad (34)$$

where V_{ref} is usually V_∞ , unless V_∞ is zero. Force and moment coefficients are calculated by the approximations that the panelled geometry is the actual surface and that the pressure coefficient on panel i is uniform with value C_{P_i} .

First-Order Inverse

In design problem solutions, each iteration cycle is divided into an analysis-only step and a first-order inverse correction to the geometry. The former was described above. The formulation for the latter is presented here. The objective is to determine the change in surface geometry most nearly corresponding to the prescribed tangential velocity distribution in design regions. The approach is to establish to first-order the relationship between velocity and geometry perturbations. This relationship is then inverted to determine the geometry perturbation corresponding to the desired velocity perturbation.

Before proceeding with the solution formulation, it is necessary to precisely define analysis and design regions. The indexing nomenclature for the division of an airfoil element into regions is presented in figure 8. Region p is bounded by $i_A(p) \leq i \leq i_B(p)$, where i is a panel endpoint index defined earlier in figure 3. At this stage, it is assumed that all continuity requirements are satisfied. For $p \neq p_T$, the continuity requirement is that points $i_B(p)$ and $i_A(p+1)$ coincide. For $p = p_T$, the requirement is that the components of the trailing edge opening $(x_n - x_1, y_n - y_1)$ equal prescribed values. Table I summarizes the differences between analysis and design regions.

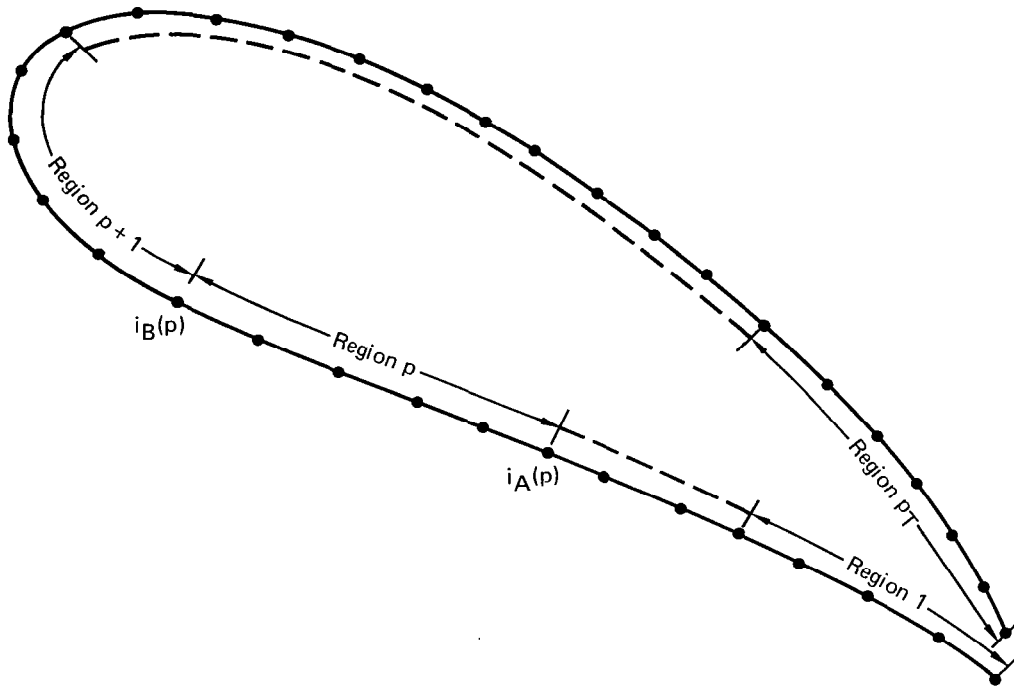


Figure 8. Division of an Airfoil Element into Regions

Region Type	Boundary Conditions		Geometry (Shape and Length)	
	Normal Velocity	Tangential Velocity	Fixed	Free
Analysis	X		X	
Design	X	X		X

Table I. Differences Between Analysis and Design Regions

The index PTYPE identifies the type of region. Both PTYPE = 0 and 1 designate analysis regions. The difference is that a region of PTYPE = 1 is free to translate in the (x,y)-coordinate system while satisfying continuity requirements, whereas the location of a region of PTYPE = 0 will remain fixed. The freedom to translate is sometimes useful if the analysis region is nestled between two design regions. Of course, no analysis region is allowed to rotate, change shape, stretch, or shrink. PTYPE = 2 and 3 designate design regions. A region of PTYPE = 3 is free to change geometry while satisfying continuity requirements with the adjacent regions. PTYPE = 2 is the same as PTYPE = 3, except that for PTYPE = 2, two degrees of freedom are eliminated by prescribed fixed values for the (x,y)-coordinates of point $i_A(p)$. A region of PTYPE = 0 cannot be immediately

followed by a region p of $PTYPE = 2$, because continuity requirements alone would fix the location of $i_A(p)$. In that case, $PTYPE(p)$ should be selected as 3. Table II defines the allowable ordering of regions on an airfoil element.

If $PTYPE(p)$ is	then $PTYPE(p+1)^*$ can be
0 (Analysis)	0 or 3 only
1 (Analysis)	1 or 3 only
2 (Design)	0, 1, 2, or 3
3 (Design)	0, 1, 2, or 3

* If $p = p_T$, replace $(p+1)$ by 1.

Table II. Permissible Ordering of Region Types

There are two additional restrictions. First, at least one region per element must be $PTYPE = 0$ or 2 in order to prevent the entire element from unrestricted translation in space. Second, the user must divide the element into regions in such manner that any sharp corners are located at the intersection of two regions. This second restriction simplifies the indexing but does not limit the solution generality of the method. That is, it is permissible for adjacent regions to be both analysis or both design, as identified in Table II.

It is convenient to designate a set of adjacent regions that are free to move as a "group of free regions". On any airfoil element q , each group of free regions is assigned an index IGP ($1 \leq IGP \leq NGP$). The regions included in group IGP are

$$p_A(IGP), p_{A+1}, \dots, p_{B-1}, p_B(IGP).$$

The locations of $i_A(p_A)$ and $i_B(p_B)$ are fixed, but all intermediate points are free to move. If the trailing edge is in the midst of a group of free regions, then the regions included in the group are ordered as follows:

$$p_A, p_{A+1}, \dots, p_{T-1}, p_T, 1, 2, \dots, p_{B-1}, p_B.$$

Each region of $PTYPE = 1, 2$, or 3 will be part of a group of free regions. The assignment of group indexing IGP , $p_A(IGP)$ and $p_B(IGP)$ is performed automatically by Program MAAD.

The transformation of a design region during an iteration cycle is illustrated in figure 9. The free stream velocity with respect to the (x,y) -system (i.e., V_∞ and α) will not change. Although the normal direction of each panel changes, the value V_{N_i} remains equal to the prescribed value $V_{N_{iP}}$. The change in shape is completely defined by the array $\delta\theta_i$ [$i_A \leq i \leq (i_B-1)$]. The ratio of surface distance of the region after transformation to the distance before transformation is $(1 + \delta SF)$. It is noted that the percentage length change is the same for every panel in the region. Therefore, the prescribed tangential velocity array $V_{T_{iP}}$ describes a fixed distribution of velocity versus normalized surface distance in the region.

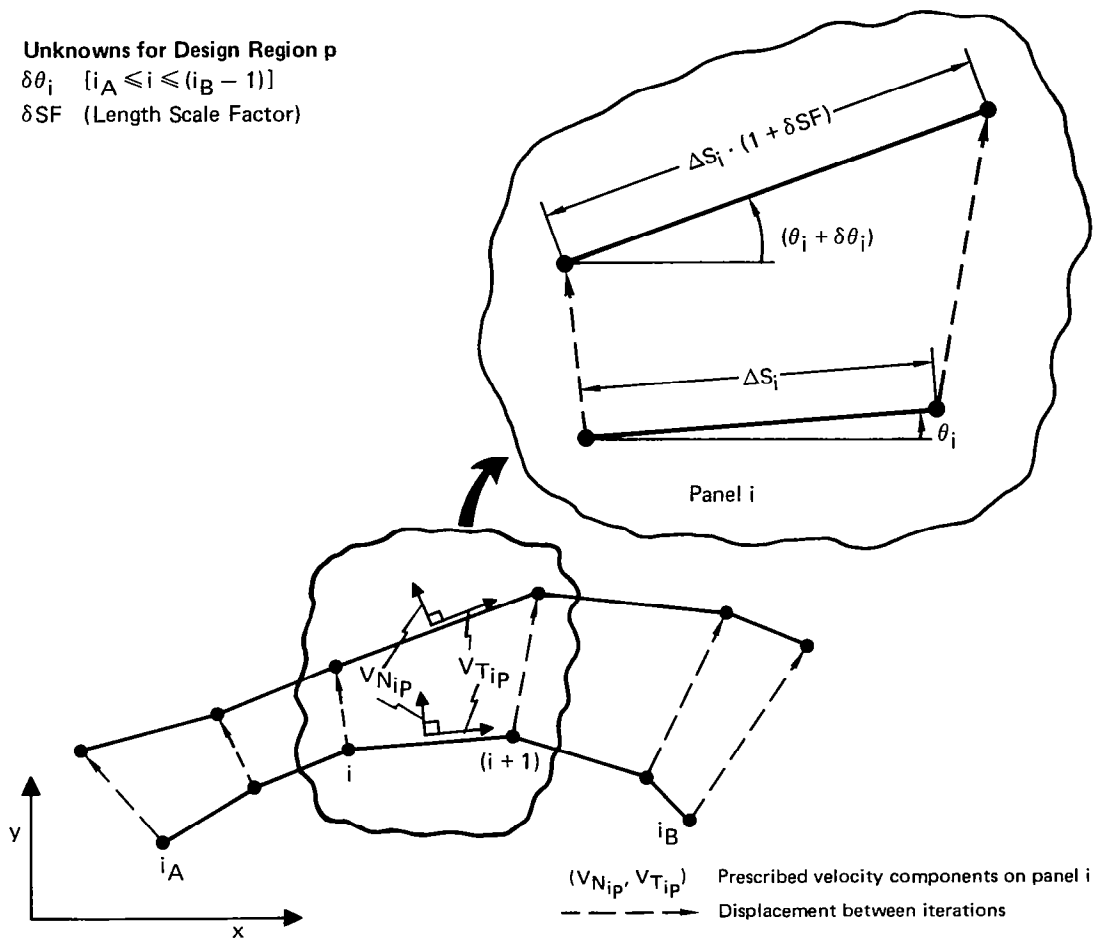


Figure 9. Transformation of a Design Region Between Successive Iteration Cycles

The displacement between iterations of point i of design region p in figure 9 is

$$\delta x_i = \delta x_{i_A} + \sum_{j=i_A}^{(i-1)} \Delta s_j \{(1 + \delta SF) \cos(\theta_j + \delta\theta_j) - \cos\theta_j\} \quad (35)$$

$$\delta y_i = \delta y_{i_A} + \sum_{j=i_A}^{(i-1)} \Delta s_j \{(1 + \delta SF) \sin(\theta_j + \delta\theta_j) - \sin\theta_j\} \quad (36)$$

Equations (35) and (36) can be linearized.

$$\delta x_i = \delta x_{i_A} + \sum_{j=i_A}^{(i-1)} \Delta s_j \{-\sin\theta_j \delta\theta_j + \cos\theta_j \delta SF\} \quad (37)$$

$$\delta y_i = \delta y_{i_A} + \sum_{j=i_A}^{(i-1)} \Delta s_j \{+\cos\theta_j \delta\theta_j + \sin\theta_j \delta SF\} \quad (38)$$

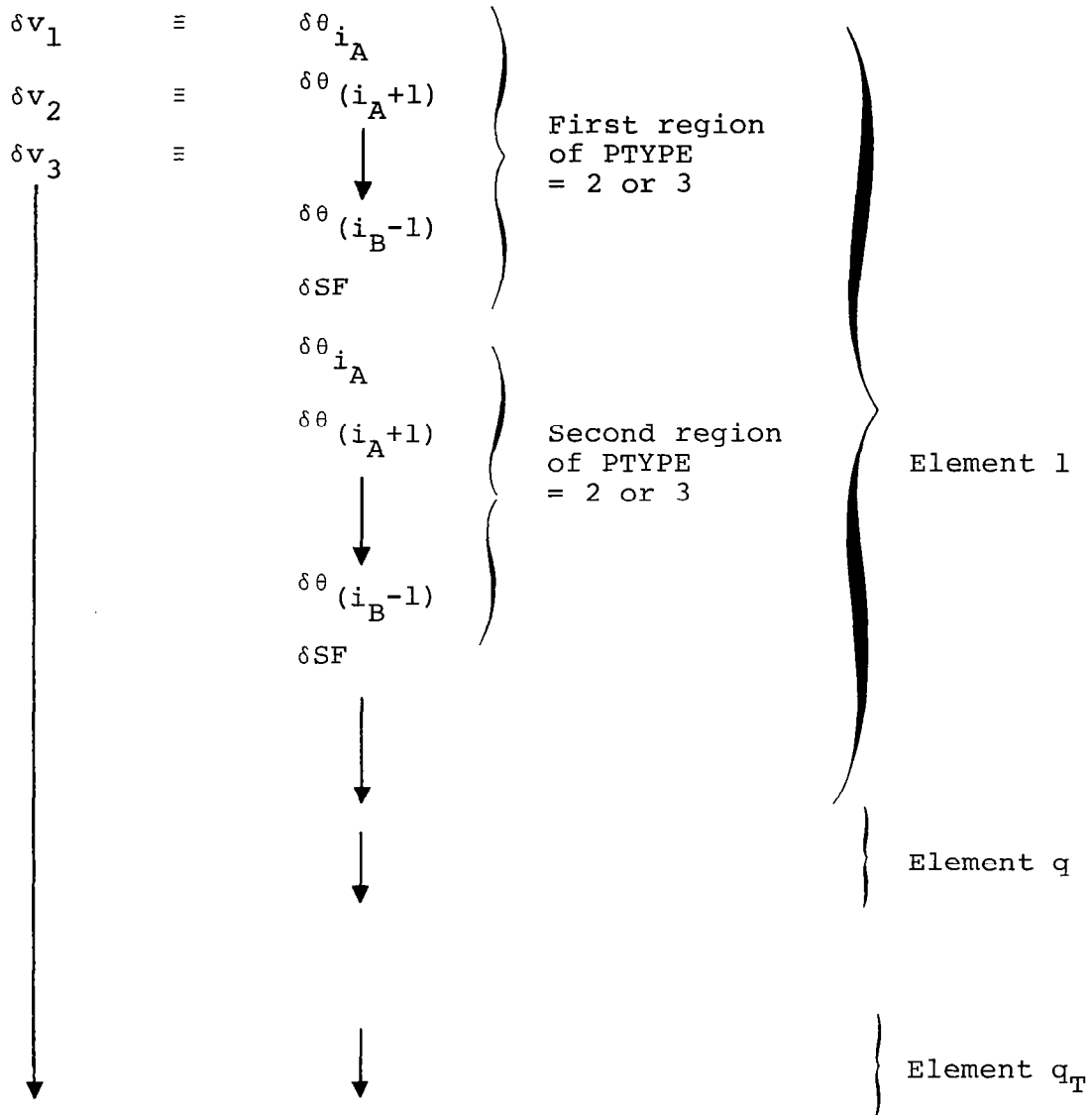
By applying the indexing nomenclature for the group of free regions associated with design region p , the terms δx_{i_A} and δy_{i_A} in equations (37) and (38) can be expressed as functions of the geometry change of preceding regions. Equations (37) and (38) become

$$\delta x_i = \sum_{p_A}^p \sum_{j=i_A}^{i_C} \Delta s_j \{-\sin\theta_j \delta\theta_j + \cos\theta_j \delta SF\} \quad (39)$$

$$\delta y_i = \sum_{p_A}^p \sum_{j=i_A}^{i_C} \Delta s_j \{+\cos\theta_j \delta\theta_j + \sin\theta_j \delta SF\} \quad (40)$$

where $i_C = (i_B - 1)$ if the region under summation is not p and $i_C = (i-1)$ if the region is p . Equations (39) and (40) apply not only for design regions but for analysis regions of PTYPE = 1 as well. Of course, if PTYPE(p) = 1, the values $\delta\theta_j$ and δSF for region p are identically zero and are ignored.

The complete set of geometric unknowns in a design problem is set up as an array δv_j , ordered as follows:



The method for establishing the first-order relationship between velocity and geometry perturbations will now be described. The procedure is to repeat every step described above in the analysis-only solution formulation. This time, however, each quantity is expanded by its differential with respect to the variable δv_k (defined above). The resulting differential analogue of equation (30) is in the form

$$\sum_j \{C_{ij} du_j + u_j \sum_k \left(\frac{\partial C_{ij}}{\partial v_k} dv_k \right)\} = \sum_k \left(\frac{\partial RHS_i}{\partial v_k} dv_k \right) \quad (41)$$

In equation (41), C_{ij} and u_j are obtained from the previous analysis-only solution. The differentiation of C_{ij} and RHS_i is performed in three steps. First, derivatives are established with respect to ξ_P , η_P , and s . Second, differentials $d\xi_P$ and $d\eta_P$ are expressed in terms of $d\theta_i$, dx_i , dy_i , dx_{i+1} , dy_{i+1} , dx_P , and dy_P (where "i" refers to an influencing panel and "P" to a control point). Third, equations (39) and (40) are used to express the differentials in terms of $d\theta_j$ and dSF , i.e., in terms of dv_k .

Differentials of the induced potential functions (19) - (22) are provided in the form

$$d() = \frac{\partial()}{\partial \xi_P} d\xi_P + \frac{\partial()}{\partial \eta_P} d\eta_P + \frac{\partial()}{\partial s} ds \quad (42)$$

$$d\phi_{S1} = \frac{1}{2\pi} \{F_A d\xi_P + F_B d\eta_P + F_C ds\} \quad (43)$$

$$d\phi_{V1} = \frac{1}{2\pi} \{F_B d\xi_P - F_A d\eta_P + [F_D - (\beta + \frac{\pi}{2})] ds\} \quad (44)$$

$$\begin{aligned} d\phi_{S2} = \frac{1}{2\pi} \{ & [-1 + (\frac{\xi_P}{s}) F_A + (\frac{\eta_P}{s}) F_B] d\xi_P \\ & + [(\frac{\xi_P}{s}) F_B - (\frac{\eta_P}{s}) F_A] d\eta_P \\ & + [+ (\frac{\xi_P}{2s}) - \frac{F_A}{2} (F_E + \frac{1}{4}) - (\frac{\xi_P \eta_P}{s^2}) F_B] ds\} \end{aligned} \quad (45)$$

$$\begin{aligned} d\phi_{V2} = \frac{1}{2\pi} \{ & [(\frac{\xi_P}{s}) F_B - (\frac{\eta_P}{s}) F_A] d\xi_P \\ & + [+ 1 - (\frac{\xi_P}{s}) F_A - (\frac{\eta_P}{s}) F_B] d\eta_P \\ & + [- (\frac{\eta_P}{2s}) - \frac{F_B}{2} (F_E + \frac{1}{4}) + (\frac{\xi_P \eta_P}{s^2}) F_A] ds\} \end{aligned} \quad (46)$$

From equations (7) and (8),

$$\begin{aligned} d\xi_P = & +\eta_P d\theta_i + \cos\theta_i [dx_P - \frac{1}{2}(dx_i + dx_{i+1})] \\ & + \sin\theta_i [dy_P - \frac{1}{2}(dy_i + dy_{i+1})] \end{aligned} \quad (47)$$

$$\begin{aligned}
d\eta_P = & - \xi_P d\theta_i + \cos\theta_i [dy_P - \frac{1}{2}(dy_i + dy_{i+1})] \\
& - \sin\theta_i [dx_P - \frac{1}{2}(dx_i + dx_{i+1})] \quad (48)
\end{aligned}$$

Equations (39), (40), (47), and (48) are used to express $d\xi_P$ and $d\eta_P$ in terms of the independent differentials, $d\theta_j$ and dSF .

Following evaluation of the derivatives, equation (41) is expressed in the form

$$\sum_j C_{ij} du_j = \sum_k D_{ik} dv_k \quad (49)$$

The system of linear equations (49) is pre-multiplied by the matrix inverse of C_{ij} , with the following result:

$$\begin{aligned}
du_\ell &= \sum_i \{ [C_{\ell i}]^{-1} \sum_k (D_{ik} dv_k) \} \\
&\equiv \sum_k (G_{\ell k} dv_k) \quad (50)
\end{aligned}$$

where the array $G_{\ell k}$ is defined by equation (50).

The final desired velocity-geometry perturbation relationships are generated by differentiating equations (31) and (32) with respect to θ_i , θ_{Ei} , γ_i , and γ_{i+1} . With the aid of equation (33) and the fact that dSF and $d\theta_j$ are equivalent to dv_k , plus the fact that equation (50) provides the relationship between vortex and geometry differentials, it is possible to express dV_{Ti} and dV_{TEi} in the following form.

$$dV_{T_i} = \sum_j A_{ij} dv_j \quad (51)$$

$$dV_{T_{E_i}} = \sum_j A_{Eij} dv_j \quad (52)$$

The calculated arrays A_{ij} and A_{Eij} are exactly the velocity partial derivatives of the panel method analysis solution. For example, suppose that the analysis problem has been solved by Program MAAD for two geometries, where the difference in geometries is defined by arbitrary finite values in the array δv_j and where the difference in calculated tangential velocity components of panel i is δV_{Ti} . Then the limiting conditions as all values δv_j approach zero will be

$$\lim_{\delta v_j \rightarrow 0} \left[\frac{\delta V_{T_i}}{\sum_j A_{ij} \delta v_j} \right] = 1 \quad (53)$$

In a design problem, values $V_{T_{i_p}}$ and $V_{T_{E_{i_p}}}$ are prescribed for each region of $PTYPE = 2$ or 3 . The solution approach is to use equations (51) and (52) to find the corresponding geometry perturbation. It may appear that one could simply insert desired values δV_{T_i} into the left-hand-side of equation (51) and then solve for δv_j . However, A_{ij} is usually an ill-conditioned matrix. Furthermore, there is no guarantee that geometric continuity requirements would be met. For those reasons, it is more appropriate to minimize the function E .

$$\begin{aligned} E \equiv & \sum_q \sum_p \left\{ \sum_{i=i_A}^{(i_B-1)} \left(\frac{\Delta s_i}{S_T} \right) [V_{T_{i_p}} - V_{T_i} - \sum_j A_{ij} \delta v_j]^2 \right. \\ & + \sum_{i=i_A}^{i_B} \left(\frac{\Delta s_i + \Delta s_{i-1}}{2S_T} \right) [V_{T_{E_{i_p}}} - V_{T_{E_i}} - \sum_j A_{E_{ij}} \delta v_j]^2 \\ & + \left[\left(\frac{W^2}{S_T} \right) \sum_{i=i_A}^{(i_B-1)} \Delta s_i \right] \delta SF^2 \} \\ & + \sum_q \sum_{IGP} \lambda_{x,IGP} \left\{ \sum_{p=p_A}^{p_B} \sum_{k=i_A}^{(i_B-1)} \Delta s_k (-\sin\theta_k \delta\theta_k + \cos\theta_k \delta SF) \right\} \\ & + \sum_q \sum_{IGP} \lambda_{y,IGP} \left\{ \sum_{p=p_A}^{p_B} \sum_{k=i_A}^{(i_B-1)} \Delta s_k (+\cos\theta_k \delta\theta_k + \sin\theta_k \delta SF) \right\} \end{aligned} \quad (54)$$

Equation (54) requires explanation. The equation expresses the mean-square difference between calculated and prescribed tangential velocity distributions, with Lagrangian constraints for satisfaction of continuity requirements. Only regions of $PTYPE = 2$ or 3 are to be included in the summation. S_T is defined as the perimeter of element q . In the term

$$\left(\frac{\Delta s_i + \Delta s_{i-1}}{2S_T} \right),$$

Δs_i and Δs_{i-1} are to be neglected if $i = i_B$ and i_A , respectively. At sharp corners, VTE_{ip} is ignored. A weighting factor W^2 is selected for each design region by the user to control the stretching. A very small value such as 10^{-5} has no significant effect. However, a large value such as 10^{+5} will suppress the length change. An additional option available to the user is the stipulation that two or more successive design regions in a group of free regions share a common value for δSF . This is achieved by consolidating the coefficients of δSF for the appropriate regions and then removing the extra unknown(s) from the array δv_j .

The unknowns in equation (54) are δv_j (which is equivalent to $\delta \theta_k$ and δSF in accordance with the definition of δv_j) and the Lagrangian multipliers $\lambda_{x,IGP}$ and $\lambda_{y,IGP}$. The unknowns are determined by setting equal to zero the derivative of E with respect to each unknown and then solving the resulting system of linear equations by a standard matrix method.

After the array δv_j is calculated, the geometry is corrected one group of free regions at a time. Starting with panel i_A of region p_A , the panel is stretched and rotated the required amount. This provides new coordinates for point i_{A+1} . The procedure is repeated for panel i_{A+1} , etc., until all panels in the group of free regions are included. Then the new coordinates of point i_B of region p_B are examined to verify that continuity requirements are satisfied. Even though the Lagrangian constraints of equation (54) provide satisfaction of continuity requirements, the constraints are only first-order accurate with respect to δv_j . Define the discontinuity vector (DXB, DYB) as

$$DXB \equiv [x_{i_B(p_B)}]_{NEW} - [x_{i_B(p_B)}]_{REQUIRED} \quad (55)$$

$$DYB \equiv [y_{i_B(p_B)}]_{NEW} - [y_{i_B(p_B)}]_{REQUIRED} \quad (56)$$

If the magnitude of $\sqrt{DXB^2 + DYB^2}$ is greater than some very small tolerance, it is necessary to make a closure correction to the geometry. What is desired is a new set of values $\delta \theta_i$ and δSF for each design region that will bring $\sqrt{DXB^2 + DYB^2}$ to within the prescribed tolerance. It is important for the closure correction to change the geometry as little as possible. This is accomplished by minimizing a new error function E .

$$\begin{aligned}
E \equiv & \sum_{p=p_A}^{p_B} \left\{ \left[\sum_{i=i_A}^{(i_B-1)} \Delta s_i (\delta \theta_i)^2 \right] + (W^2+1) (DST_p) (\delta SF)^2 \right\} \\
& + \lambda_x \left\{ DXB + \sum_{p=p_A}^{p_B} \left[(DX_p) \delta SF - \sum_{i=i_A}^{(i_B-1)} \Delta s_i \sin \theta_i \delta \theta_i \right] \right\} \\
& + \lambda_y \left\{ DYB + \sum_{p=p_A}^{p_B} \left[(DY_p) \delta SF + \sum_{i=i_A}^{(i_B-1)} \Delta s_i \cos \theta_i \delta \theta_i \right] \right\} \quad (57)
\end{aligned}$$

where

$$DST_p \equiv \sum_{i=i_A(p)}^{(i_B(p)-1)} \Delta s_i \quad (58)$$

$$DX_p \equiv \sum_{i=i_A(p)}^{(i_B(p)-1)} \Delta s_i \cos \theta_i \quad (59)$$

$$DY_p \equiv \sum_{i=i_A(p)}^{(i_B(p)-1)} \Delta s_i \sin \theta_i \quad (60)$$

In equation (57), only regions of PTYPE = 2 or 3 are to be included in the summation over p. The unknowns are $\delta \theta_i$, δSF , λ_x , and λ_y , where λ_x and λ_y are Lagrangian multipliers. The first-order Lagrangian constraints correspond to the elimination of the discontinuity vector (DXB, DYB). The weighting factor W^2 and the option in which successive design regions share a common length variation δSF apply to equation (57) in the same manner described for equation (54).

E is to be minimized with respect to the unknowns.

$$0 = \frac{\partial E}{\partial (\delta \theta_j)} = (2 \Delta s_j) \delta \theta_j - (\Delta s_j \sin \theta_j) \lambda_x + (\Delta s_j \cos \theta_j) \lambda_y \quad (61)$$

$$0 = \frac{\partial E}{\partial (\delta SF)} = [2 \cdot DST_p \cdot (W^2 + 1)] \delta SF + DX_p \cdot \lambda_x + DY_p \cdot \lambda_y \quad (62)$$

A mathematical artifice which will result in reduced computing effort is to multiply equations (61) and (62) by appropriate factors and then sum the products.

$$0 = \sum_{p=p_A}^{p_B} \left\{ \left[\sum_{j=i_A}^{(i_B-1)} - \sin\theta_j \frac{\partial E}{\partial (\delta\theta_j)} \right] + \frac{DX_p}{DST_p (W^2 + 1)} \frac{\partial E}{\partial (\delta SF)} \right\} \quad (63)$$

$$0 = \sum_{p=p_A}^{p_B} \left\{ \left[\sum_{j=i_A}^{(i_B-1)} + \cos\theta_j \frac{\partial E}{\partial (\delta\theta_j)} \right] + \frac{DY_p}{DST_p (W^2 + 1)} \frac{\partial E}{\partial (\delta SF)} \right\} \quad (64)$$

By substituting the right-hand-sides of equations (61) and (62) into equations (63) and (64), and then by applying the fact that the Lagrangian constraint functions of equation (57) are equal to zero, equations (63) and (64) become

$$2 \cdot DXB = + \lambda_x \sum_{p=p_A}^{p_B} \left[\frac{(DX_p)^2}{DST_p (W^2 + 1)} + \sum_{j=i_A}^{(i_B-1)} \Delta s_j \sin^2\theta_j \right] \\ + \lambda_y \sum_{p=p_A}^{p_B} \left[\frac{(DX_p)(DY_p)}{DST_p (W^2 + 1)} - \sum_{j=i_A}^{(i_B-1)} \Delta s_j \sin\theta_j \cos\theta_j \right] \quad (65)$$

$$2 \cdot DYB = + \lambda_x \sum_{p=p_A}^{p_B} \left[\frac{(DX_p)(DY_p)}{DST_p (W^2 + 1)} - \sum_{j=i_A}^{(i_B-1)} \Delta s_j \sin\theta_j \cos\theta_j \right] \\ + \lambda_y \sum_{p=p_A}^{p_B} \left[\frac{(DY_p)^2}{DST_p (W^2 + 1)} + \sum_{j=i_A}^{(i_B-1)} \Delta s_j \cos^2\theta_j \right] \quad (66)$$

Equations (65) and (66) provide a 2 x 2 system of linear equations which are solved for λ_x and λ_y . Then equations (61) and (62) provide values immediately for each of the other unknowns, $\delta\theta_j$ and δSF .

Using the set of values for $\delta\theta_j$ and δSF , the geometry is corrected and a new discontinuity vector (DXB,DYB) is generated. The closure correction procedure is repeated as many times as necessary to bring $\sqrt{DXB^2 + DYB^2}$ to within the prescribed tolerance. Usually, one or two times are sufficient.

It is noteworthy that the closure correction procedure is also applied to the starting geometry in design problems before any aerodynamic calculations are performed. This significantly simplifies user input requirements. As illustrated in figure 1, large discontinuities are permitted. Program MAAD will automatically generate the desired closure without changing the relative panel length distribution in each design region.

Following the closure correction in a design problem iteration cycle, a test is performed to determine whether any two panels intersect improperly. The only acceptable intersections are, of course, between panels i and $i-1$ at point i . Improper intersections destroy the separation between the real and imaginary flow fields, thereby violating the theoretical requirements. There can be situations in which the user will have to redefine either the starting geometry, prescribed tangential velocity distribution, or gap between airfoil elements. However, Program MAAD has an option for increasing the thickness of an airfoil element if the upper and lower surfaces overlap. This option is usually sufficient to eliminate improper panel intersections.

At this stage, the inverse step of a design problem iteration cycle is complete. All data necessary for the analysis step of the next iteration cycle has been calculated.

Prediction Accuracy of Analysis Solutions

In references 1 and 2, predictions by the analysis method of Program MAAD (using constant source panels) were compared with predictions by both a low order and a higher order method that impose flow tangency boundary conditions directly. It was concluded that the MAAD method is competitive with the higher order formulation for a wide variety of geometries. Rather than repeat the detailed analysis examples, a brief discussion on the relative prediction accuracies of the three methods is presented here.

Figures of merit for prediction accuracy are the calculated drag and the difference between lift calculated by pressure integration and circulation for solid, closed airfoils. Analytically, both the drag and lift difference are zero. For single element airfoils modelled by from thirty to forty panels, the drag coefficient is typically on the order of 0.0005 for both the MAAD method and higher order method, versus 0.0025 for the low order flow tangency method. Similarly, the lift difference is typically 0.001 for the MAAD and higher order methods, versus 0.005 for the low order flow tangency method.

For a circular cylinder represented by twenty equal length panels, the surface distribution of relative error in calculated midpoint velocities is essentially uniform for each of the three methods. Specifically, the error is 2.06% for the low order flow tangency method, 0.22% for the MAAD method, and 0.05% for the higher order method.

It is noteworthy that there is seldom any appreciable difference in prediction accuracy between the use of constant and linear source panels in Program MAAD. Furthermore, the extrapolated bisector Kutta condition (using the recommended value $\kappa_2 = 0.02$) will generate a lift coefficient that is typically within a tolerance $\Delta C_l < 0.01$ of the mathematically exact value, whether the panels in the MAAD method have constant or linear source distributions. This 0.01 tolerance is based on the use of from 30 to 40 panels to model a single element airfoil.

The reason behind the good prediction accuracy of the MAAD method centers on the use of internal potential boundary conditions. A flat panel source-vortex model characteristically underpredicts tangential velocity at panel centers, but overpredicts near endpoints. On the other hand, the average velocity between adjacent panel centers, which is the difference in potential, is significantly more accurate.

Although it is true that the MAAD method exhibits higher order prediction accuracy in most practical problems, there are exceptions. For example, the predicted tangential velocities induced by positive blowing on both the upper and lower surfaces of a thin, cambered airfoil will exhibit low order accuracy. However, it is believed that such limitations are outweighed by the simplicity of the basic formulation, especially when applied to the more complex problem of design.

Example Design Solutions

Five design solutions are presented to demonstrate the flexibility of Program MAAD. It is noted that in the example solutions, constant source panels were used in the program. The linear source feature described in the preceding formulation sections was added after the figures were prepared. However, some of the examples have since been repeated using linear sources, and there are no significant differences in the results.

A typical design solution requires five iteration cycles, where each cycle requires 100%-300% more computing time than an analysis-only solution. On the CDC CYBER 175, a two-element airfoil represented by a total of 70 panels requires 20 seconds computing time per iteration cycle for a design-only solution. The program can handle as many as five airfoil elements simultaneously.

The selection of examples is intended to demonstrate design solution characteristics for a variety of applications. Included are two design-only solutions for two-element airfoils. The design of a cavitation body illustrates the value of the variable panel length feature. The ability to modify airfoils to offset the effects of wind tunnel interference is demonstrated for a Liebeck high-lift geometry. A simple separated flow model is presented in which the pressure gradient in the recompression region is calculated by the program.

The first example was solved previously by the analysis-only/design-only method of references 1 and 2. The identical solution by Program MAAD is presented here to demonstrate prediction accuracy and convergence properties. In figure 10, the analysis-only solution for a two-element airfoil is compared to an exact analytical conformal mapping solution by Williams (reference 8). Notice that the lift predicted using the extrapolated bisector Kutta condition ($\kappa_2 = 0.02$) is quite accurate. Not shown in figure 10 is a comparison made at the exact $C_L = 2.03$ between calculations by Program MAAD and the higher order analysis method of reference 5. Over the complete two-element airfoil boundary modelled by 66 panels, the average magnitude of the difference in calculated pressure coefficients is less than 0.005, demonstrating the good agreement between Program MAAD and the higher order formulation. A design-only problem was established by unwrapping both airfoil elements to provide the open rectangle starting geometry of figure 11. The velocity distribution calculated by Program MAAD for the analysis solution of figure 10 was prescribed on the starting geometry. A very large length weighting factor was selected for each region to prevent any change in panel lengths. The converged geometry generated by Program MAAD in five iteration cycles is virtually identical to the target geometry of figure 10. Specifically, the coordinates at all 66 panel endpoints differ by less than one thousandth of one percent of the main element chord.

In the second example, the problem is to design a symmetric solid airfoil with a flat plate nose and tail such that at zero incidence the upper and lower surfaces have a constant velocity $V = 1.50 V_\infty$ ($C_p = -1.25$). A square was selected as the starting geometry (figure 12). The flat plate nose and tail are analysis regions, selected as PTYPE = 0 and 1, respectively. The upper and lower surface design regions are both PTYPE = 3. A very small weighting factor ($W = 10^{-5}$) was selected for both of the design regions in order to allow unrestricted stretching. The design solution converged to within plotting tolerances in five iteration cycles, and the calculated velocities agree well with the prescribed distribution. The ability of Program MAAD to calculate both shape and surface distance was essential to the design of this cavitation geometry, for which the chord was unknown.

In the third example, the geometry of a Liebeck airfoil was modified to offset non-uniform flow angularity induced by simulated wind tunnel walls. The modification was conducted for a

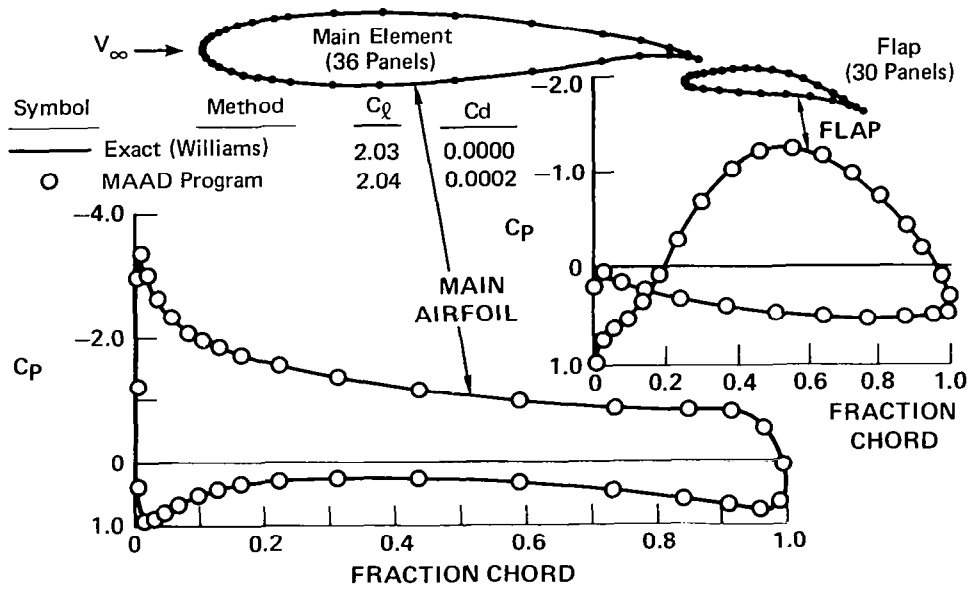


Figure 10. Two-Element Airfoil Analysis Solution

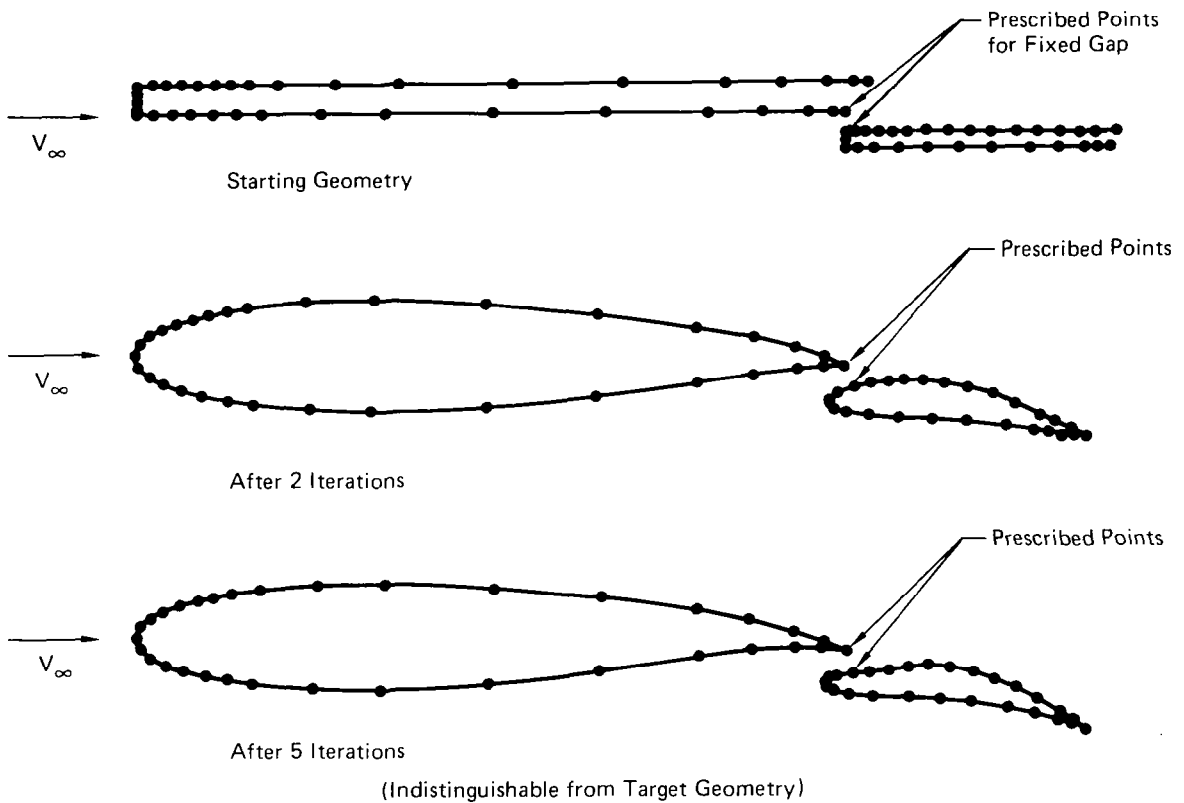


Figure 11. Two-Element Airfoil Design Solution

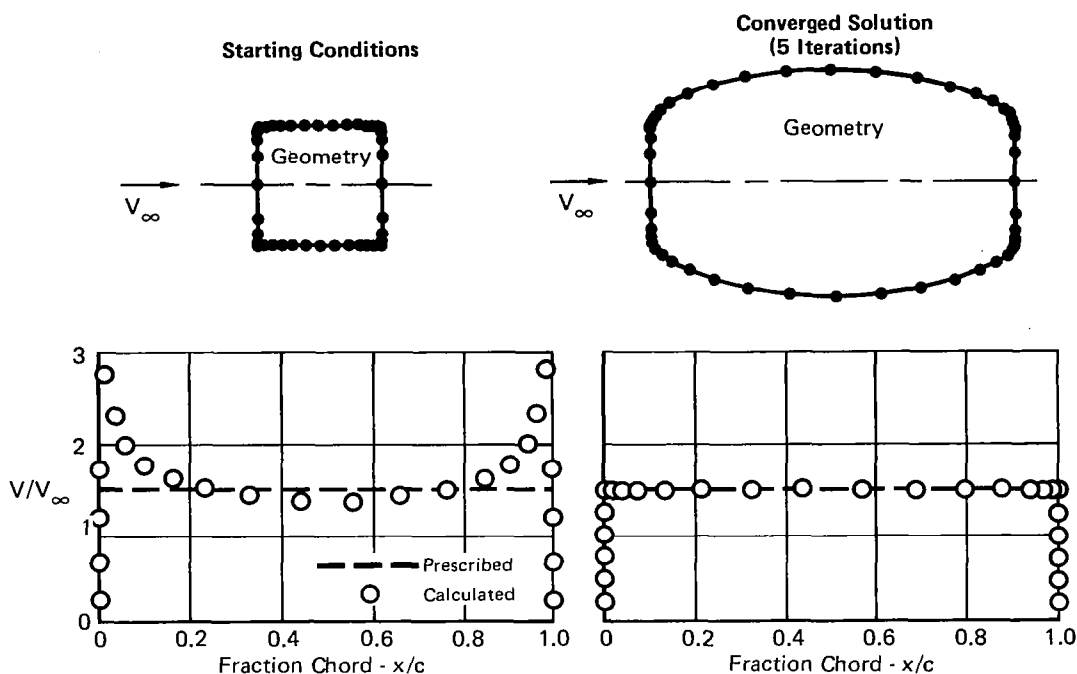


Figure 12. Design of a Constant Pressure Geometry

test section height-to-airfoil chord ratio of two. Although much larger ratios are standard in practice, here the objective is to evaluate the design method for very strong interference. The airfoil was positioned approximately midway between the walls and pivoted at the upper surface quarter chord point. Blockage effects were accounted for by applying an average channel velocity equal to $0.9822 V_{ref}$, where V_{ref} is the reference velocity for C_D and C_L . The three pressure distributions presented in figure 13 were calculated by Program MAAD at the common lift coefficient $1.80 C_{L}$, corresponding to the Liebeck airfoil in unbounded flow at 11.2° incidence (reference 9). In spite of correcting the channel velocity for blockage and correcting the chord incidence for the average induced flow angularity, the pressure distribution of the unmodified Liebeck airfoil in the wind tunnel reveals significant wall effects. The design solution was generated by prescribing the unbounded flow pressure distribution and then solving for the geometry (including chord incidence) in the presence of tunnel walls with channel velocity $0.9822 V_{ref}$. To within plotting tolerances, the design solution completely offsets the effect of tunnel walls on the calculated pressure distribution.

In obtaining the design solution of figure 13, the airfoil element was divided into four design regions. Region $p=1$ spanned most of the lower surface, region $p=2$ encompassed seven panels surrounding the stagnation point, region $p=3$ terminated at the upper surface quarter chord pivot point, and region $p=4$ covered the

remainder of the upper surface. The length weighting factors selected for the four regions were, respectively, $W = 10^{-5}$, 10^{-5} , 10^{+5} , 10^{+5} . The low weighting on the first two regions allowed the arc length location of the stagnation point and the velocity gradient near the stagnation point freedom to adjust. This approach can be extremely effective in converting what would otherwise be a nonexistent prescribed velocity distribution into approximately the closest possible existing distribution, without disturbing the prescribed velocities.

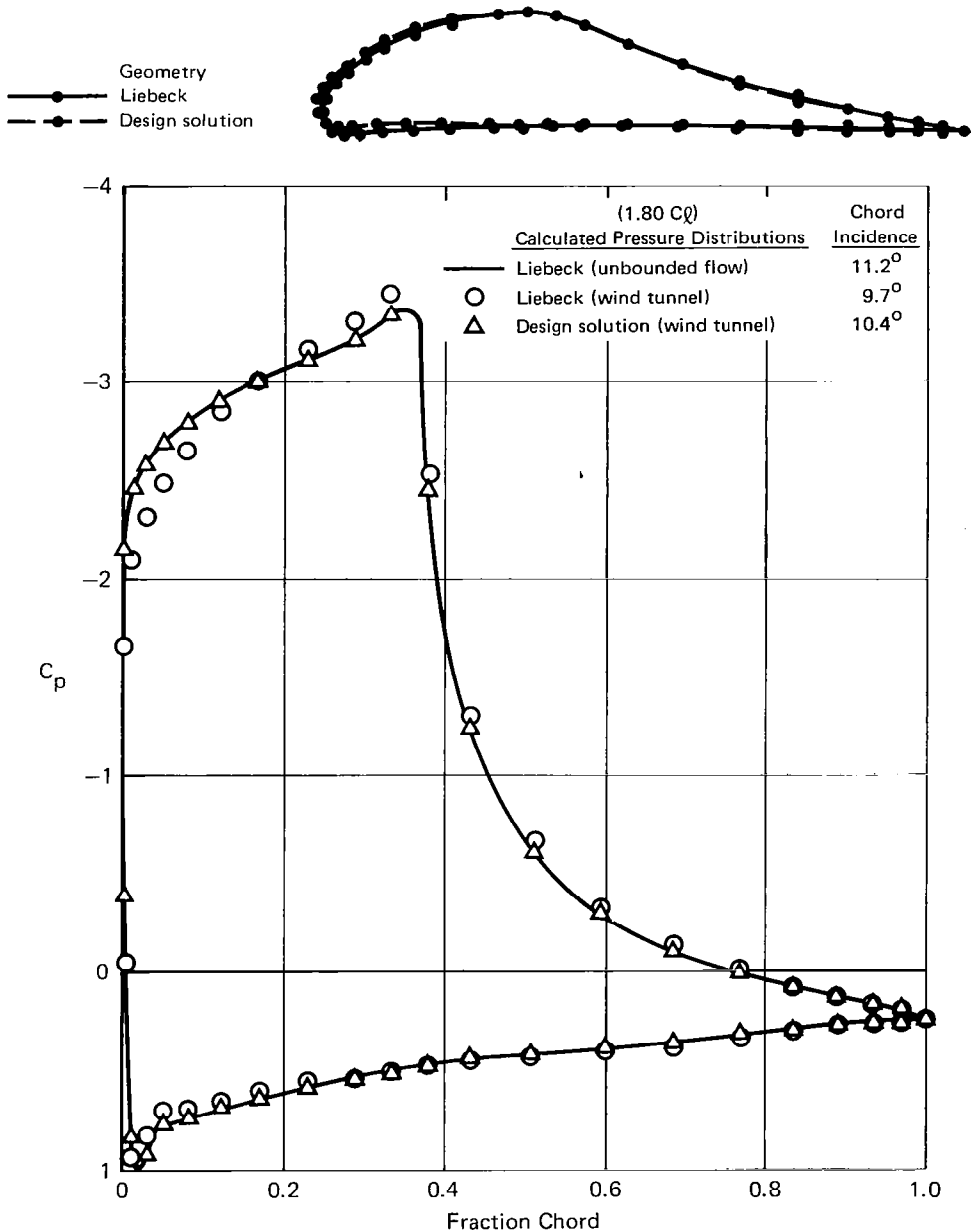


Figure 13. Design to Eliminate Wind Tunnel Wall Effects

The two element airfoil of figure 14 was designed by Program MAAD on an interactive graphics system by applying the high lift rules of Liebeck and Smith (references 9-11). Both the adaptation of Program MAAD for interactive graphics and the two-element design were conducted as part of the 1978 MCAIR Independent Research and Development Program. The design pressure distribution was established for a Reynolds number of approximately 5 million, $C_L = 4.7$, and $\alpha = 25^\circ$. The reference length is the extended chord C of figure 14. Both elements are designed for the steepest possible upper surface pressure gradient without inducing turbulent separation (reference 12). This allows for a very low pressure upper surface roof-top acceleration region. The presence of the short chord rear element raises the trailing edge (dumping) velocity of the main element. This allows for the magnification of the upper surface pressure distribution of the main element beyond that of the rear element without increasing the likelihood of separation. The lower surface of each element was designed to be as close to the maximum stagnation pressure as possible while maintaining reasonable thickness for structural purposes.

Prescribed	Increased C_L		Reduced C_D
	Upper	Lower	
(1) Stratford Pressure Rise	X		X
(2) Maximum Dumping Velocity	X		
(3) Roof Top Acceleration			X
(4) Nearly Stagnant Lower Surface		X	X

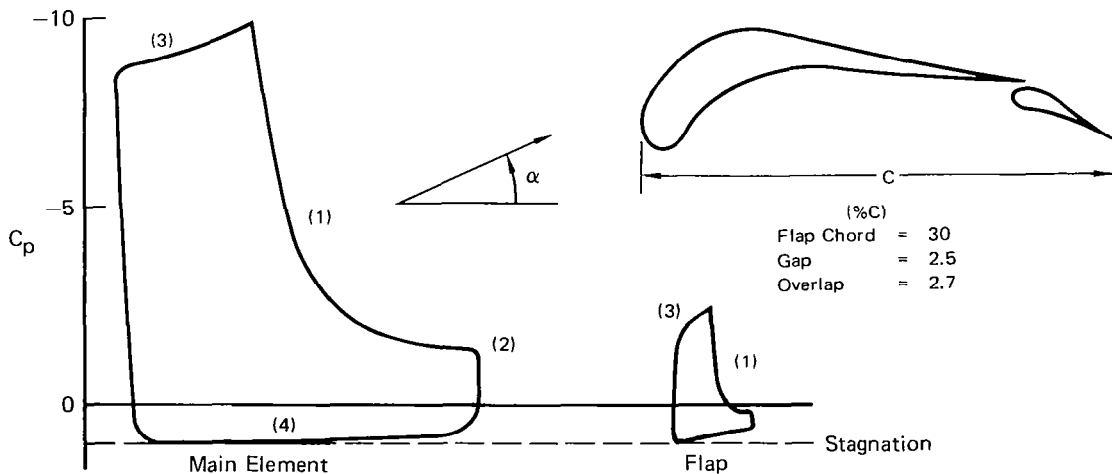


Figure 14. Automated High Lift Design Solution
 $4.7 C_L$ at $25^\circ \alpha$

A simple model for predicting the pressure distribution on an airfoil with trailing edge separation is presented in figure 15. The model is based on semi-empirical rules for the behavior of pressure distributions in separated flow. By using the mixed analysis-design mode of Program MAAD, the corresponding geometry of the wake can be generated. The combined airfoil-wake geometry is represented as a closed streamline. The wake consists of a constant pressure upper surface region ($p=3$) followed by upper and lower recovery regions ($p=4$ and 1). All the regions are $PTYPE = 3$, except for the solid airfoil region $p = 2$, which is $PTYPE = 0$. A very large length weighting factor ($W = 10^{+5}$) is selected for region $p = 3$. Therefore, the upper recovery region $p = 4$ will begin approximately directly above the trailing edge of the actual solid airfoil. The prescribed velocity recovery in both regions $p = 1$ and 4 varies linearly from the separation velocity level V_W to a nominal value slightly less than free stream. This will generate zero wake loading. A very small length weighting factor ($W = 10^{-5}$) is selected for regions $p = 1$ and 4. Consequently, the wake length is free to change. The program will indirectly generate the recovery pressure gradient by determining the coordinates of the wake trailing edge that are consistent with the entire model. This is in contrast to the wake model established by Henderson (reference 13), in which the recovery pressure gradient is essentially fixed a priori.

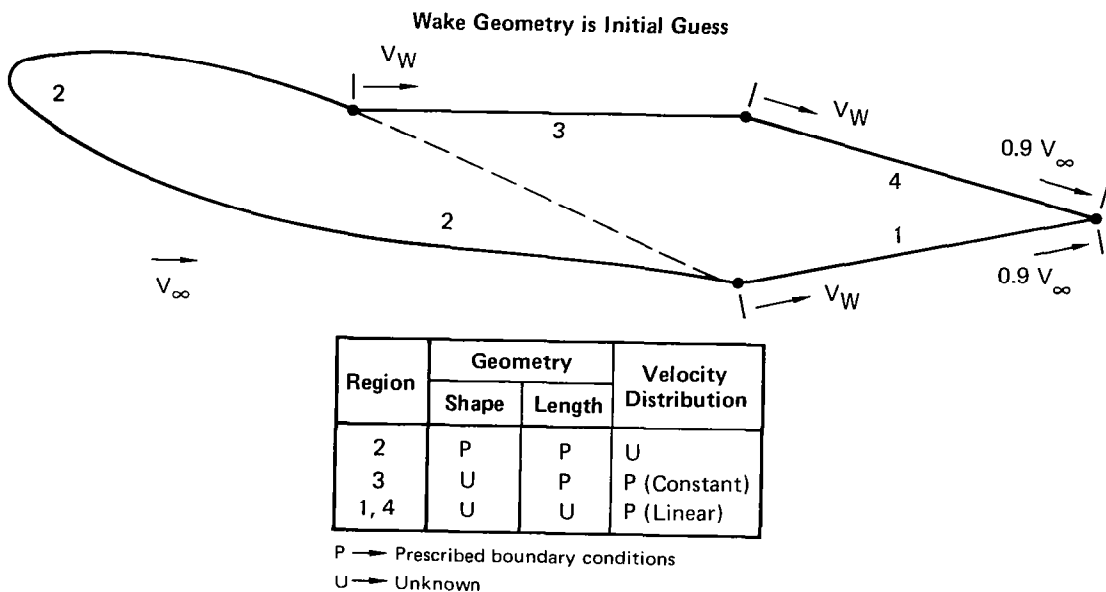


Figure 15. Wake Model for External Inviscid Flow Field

The application of the wake model of figure 15 to a NACA 633-018 airfoil at 15.6° incidence is illustrated in figure 16. The wind tunnel data of reference 14 was used to establish both the separation point location and wake velocity V_W for the wake model. The agreement between calculated and experimental pressures is good, indicating that the present model is reasonable. It is noted that the effects of the boundary layer displacement and the wake mass flux deficit were neglected. It is anticipated that by coupling the equations of integral viscous flow theory with the existing inviscid velocity-geometry perturbation functions of Program MAAD, it will be possible to accurately solve for strong viscous-inviscid interactions without resorting to empirical rules.

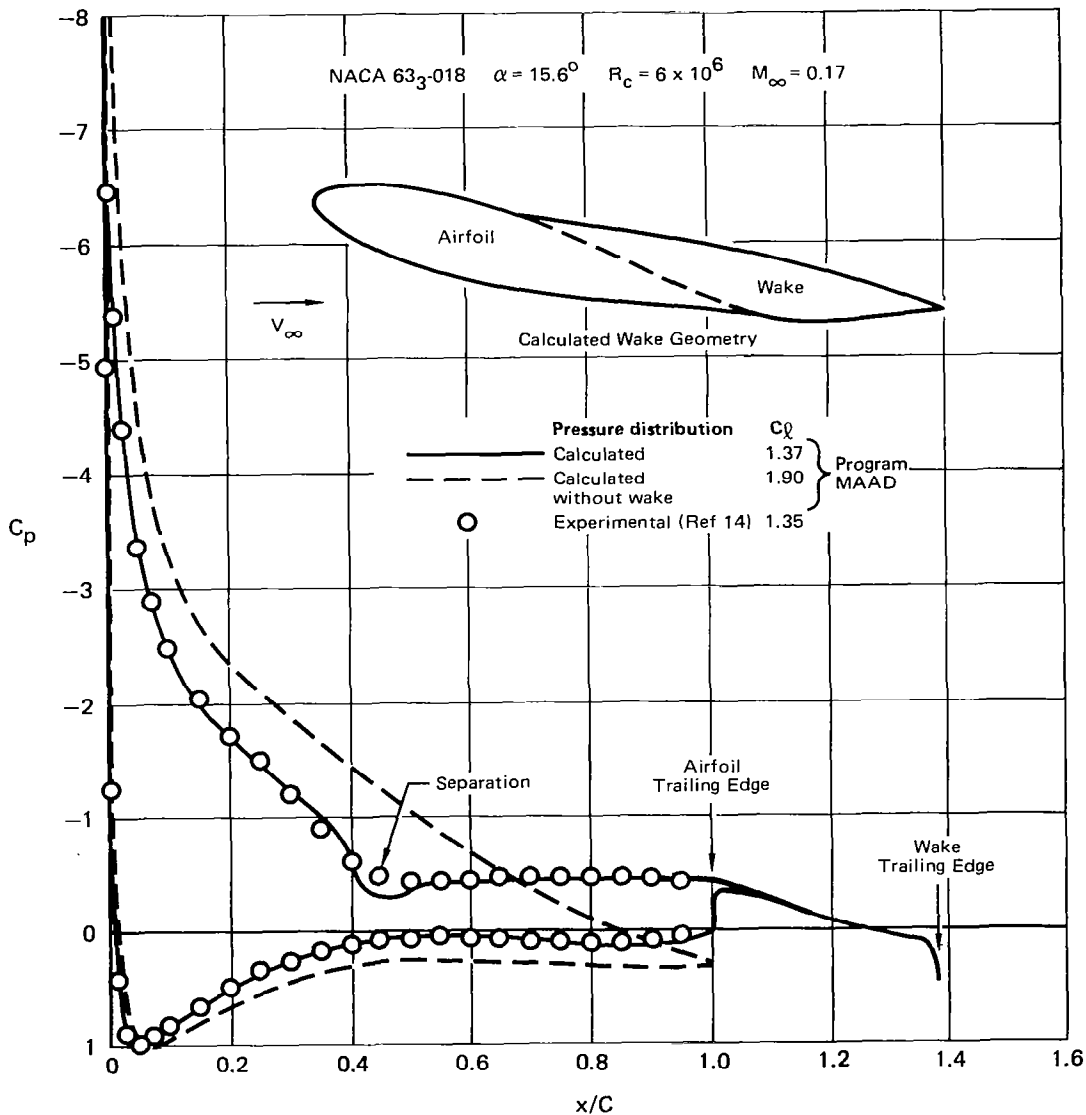


Figure 16. Airfoil-Wake Solution

Recommendations and User Guidelines

Program MAAD is an accurate and reliable method for handling a wide variety of two-dimensional, incompressible, potential flow problems. Basic user guidelines and recommendations for further program development are briefly described here.

Design solution convergence is usually very good, provided that the prescribed velocity distribution is reasonably close to an existing distribution. For every geometry there is an existing pressure distribution; however, the converse is not true. Fortunately, in the iteration process, the program will generate a velocity distribution in the analysis step that will guide the user toward necessary modifications in the prescribed distribution. This guidance is especially helpful if interactive graphics are used.

In design-only problems, the user is often faced with the dilemma of where to prescribe the stagnation point and how steep to make the local velocity gradient. There are two approaches. First, let the program run through two or three iteration cycles. If the stagnation location and local gradient are inconsistent with the remainder of the prescribed distribution, the designed leading edge region will appear saw-toothed. The user can then smooth the leading edge and run an analysis solution to determine an existing distribution to prescribe in the vicinity of the stagnation point. The second and simpler approach is to divide the element into three or more regions, one spanning the lower surface with low length weighting, one in the vicinity of the stagnation point with low weighting, and one covering the upper surface with high weighting. As described in the third solution example, this second approach will automatically generate the proper adjustment to the stagnation region.

In the modelling of bounded flow problems such as wind tunnel simulation, there are two rules. First, the net velocity flux through all boundaries must be zero, which is a direct consequence of the continuity equation. Second, it is desirable to define values for V_∞ and α that approximately correspond to the average anticipated fluid velocity. Theoretically, any values are acceptable because there is no physical free stream in a completely bounded flow. However, prediction accuracy and design solution convergence are usually enhanced if reasonable values are selected.

It is recommended that Program MAAD be operated on a computer system providing twelve or more significant figures. This is important only for exceptionally thin airfoils. It can be shown mathematically that the calculated loading is a function of the difference in potential between adjacent upper and lower control points. If the control points are sufficiently close, then the difference in potential can be several significant figures less accurate than the potential. For this reason, the possible future introduction to the program of intermediate and far field influence coefficient expansions should be approached with caution.

Although there are many conceivable improvements that could be made to Program MAAD with respect to both extended capability and computing efficiency, two are most worthy of mention. The first is to extend the method to handle multi-energy flows such as jets. An obvious approach would be to solve for the combined source-vortex distribution and geometry that simultaneously satisfy internal and external boundary conditions for the two (or more) flows of different potential. Another approach that would not increase computing effort significantly but would retain the benefits of Green's third identity would be to handle a real and an imaginary internal flow in concert with a real and an imaginary external flow. The second conceivable improvement to Program MAAD is to implement an accurate method for handling airfoils with finite thickness trailing edges, which is the subject of the next section.

KUTTA CONDITION FOR FINITE TRAILING EDGE THICKNESS

For airfoils with sharp trailing edges, the previously described extrapolated bisector Kutta condition of the Multi-Element Airfoil Inviscid Analysis and Design Program (MAAD) typically provides calculated lift coefficients that differ by less than 0.01 from the exact analytic value. Even this small error will vanish as the number of panels is increased indefinitely. However, many advanced airfoils have trailing edge thicknesses of 1/4 to 3/4 percent chord, and for these airfoils Program MAAD characteristically overpredicts the lift by ten to twenty percent. Furthermore, the error does not diminish with increased panel density. The overprediction results from the common practice of not panelling the base. Consequently, the local flow is not properly modelled and the correct circulation is not generated. A method for modelling the base has been established which typically improves the lift predictions by a factor of ten.

The objective of the method is to use base panelling to generate smooth flow off both the upper and lower surface trailing edges. The extrapolated bisector Kutta condition is replaced by the base panel control equations defined in figure 17. The upper and lower surface velocities immediately upstream of the trailing edge are V_U and V_L , respectively. The velocities will be tangent to the surface unless nonzero normal velocity boundary conditions are prescribed. The velocity component in the direction of the trailing edge bisector (V_B) is to vary linearly from V_{BU} at the upper surface to V_{BL} at the lower surface. Here the trailing edge bisector is defined as the line intersecting the mid-point of the base at an angle equal to the average of the upper and lower surface trailing edge angles.

The number of panels used to model the base is not especially significant. One or two is usually adequate. It is recommended that the values for V_U , V_L , V_{BU} , and V_{BL} be calculated by linearly extrapolating the mid-point velocities of neighboring panels to the upper and lower surface trailing edges.

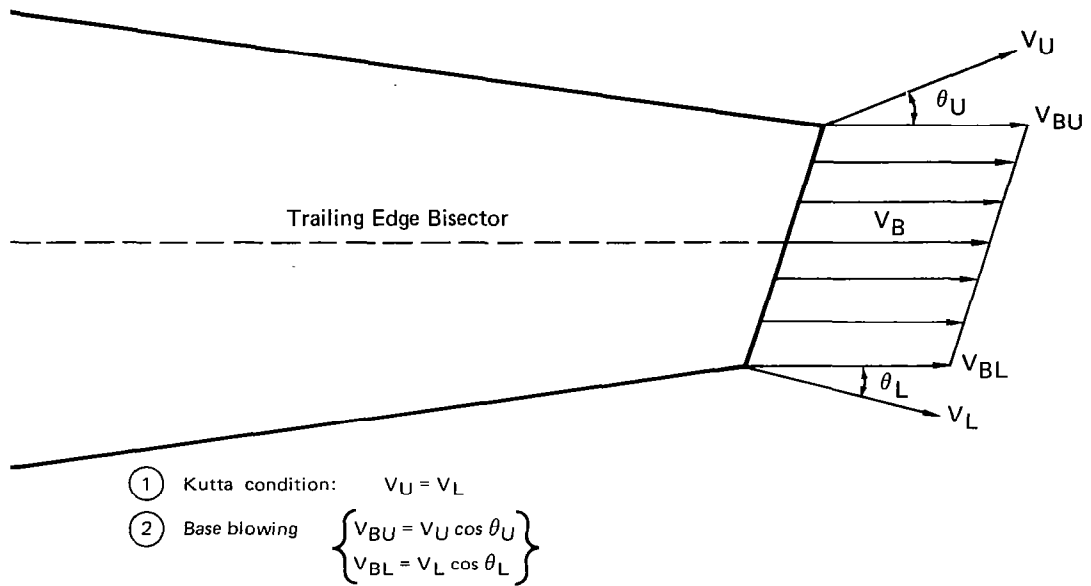


Figure 17. Base Panel Control Equations

The base panel control equations have not been coded explicitly for Program MAAD. Therefore, it is presently necessary to satisfy them manually by the proper combination of linearly independent velocity distributions for a unit free stream, unit circulation, unit constant base blowing, and unit linear base blowing. The proper combination is uniquely determined by the base panel equations of figure 17. This approach was used in the examples presented below.

The examples compare the inviscid solution predictions of four methods applied to airfoils with finite thickness trailing edges. The methods are (1) Catherall-Sells (reference 15), (2) Oellers (reference 16), (3) Program MAAD with the extrapolated bisector Kutta Condition and no base panels, and (4) Program MAAD with the present base panel modelling. The Catherall-Sells conformal mapping method is virtually exact for sharp trailing edge airfoils and provides reasonably smooth flow at the corners of a blunt base. Therefore, Catherall-Sells is considered to be a standard of comparison. The Oellers vortex-only panel method does not provide smooth flow at a blunt base, but the Oeller equal pressure upper surface-lower surface Kutta condition generates reasonably accurate lift predictions. The geometries examined were the three simple symmetric airfoils of figure 18 and the Whitcomb advanced airfoil of figure 19. Identical input coordinate definition was used for each of the four prediction methods. The base was left unpanelled except for the Program MAAD calculations using the present base model-

ling. In every example, piecewise constant source distributions were used in Program MAAD. In each of the four methods, the lift coefficient is referenced by the (maximum) airfoil chord and was calculated by integrating the pressure force acting normal to \vec{V}_∞ .

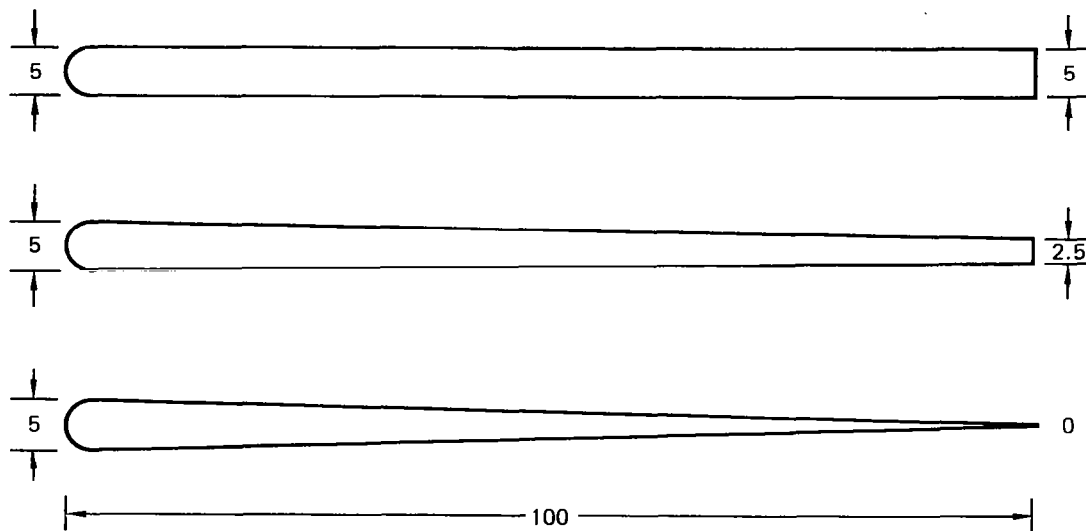


Figure 18. Symmetric Airfoils Selected for Blunt Base Analysis

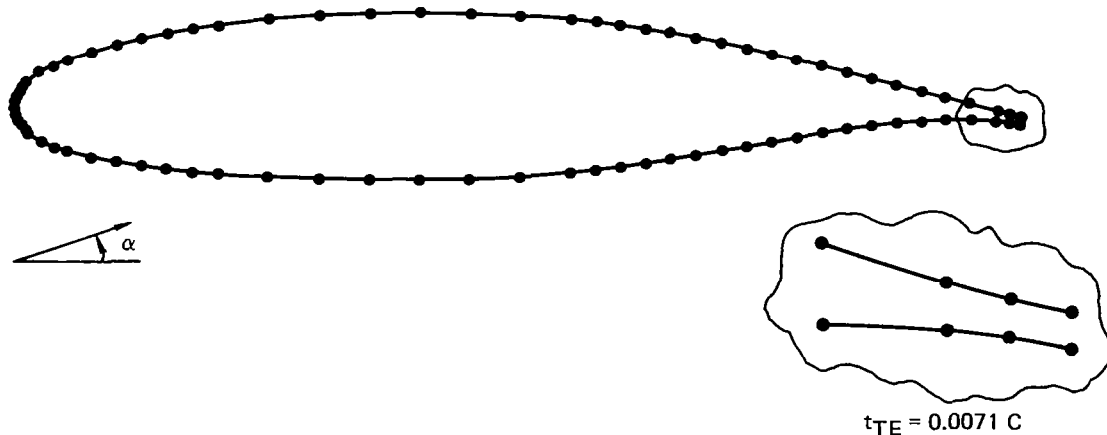


Figure 19. GAW-1 Airfoil

For each of the three symmetric airfoils of figure 18, 120 panels were used to represent the geometry forward of the trailing edge. The panelling is sufficiently dense that the difference in the predictions of the four methods should be dominated by the base modelling and not by numerical discretization. Depending upon the trailing edge thickness, the base was represented by either 10, 5, or 0 panels. Solid body boundary conditions were prescribed ahead of the base.

Plotted as a function of base (trailing edge) thickness in figure 20, the predicted lifts for all four methods attain a common value as trailing edge thickness vanishes. However, the lift is significantly over-predicted by Program MAAD in the cases for which a finite base was left unpanelled. Clearly, the present base modelling alleviates the problem. The accuracy is also evident in the pressure and velocity distributions of figures 21 and 22.

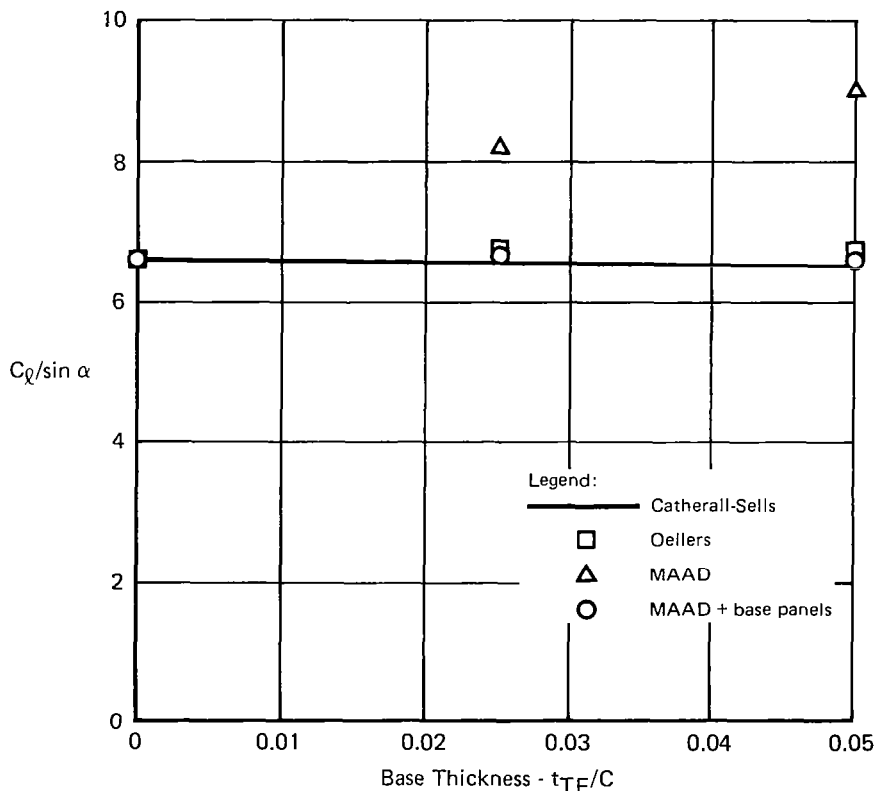


Figure 20. Lift Prediction for Symmetric Blunt Base Airfoils

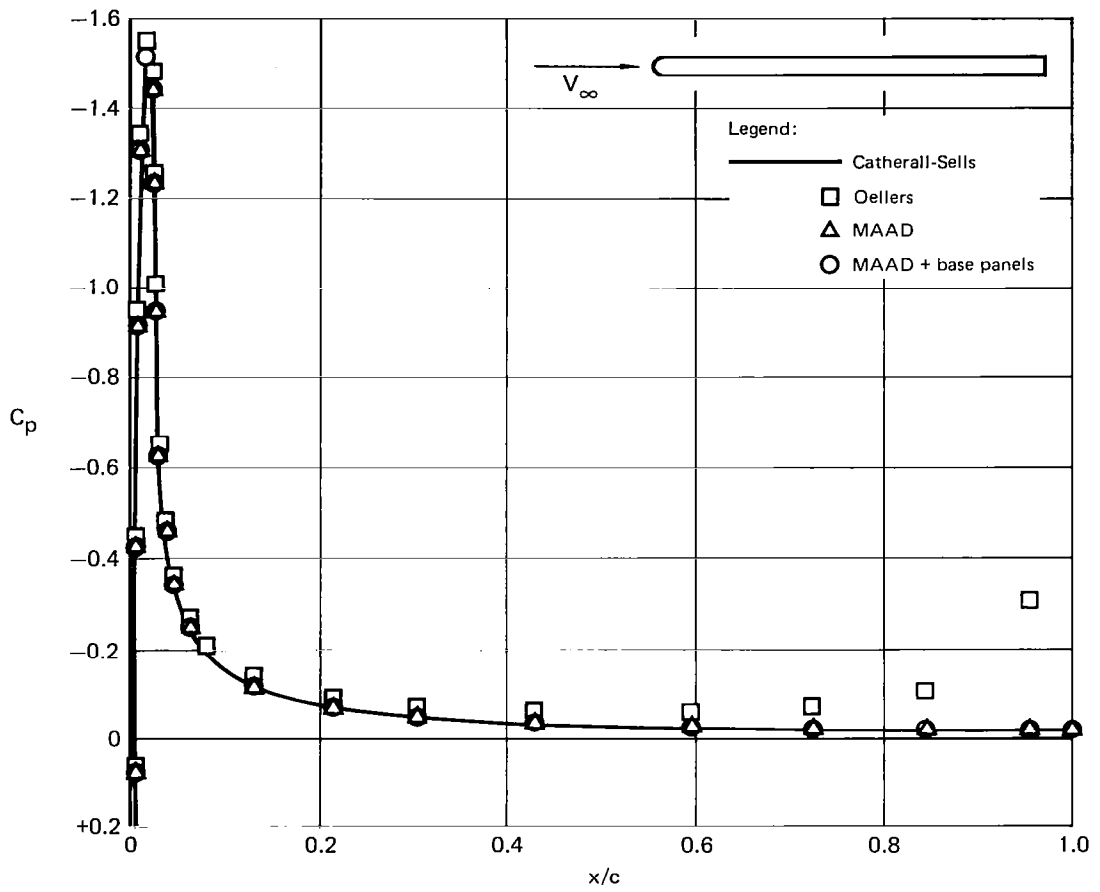


Figure 21. Blunt Base Airfoil Analysis (0° Incidence)

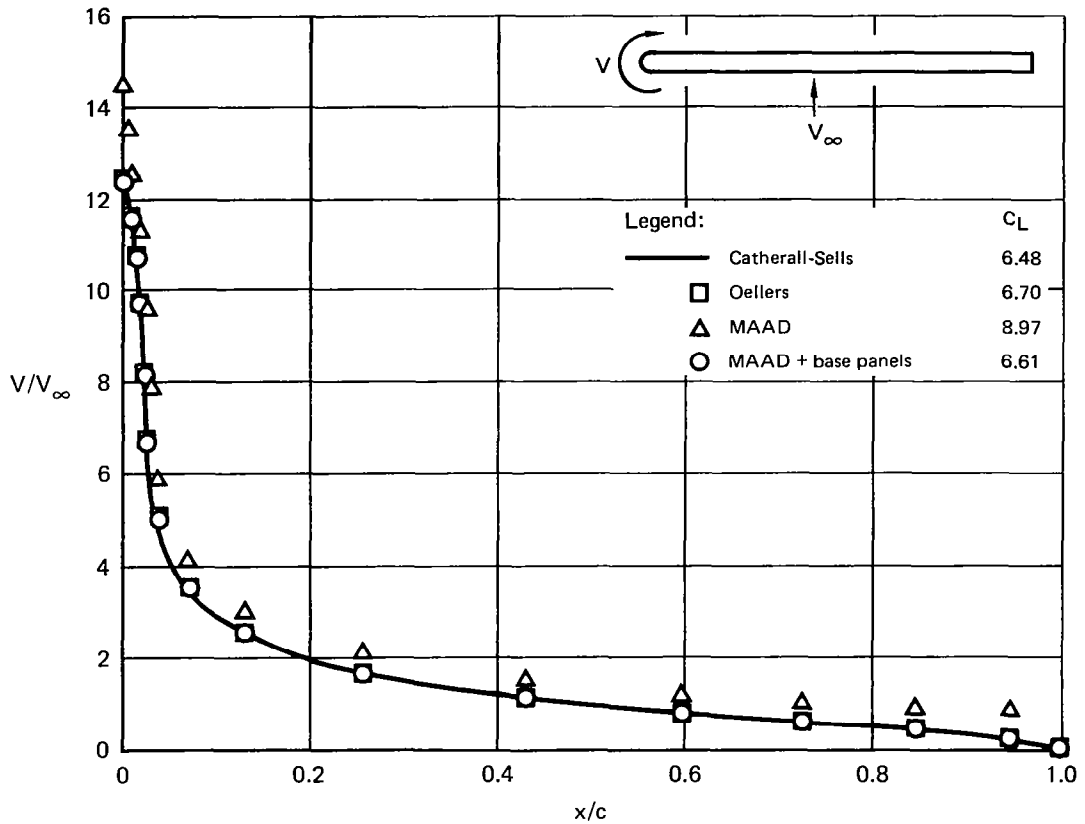


Figure 22. Blunt Base Airfoil Analysis (90° Incidence)

For the GAW-1 Airfoil of figure 19, lift prediction error is plotted against angle of attack in figure 23. Here the error is defined as the difference between the calculated lift and the lift predicted by Catherall-Sells. With only two panels, the base modelling reduces the Program MAAD error by an approximate factor of ten.

Although the present base modelling method was developed for Program MAAD, the method can be implemented directly in any surface panelling program. The modelling is a simple but effective approximation to the fact that no real fluid can turn a sharp corner on an impermeable surface.

THREE-DIMENSIONAL POTENTIAL FLOW METHOD

In 1978 a surface panel-method computer program was developed for solving incompressible potential flow analysis problems for arbitrary lifting or nonlifting three-dimensional geometries (reference 1). When applied to thin wings, the program demonstrated significantly better prediction accuracy than the Hess (Douglas Neumann) source method (reference 17). This improvement was the anticipated result of using the mild source-doublet

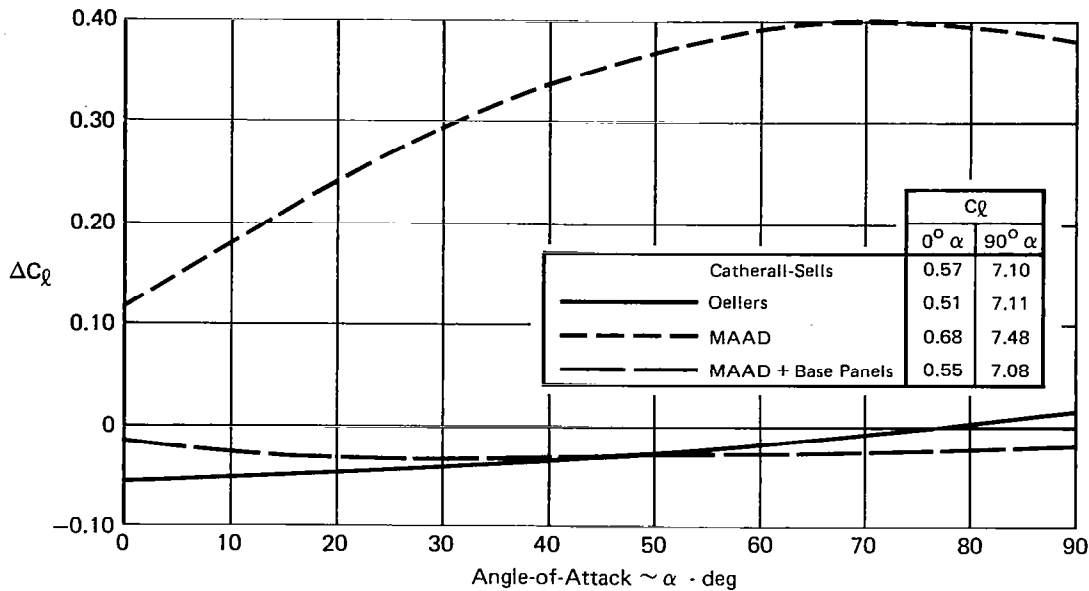


Figure 23. Lift Prediction Error for GAW-1 Airfoil

$$\Delta C_l \equiv C_l - C_l \text{ Catherall}$$

distribution of Green's third identity in place of a distribution having strong source density. However, the prediction accuracy of the program was dependent upon the degree to which neighboring panels were uniform in size and shape. Furthermore, the modeling was limited to trapezoidal panels. These restrictions were eliminated as part of this contract by modifying and extending the earlier program, thereby creating the MCAIR 3-D Subsonic Potential Flow Program (Version 1), hereinafter designated the "MCAIR 3-D Program".

As in the earlier program, the geometry in the MCAIR 3-D Program is modeled by flat, quadrilateral panels with distributions of constant source and quadratic doublet density. Potential influence functions from reference 18 have been incorporated to eliminate the trapezoidal requirement of the earlier functions. The quadratic doublet distribution on each panel is established by a least squares spline fit through neighboring panel control points. In the earlier program, only nine control points were used to establish the spline fit, resulting in doublet discontinuities at panel edges and subsequent solution sensitivity to nonuniform paneling. In the MCAIR 3-D Program, twenty-one control points are used in such a manner that the spline is nearly continuous at panel edges. This spline is similar to the one developed for the Boeing PANAIR Program (unpublished); however, in the present case, the spline can be carried across the intersection of network edges, even if the intersection includes a wake. This eliminates the requirement for edge boundary condition control points on smooth geometries such as fuselages and guarantees that axisymmetric flow problems will have axisymmetric solutions.

Presented in this section is a description of the solution method. Experience with the analysis mode of the Multi-Element Airfoil Inviscid Analysis and Design Program guided the development of the MCAIR 3-D Program. In that regard, the present three-dimensional analysis method can be considered to be a nearly direct extension of the two-dimensional formulation described in a preceding section. In accordance with Green's third identity, the source density on each panel is determined by the orientation of the panel with respect to the free stream direction. The doublet distribution is calculated by requiring that the internal perturbation potential be zero at selected control points, corresponding to a uniform imaginary internal flow. It is recommended that the reader be acquainted with the theoretical and numerical background presented in reference 1. The formulation for the MCAIR 3-D Program is described below, to be followed by a simple wing example solution.

Geometry Panel Modeling

The surface of each body in the flowfield is divided by the user into one or more sections (figure 24), where each section will be further subdivided into panels. A typical section is a wing, tail, or part of a fuselage. A body is defined as any closed surface with an interior, such as an airplane, sphere, or toroid. Canard-wing-tail geometries and slotted flap wings are permitted. However, the user must define the wake trajectory a priori. The division of a body into sections must be performed such that one side of each section is wetted by the real external flow and the other by the imaginary internal flow. If there are one or two planes of symmetry, only the geometry on one side of the plane(s) is defined, and the image geometry will be generated automatically.

With the exception of the following two restrictions, the division of a body into sections is arbitrary. First, a section cannot be multiply connected in the sense that there are holes in the surface. Second, every sharp edge on a body must be aligned with section edges, where a sharp edge is defined as the locus of points at which there is a discontinuity in the surface normal direction.

Although open wing tips and open fuselage bases are permitted in the MCAIR 3-D Program, it is recommended that they be closed in accordance with the definition of a body. The closing seals the boundary between the real external and the imaginary internal flows. Of course, physical openings such as flow-through nacelles should not be closed.

The difference between a lifting and nonlifting body is dictated by the presence or absence of an intersecting wake. A wake is divided into sections in the same sense as a body, except that a wake is a sheet and not a closed geometry with an interior. No part of a wake can lie in the interior of a body.

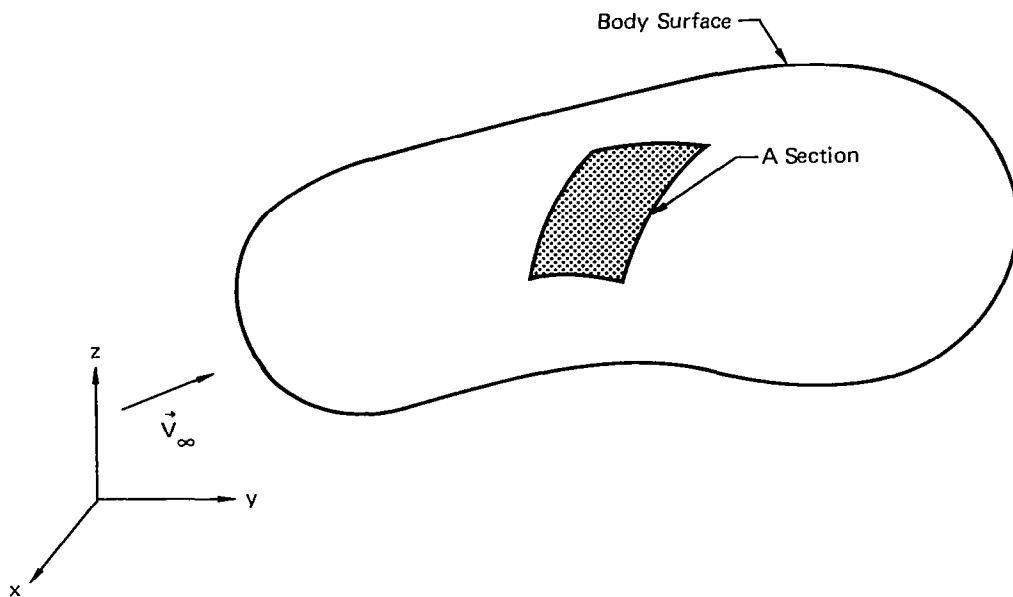


Figure 24. A Section of a Body Surface

One edge of a wake section will be assigned control points to determine the lift. That edge must coincide with a sharp edge of a body. Typically, this will correspond to the intersection of a wake with a wing trailing edge. The opposite wake edge, usually designated the starting vortex, can also intersect a body section at a sharp edge. In most cases, however, the starting vortex will be positioned several body lengths downstream to simulate a semi-infinite trailing vortex sheet. Either of the two remaining wake section edges can intersect an edge of another wake section, intersect a body section, or be free of any intersections. The intersection with a body section can occur along any path of panel edges selected and identified by the user. On an airplane, the inboard wake edge should follow the contour of the fuselage, even if the fuselage is tapered.

Each section is assigned an index i_s ($1 \leq i_s \leq n_s$). The type of section is identified by $STYPE(i_s)$, equal to 1 for a body section and 2 for a wake. A third type, designated a vortex loop, is also available. The difference between a vortex loop and a wake section is that for the former, a single edge control point is used to determine a uniform doublet distribution.

The subdivision of a section into panels is performed using the rectangular indexing nomenclature of figure 25. It is noted that only the indexing is rectangular, not the section or panel geometries. If the section in figure 25 is on a body, the exterior is assumed to be on the viewer's side of the figure. Cumulative point and panel indices are defined as:

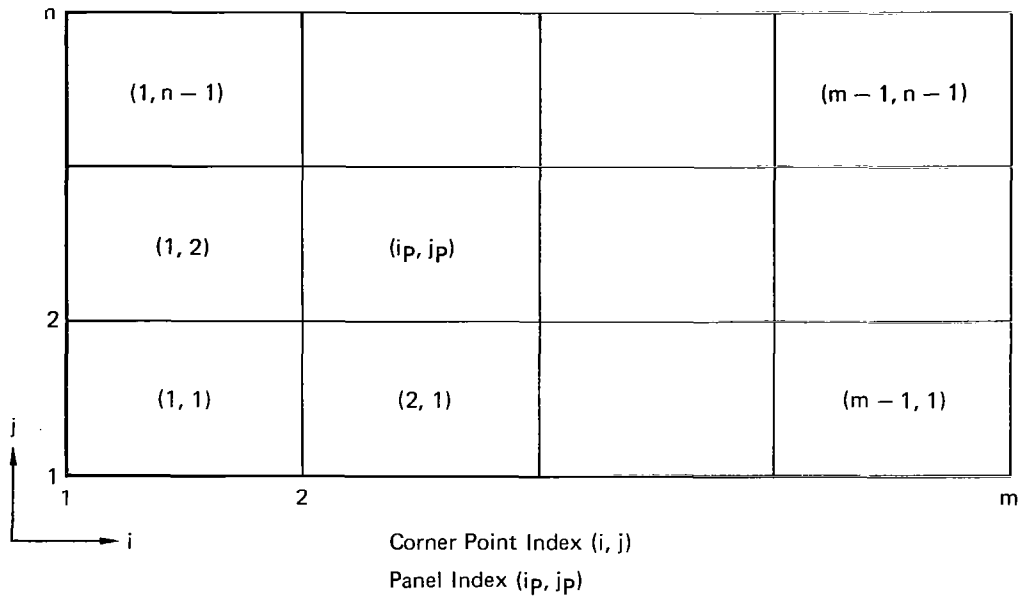


Figure 25. Indexing Nomenclature for a Section of Panels

$$k \equiv k_o(i_s) + (i-1) \cdot n + j \quad (67)$$

$$k_p \equiv k_{p_o}(i_s) + (i_p-1) \cdot (n-1) + j_p \quad (68)$$

where $k_o(i_s)$ and $k_{p_o}(i_s)$ are respectively equal to the total number of corner points and panels on preceding sections 1 through (i_s-1) . Coordinates (x, y, z) are input for each corner point k . With the exception of points on a section edge, each point k is a corner of four surrounding panels. At the intersection of two sections, there is no requirement that the sections share the same point distribution along the common edge. Therefore, it is permissible for a section with dense paneling to intersect a section with sparse paneling. Except for sharp edges on a body, it is not necessary for the input point distributions of intersecting edges to lie on a common path of connected straight line segments. At sharp edges, boundary condition control points will be inserted near the intersection, and therefore gaps or overlaps perpendicular to the intersection could adversely affect the calculations.

The four edges of a section are ordered counterclockwise by index i_{SE} , where $i_{SE} = \{1, 2, 3, 4\}$ respectively corresponds to $\{j = 1, i = m, j = n, \text{ and } i = 1\}$. Each edge of each section is categorized by three values selected by the user, defined below.

ETYPA(i_{SE})

- 0 This edge is either (1) a smooth edge on a body (no surface slope discontinuity) or (2) edge number $i_{SE} = 2, 3, \text{ or } 4$ on a wake. In either case, no edge control points will be used.
- 1 Edge control points will be used. This can be a sharp edge on a body section or edge number $i_{SE} = 1$ on a wake section. In the latter case, this edge must intersect two body section edges of $ETYPA = 1$.

ETYPB(i_{SE})

- 0 This edge has finite length.
- 1 This edge is a point. This is the only place where triangular panels are allowed.

ETYPC(i_{SE})

- 0 This edge does not lie on a symmetry plane.
- 1 The x-z plane is a symmetry plane, with which this edge is coincident.
- 2 The x-y plane is a symmetry plane, with which this edge is coincident.

A schematic of boundary condition control points on a body section is presented in figure 26. There is one control point at each panel center. The edge control points are slightly retracted toward the center of the section to prevent contact with singular edge properties. All body section control points are considered to lie on the internal side of a panel.

For a wake section, all control points are omitted except for those on edge $i_{SE} = 1$. Each wake control point is double-valued, i.e., there is one point slightly above and one slightly below the panel plane. As a Kutta condition, the average velocity between the two points will be set to zero. The direction of the vector connecting the two points is input by the user.

Each panel (i_p, j_p) of section i_s is described by the four corner points $(i, j) = (i_p, j_p), (i_p+1, j_p), (i_p+1, j_p+1), (i_p, j_p+1)$. In figure 27, these four points have been locally reindexed as $i = 1, 2, 3, 4$, respectively. The edge midpoints are $i = 5, 6, 7, 8$ and the panel center is $i = 9$. Here the four corner points will be adjusted to form a planar quadrilateral

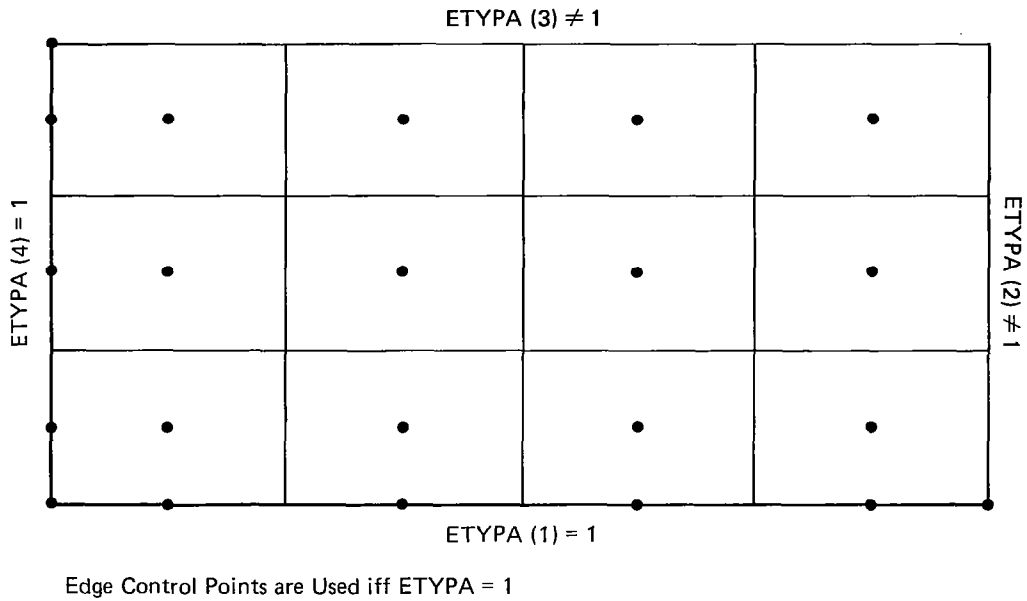


Figure 26. Control Point Locations on a Section

panel, and a local (ξ, η, ζ) - Cartesian coordinate system will be defined in relation to the general system (x, y, z) of figure 24.

Using the local indexing nomenclature of figure 27, the panel center is determined.

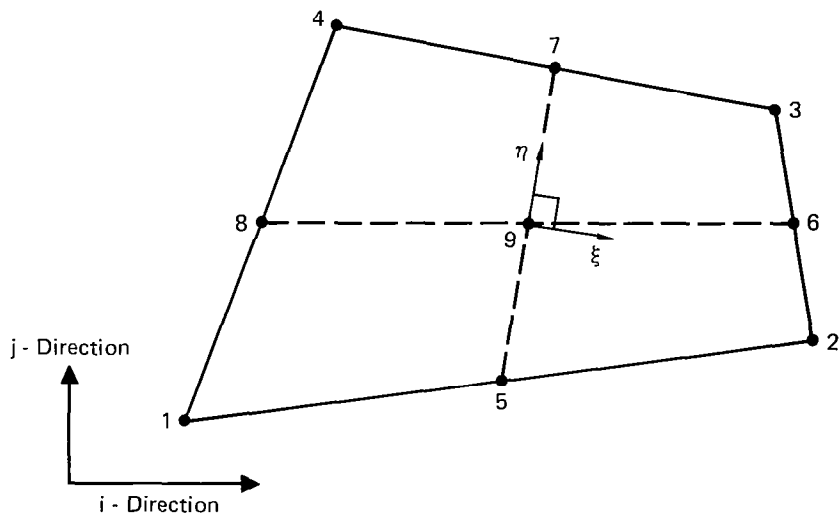


Figure 27. Local Indexing Nomenclature and Coordinate System for a Panel

$$\begin{pmatrix} x_9 \\ y_9 \\ z_9 \end{pmatrix} = \frac{1}{4} \begin{pmatrix} x_1 + x_2 + x_3 + x_4 \\ y_1 + y_2 + y_3 + y_4 \\ z_1 + z_2 + z_3 + z_4 \end{pmatrix} \quad (69)$$

Define P_{ij} as follows:

$$\vec{P}_i \equiv \begin{pmatrix} P_{i1} \\ P_{i2} \\ P_{i3} \end{pmatrix} \equiv \begin{pmatrix} x_i - x_9 \\ y_i - y_9 \\ z_i - z_9 \end{pmatrix} \quad (1 \leq i \leq 9) \quad (70)$$

Vector \vec{P}_i is the displacement of point i from the panel center.

Unit vectors for the (ξ, η, ζ) -system are defined, in conjunction with a rotation matrix $[a_{ij}]$.

$$\vec{e}_\eta \equiv (a_{21}, a_{22}, a_{23}) \equiv \frac{(\vec{P}_7 - \vec{P}_5)}{|\vec{P}_7 - \vec{P}_5|} \quad (71)$$

$$\vec{e}_\zeta \equiv (a_{31}, a_{32}, a_{33}) \equiv \frac{(\vec{P}_6 - \vec{P}_8) \times \vec{e}_\eta}{|(\vec{P}_6 - \vec{P}_8) \times \vec{e}_\eta|} \quad (72)$$

$$\vec{e}_\xi \equiv (a_{11}, a_{12}, a_{13}) \equiv (\vec{e}_\eta \times \vec{e}_\zeta) \quad (73)$$

Unit vector \vec{e}_ζ is normal to the panel, directed toward the real flow if the panel is part of a body section. The rotation matrix $[a_{ij}]$ provides the conversion between the local and general coordinate systems.

$$\begin{pmatrix} \vec{e}_\xi \\ \vec{e}_\eta \\ \vec{e}_\zeta \end{pmatrix} = [a_{ij}] \begin{pmatrix} \vec{e}_x \\ \vec{e}_y \\ \vec{e}_z \end{pmatrix} \quad (74)$$

The coordinates of the nine points in figure 27 are established in the (ξ, η, ζ) -system.

$$\begin{pmatrix} \xi_i \\ \eta_i \\ \zeta_i \end{pmatrix} = \sum_{k=1}^3 \begin{pmatrix} a_{1k} \\ a_{2k} \\ 0 \end{pmatrix} P_{ik} \quad (1 \leq i \leq 9) \quad (75)$$

It is noted that $\zeta_i = 0$ for all nine points, thereby providing the desired planar adjustment.

The planar adjustment affects the four corner points, $i = \{1, 2, 3, 4\}$. Consequently, small gaps or overlaps can occur between panels. These geometric discontinuities are of little significance unless control points are in the immediate vicinity, which is the case with edge control points. Therefore, the planar adjustment is modified such that a panel edge will not be disturbed if that edge is either a sharp edge of a body section or an edge of a wake section. The preceding statement can apply to no more than one edge or two intersecting edges per panel.

Singularity Distributions on a Panel

The effect of each panel on the flow is represented by a constant source distribution and a quadratic doublet distribution. The source strength is identically zero on all wake panels. For body panels, the strength is determined immediately by the application of Green's third identity,

$$\sigma = V_{Np} - \vec{V}_\infty \cdot \vec{e}_\zeta \quad (76)$$

where V_{Np} is the prescribed normal velocity boundary condition at the panel center. The doublet distribution is established by fitting a least-square-error quadratic to the doublet strengths at the nine points of figure 27. The least squares fit is established before boundary conditions are satisfied, which means that values for the doublet strengths must be treated as unknowns.

The quadratic doublet distribution on a panel is

$$\mu(\xi, \eta) = \beta_1 + \beta_2 \xi + \beta_3 \eta + \beta_4 \xi^2 + \beta_5 \xi \eta + \beta_6 \eta^2 \quad (77)$$

where the coefficients β_i ($1 \leq i \leq 6$) are constants. If μ_j designates the doublet strength at point j of figure 27 ($1 \leq j \leq 9$), it is desired to calculate the matrix b_{ij} such that

$$\beta_i = \sum_{j=1}^9 b_{ij} \mu_j \quad (1 \leq i \leq 6) \quad (78)$$

Matrix b_{ij} dictates the influence of each doublet strength μ_j on each quadratic coefficient β_i . By using the method of least squares, b_{ij} will be calculated as a function of the coordinates of the nine points on the panel.

The procedure is to minimize the error function E.

$$E \equiv \sum_{j=1}^8 W_j^2 [\beta_1 + \beta_2 \xi_j + \beta_3 \eta_j + \beta_4 \xi_j^2 + \beta_5 \xi_j \eta_j + \beta_6 \eta_j^2 - \mu_j]^2 \quad (79)$$

In order to guarantee that the panel center doublet strength is obtained, β_1 is set exactly equal to μ_9 . The weighting factor W_j^2 is equal to 1.00, unless j is an edge control point, in which case the value 10^4 is used to force the doublet distribution through the control point value. If point j is an edge control point, the values ξ_j and η_j are replaced by $(1 - \epsilon)\xi_j$ and $(1 - \epsilon)\eta_j$, where ϵ ($\ll 1$) is an input value that dictates the retraction of edge control points. Equation (79) is minimized with respect to the five unknowns $\beta_2, \beta_3, \beta_4, \beta_5$, and β_6 . This leads to a five by five system of linear equations. Matrix inversion and multiplication then provide the values b_{ij} for equation (78).

In principle, it would be possible to place nine boundary condition control points on each body panel, where each control point would correspond to one unknown value μ_j . However, the computing time would be prohibitive. It is more desirable to maintain the control points of figure 26 and establish each μ_j as a weighted average of the doublet strengths at neighboring control point locations. For wake sections, the weighted average is established under the constraint that the doublet strength be constant along the panel edges aligned with any fixed value of i in figure 25. By substituting the weighted average into equation (78) and then substituting equation (78) into (77), the quadratic doublet distribution on a panel is determined as a function of the unknown control point doublet strengths. The procedure for establishing the weighted average is the subject of the following section.

Doublet Strength at Panel Edges

Illustrated in figure 28 are the control stations that determine the quadratic doublet distributions of all panels in the section. In other words, if the doublet strength at each point (i_μ, j_μ) were known, then equation (78) would provide quadratic coefficients for equation (77). The fact that adjacent panels share common control stations at corners and edge midpoints limits the magnitude of doublet discontinuity along panel edges, regardless of panel spacing. Only the control stations that are also boundary condition control points are independent.

The doublet strength at each of the remaining stations is determined by a weighted average of the strengths at neighboring control points. This section describes the approach by which that weighting is established.

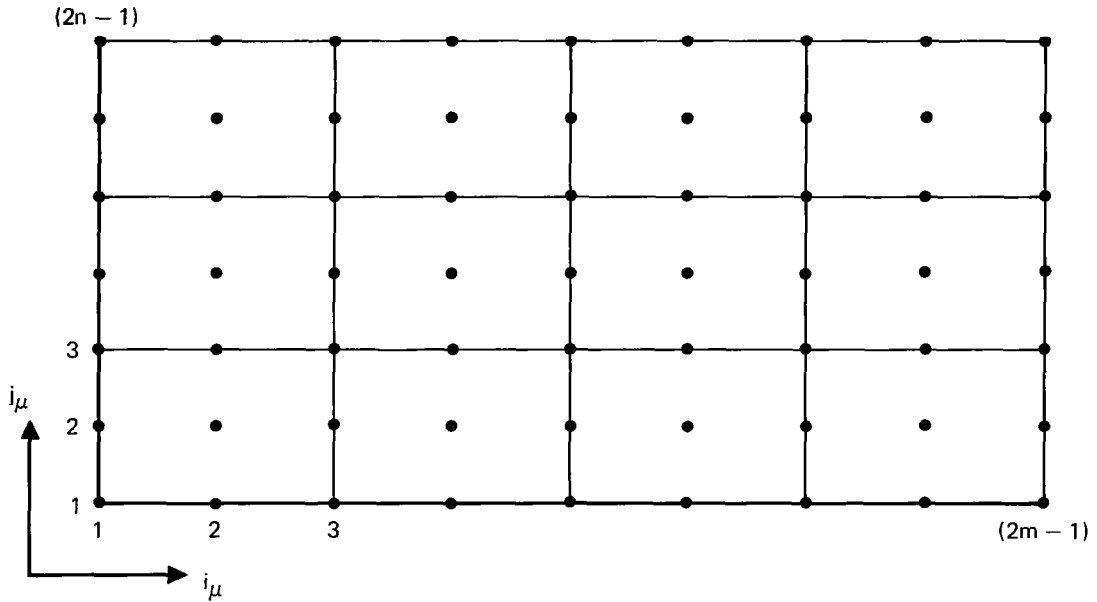


Figure 28. Doublet Spline Control Stations on a Section

Cumulative indexing is defined for the doublet control stations of all sections.

$$k_{\mu} \equiv k_{\mu_0}(i_S) + (i_{\mu} - 1) \cdot (2n-1) + j_{\mu} \quad (80)$$

where $k_{\mu_0}(i_S)$ is the total number of control stations on preceding sections 1 through $(i_S - 1)$. The doublet strength for each k_{μ} will be a weighted average of the doublet strengths at n_D neighboring k_{μ} 's, where each neighboring k_{μ} must be a control point. The neighboring locations are identified by index k_{μ_i} , where $i = 1, 2, 3, \dots, n_D$. The objective is to determine the stations k_{μ_i} and weightings c_i such that

$$\mu(k_{\mu}) = \sum_{i=1}^{n_D} c_i \cdot \mu(k_{\mu_i}) \quad (81)$$

If k_{μ} is a control point, the weighting is trivial; i.e., $n_D = 1$, $k_{\mu_i} = k_{\mu}$, and $c_i = 1$. In general, quadratic interpolation is required to determine the proper weighting. The interpolation technique will be described for panels on a body section.

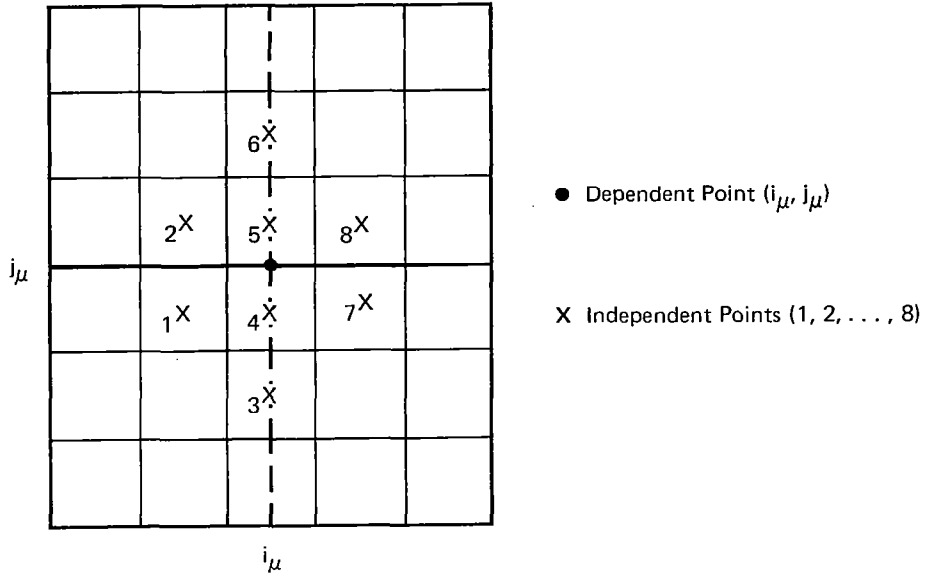


Figure 30. Local Indexing at a Doublet Edge Midpoint Control Station

If one or more wake section edges intersect any of the body panel edges within the space occupied by the n_D control points, the least squares fit will not be applied to the doublet distribution μ , but to a function u illustrated in figure 31. In the vicinity of point k_μ , the function u is equal to the doublet density μ . However, on the opposite side of each wake intersection, u is adjusted by $+\Delta\mu$, where $\Delta\mu$ is the discontinuity in doublet density on the body surface generated by the wake. Therefore, the function u is continuous with continuous gradient and is suitable for quadratic interpolation.

At this stage, it is desirable to establish a local (ξ, η, ζ) -coordinate system such that the origin is at k_μ and the ζ -axis is locally normal to the body surface. The vector \vec{P}_i is defined for $1 \leq i \leq n_D$.

$$\vec{P}_i \equiv \begin{pmatrix} P_{i1} \\ P_{i2} \\ P_{i3} \end{pmatrix} \equiv \begin{pmatrix} x \\ +y \\ +z \end{pmatrix}_{k_{\mu i}} - \begin{pmatrix} x \\ y \\ z \end{pmatrix}_{k_\mu} \quad (82)$$

where the positive sign for y and z is selected unless $k_{\mu i}$ is on the opposite side of the $y = 0$ and $z = 0$ symmetry planes, respectively. Vector \vec{P}_i is the displacement between points $k_{\mu i}$ and k_μ . The unit vector \vec{e}_ζ is a weighted average of local panel normal vectors.

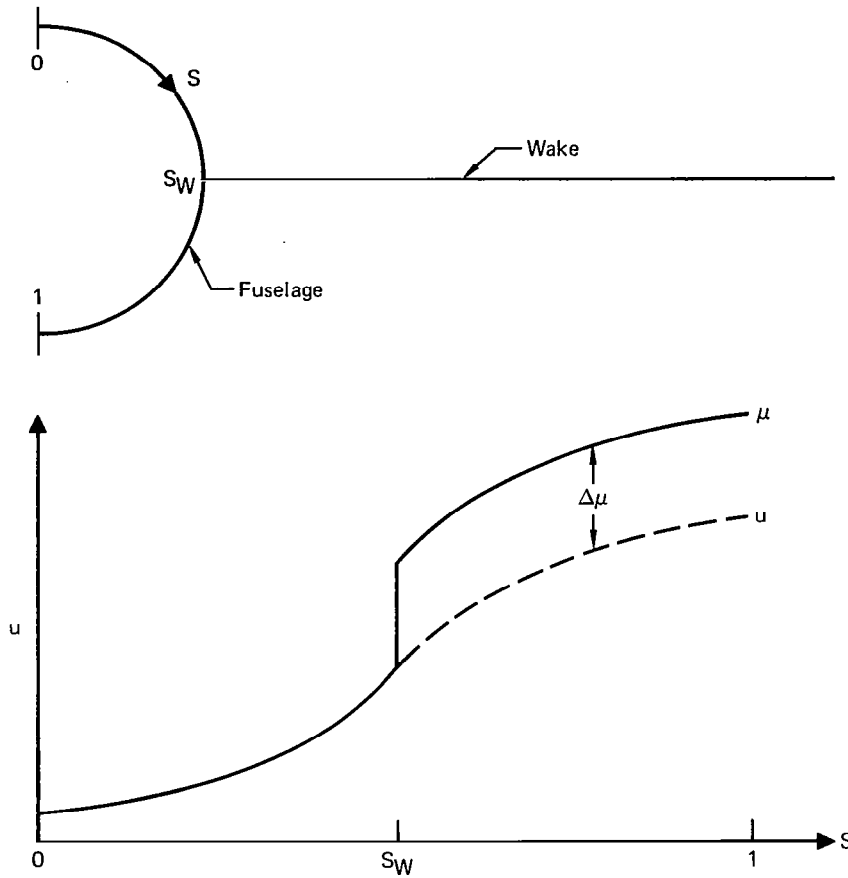


Figure 31. Doublet Discontinuity at Wake-Fuselage Intersection

$$\frac{\vec{e}_\zeta}{c} = \frac{n_D \sum_{i=1} \{n_x, \pm n_y, \pm n_z\} k_P(i)}{\sqrt{P_{i1}^2 + P_{i2}^2 + P_{i3}^2}} \quad (83)$$

where the constant c accounts for the fact that the right-hand-side is not normalized, where $k_P(i)$ is the panel on which point k_μ lies, where (n_x, n_y, n_z) is the unit normal vector of panel $k_P(i)$ in the general coordinate system, and where the summation is to include only values i that are panel centers less than one panel distant from k_μ . Once again, the sign selection depends upon whether point i is on the opposite side of a symmetry plane. \vec{e}_ξ is defined by selecting any unit vector normal to \vec{e}_ζ . It follows that \vec{e}_η is defined as $\vec{e}_\zeta \times \vec{e}_\xi$. Each point i is then assigned coordinates in the (ξ, η, ζ) -system.

$$\left\{ \begin{array}{l} \xi_i = \vec{P}_i \cdot \vec{e}_\xi \\ \eta_i = \vec{P}_i \cdot \vec{e}_\eta \\ \zeta_i = \vec{P}_i \cdot \vec{e}_\zeta \end{array} \right\} \quad (1 \leq i \leq n_D) \quad (84)$$

In order to approximately account for surface curvature, ξ_i and η_i should both be magnified by the factor $[(\xi_i^2 + \eta_i^2 + \zeta_i^2)/(\xi_i^2 + \eta_i^2)]^{1/2}$

Function $u(\xi, \eta)$ is modeled as a quadratic

$$u(\xi, \eta) = \beta_1 + \beta_2\xi + \beta_3\eta + \beta_4\xi^2 + \beta_5\xi\eta + \beta_6\eta^2 \quad (85)$$

Designating u_i as the value of u at point $k_{\mu i}$ ($1 \leq i \leq n_D$), quadratic interpolation is performed by minimizing function E .

$$E \equiv \sum_{i=1}^{n_D} W_i^2 (\beta_1 + \beta_2\xi_i + \beta_3\eta_i + \beta_4\xi_i^2 + \beta_5\xi_i\eta_i + \beta_6\eta_i^2 - u_i)^2 + 10^{-4} (\beta_4^2 + \beta_5^2 + \beta_6^2) \quad (86)$$

where W_i^2 is a weighting factor inversely proportional to the fourth power of distance between $k_{\mu i}$ and k_μ . If $k_{\mu i}$ is less than one panel width from k_μ , W_i^2 is increased by a factor of 10^4 to force a close fit. The term

$$10^{-4} (\beta_4^2 + \beta_5^2 + \beta_6^2)$$

eliminates the possibility of unbounded curvature in the quadratic. E is minimized with respect to the unknowns β_1, \dots, β_6 . The resulting system of linear equations is manipulated by standard matrix inversion and matrix multiplication techniques to provide the array c_i where

$$\beta_1 = \sum_{i=1}^{n_D} c_i u_i \quad (87)$$

The array c_i should be normalized such that $\sum_{i=1}^{n_D} c_i$ is equal to one. Since the origin of the (ξ, η, ζ) -system is at k_μ , equation (85) implies that

$$\mu(k_\mu) = \beta_1 \quad (88)$$

Combining equations (87) and (88),

$$\mu(k_\mu) = \sum_{i=1}^{n_D} c_i u_i \quad (89)$$

Equation (89) can be transformed into the desired form of equation (81) by expressing u_i as $\mu(k_{\mu i}) \pm \Delta\mu_1 \pm \Delta\mu_2 \pm \dots$, where each $\Delta\mu_j$ corresponds to a wake intersection somewhere between points k_μ and i . As stated earlier, only intersections along wake edge numbers $i_{SE} = 2$ or 4 are permitted. The doublet strength along the wake edge is constant, equal to the doublet strength at one of the two corner control points of wake edge $i_{SE} = 1$. Therefore, each $\Delta\mu_j$ can be replaced by a wake control point doublet strength. Equation (89) becomes

$$\mu(k_\mu) = \sum_{i=1}^{(n_D+n_W)} c_i \cdot \mu(k_{\mu i}) \quad (90)$$

where $i > n_D$ refers to wake control points.

If k_μ is a panel corner on a body or wake section edge of $ETYP_A = 1$, the quadratic interpolation is modified to be based upon distance along the edge. The modified interpolation involves a single variable, as opposed to the two variables ξ and η required for the surface interpolation. For a wake section, $\mu(k_\mu)$ is constrained to be a constant for all values j_μ at a fixed i_μ . This constraint corresponds to the approximation of zero pressure loading on a wake.

By substituting equation (90) into equation (78), the quadratic doublet coefficients on a panel are expressed in terms of the independent unknowns at control points.

$$\beta_i = \sum_{j=1}^9 b_{ij} \left[\sum_{\ell=1}^{(n_D+n_W)} c_\ell \cdot \mu(k_{\mu \ell}) \right] \quad (91)$$

Boundary Condition Satisfaction

There are two types of boundary conditions to be satisfied. At each body control point, the internal perturbation potential induced by the simultaneous action of all singularities is set equal to zero. At each wake control point, the average total velocity between the adjacent upper and lower Kutta condition

points is to be zero. This average velocity can be expressed as the difference in potential between the two points, less the local doublet strength on the wake at the control point.

For each control point there is one boundary condition to be satisfied and one unknown doublet strength. The boundary condition equations are established by using equations (76) and (91) in conjunction with available potential influence functions for unit distributions of constant source, constant doublet, linear doublet, and second order doublet density (reference 18).

The resulting system of linear equations is solved for the doublet strength at each control point. Equations (77) and (91) then provide the doublet distribution on every panel.

Velocity and Pressure Calculation

The calculated doublet distribution is converted to surface velocity and pressure at each body panel center, and then the forces and moments are integrated. For each body panel, the flow velocity in the local panel coordinate system is

$$\begin{aligned}
 v_{\xi} &= \vec{V}_{\infty} \cdot \vec{e}_{\xi} + \beta_2 \\
 v_{\eta} &= \vec{V}_{\infty} \cdot \vec{e}_{\eta} + \beta_3 \\
 v_{\zeta} &= \vec{V}_{\infty} \cdot \vec{e}_{\zeta} + \sigma = v_{N_p}
 \end{aligned}
 \tag{92}$$

Equation (92) expresses the fact that on a body surface the local source strength is equal to the perturbation velocity normal component and the local doublet strength is the local perturbation potential, corresponding to Green's third identity. For steady flow, Bernoulli's equation provides the local pressure coefficient.

$$C_p = 1 - \frac{v_{\xi}^2 + v_{\eta}^2 + v_{\zeta}^2}{v_{ref}^2}
 \tag{93}$$

Forces and moments are calculated under the approximations that the pressure is uniform on each panel and that the flat quadrilateral panel is the local geometry.

This completes the description of the analysis method of the MCAIR 3-D Program.

Example Solution

The MCAIR 3-D Program has been checked out for a variety of simple geometries. At the time of writing this report, the program had not been evaluated for wing-fuselage configurations. Although it is anticipated that the evaluation will be successful, only a simple isolated wing solution is available for presentation here.

The right half-wing of figure 32 was represented by five spanwise strips of panels with 10 upper and 10 lower surface panels per strip. Twenty additional panels were used to close the tip. The wake was modelled as being tangent to the local trailing edge bisector angle at each span station.

The calculated incompressible inviscid pressure distribution at two angles of attack is shown in figures 33 and 34. Unpublished experimental data is also shown for comparison. The data was taken in the presence of a fuselage at 0.6 Mach number and 6 million Reynolds number, based on the mean aerodynamic chord. Although no corrections were made for fuselage interference, compressibility, or viscosity, the calculated results agree reasonably well with the experimental data. The solution required approximately 50 seconds computing time on the CDC CYBER 175.

FIRST-ORDER EXPANSION APPROACH FOR THICK WING-FUSELAGES

The most widely recognized feature of three-dimensional surface singularity panel methods is that the numerical solution formulation is not dependent upon the type of surface geometry. A second feature that has been almost totally unrecognized is that the analytical expressions in a panel method formulation can be linearized to provide the matrix of velocity derivatives with respect to surface geometry perturbations. This approach was used for the design mode of the Multi-Element Airfoil Inviscid Analysis and Design Program (MAAD), and it is anticipated that the success of the two-dimensional design method will carry over to three-dimensional configurations.

Possibly an even more valuable application of the velocity-geometry derivative matrix is to the analysis of several wing-fuselage geometry variations at no significant additional expense. During the configuration development of most airplanes, several possible combinations of wing planform, twist, and section shape are considered. With existing surface panel methods, each combination would require one independent analysis solution. If compressibility effects were to be included, each Mach number would also require a separate solution. Since a three-dimensional analysis can cost several hundred dollars and require overnight turnaround, there is reluctance among many engineers to exercise

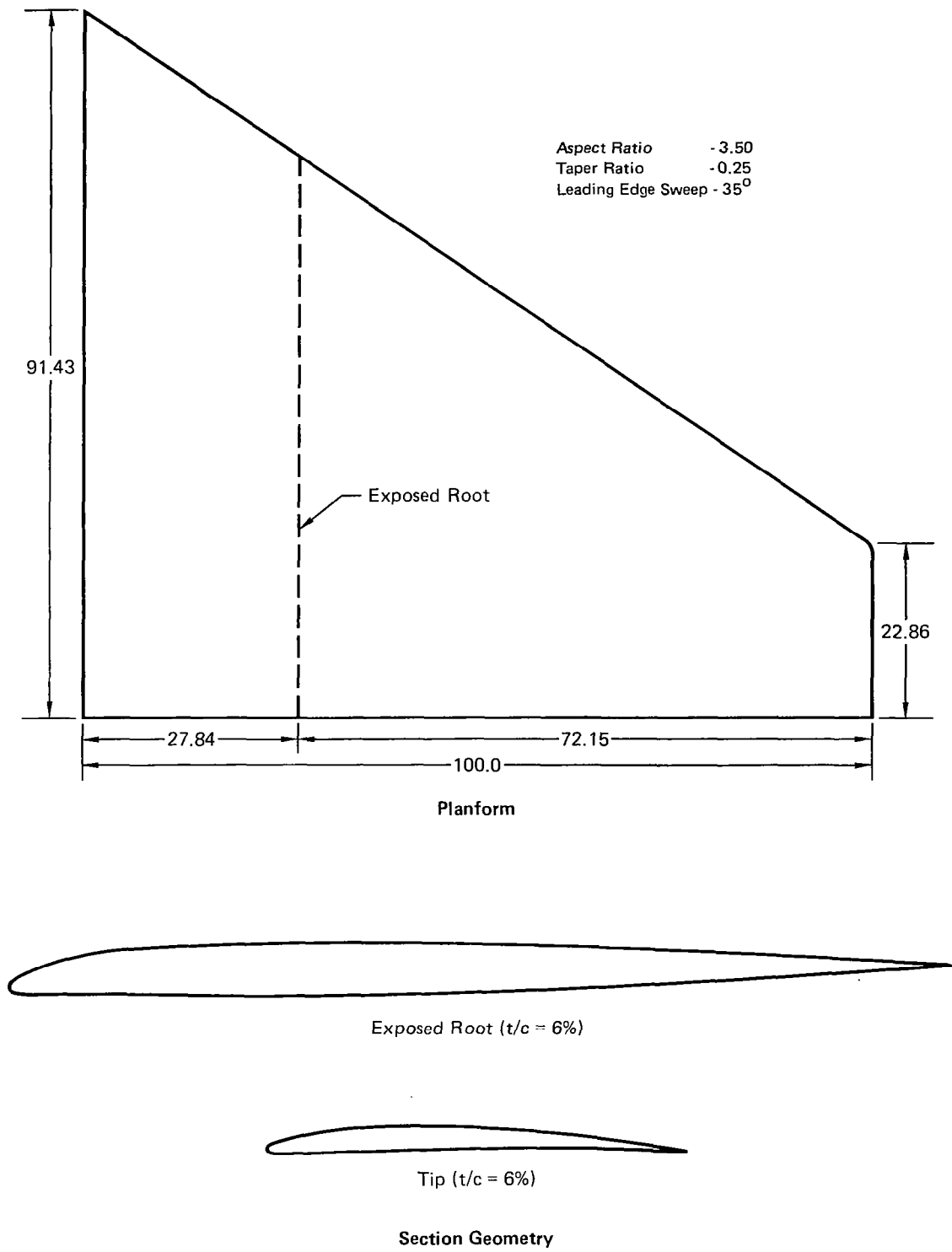


Figure 32. WLB-1 Wing Geometry

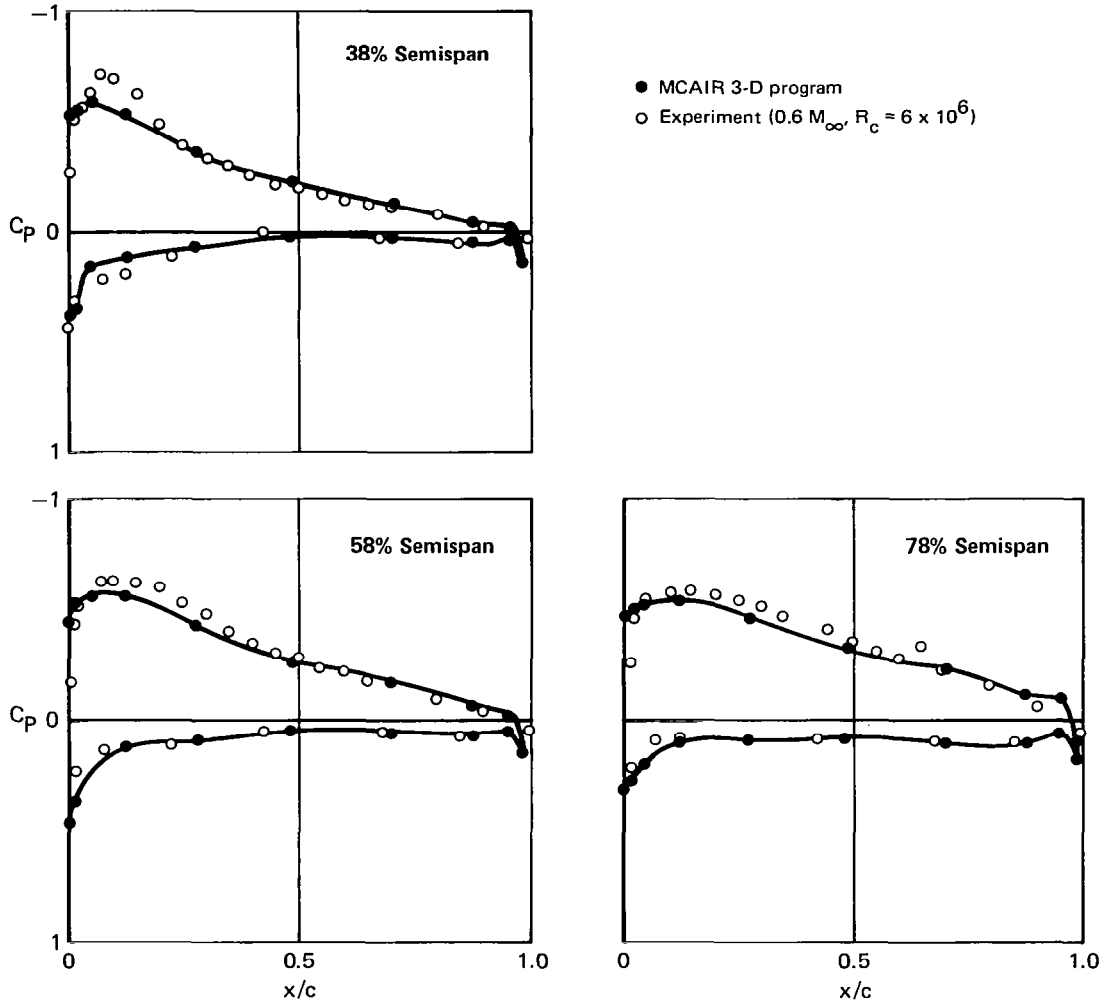


Figure 33. WLB-1 Pressure Distribution at $3.8^\circ \alpha$

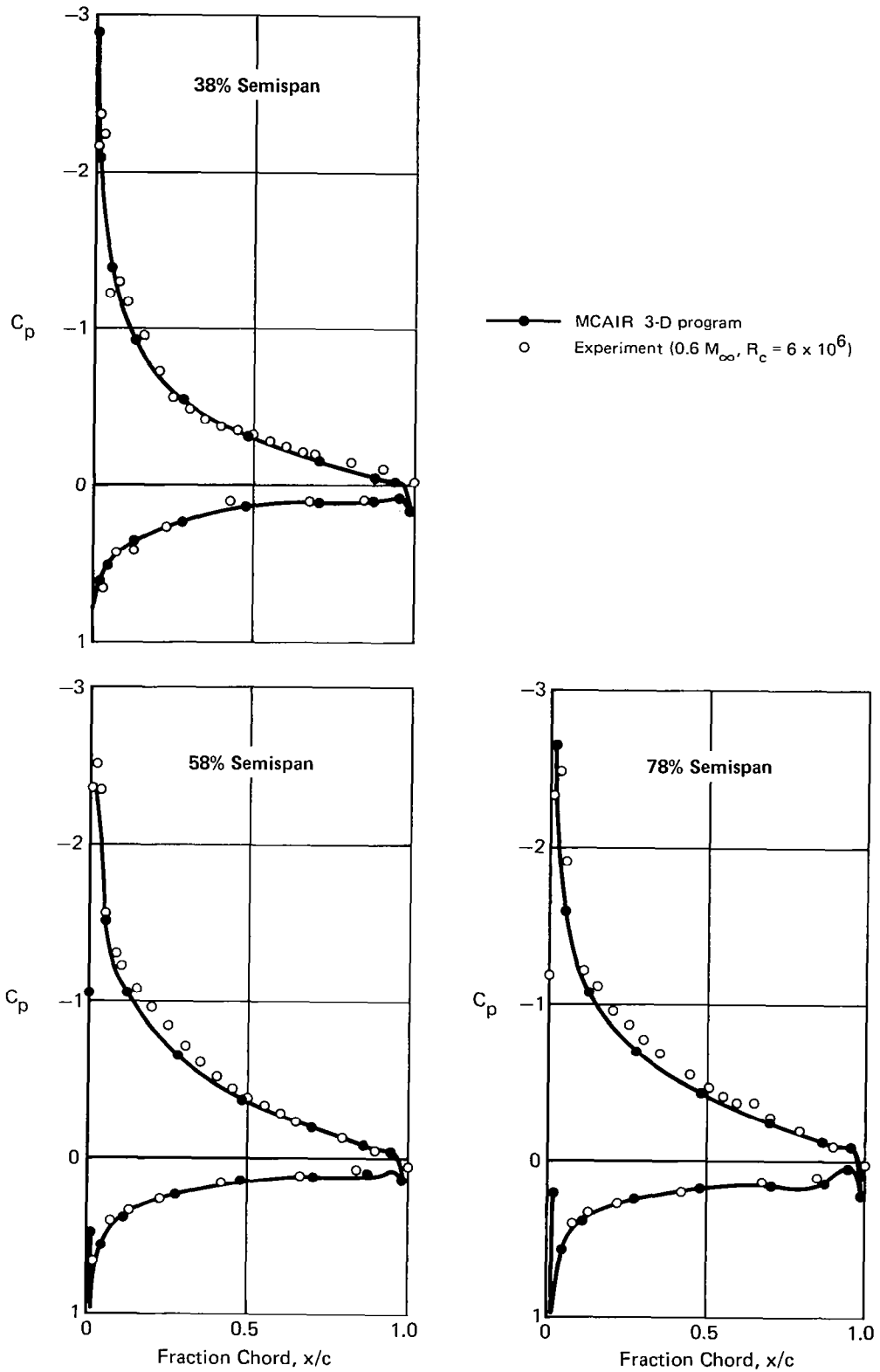


Figure 34. WLB-1 Pressure Distribution at $8.8^\circ \alpha$

surface panel methods. On the other hand, the simpler chord plane panel methods such as vortex lattice are often insufficiently accurate, particularly at leading edges and wing-fuselage intersections. It is anticipated that the dilemma would be alleviated by implementing a velocity-geometry perturbation formulation in the MCAIR 3-D program.

Outlined in this section is the approach through which arbitrary small variations in both configuration geometry and subsonic Mach number can be analyzed at very small cost. Then an approach for solving finite wing design problems will be summarized.

Low Cost Method for Analyzing Geometry Perturbations

Consider any three-dimensional geometry subject to analysis by the MCAIR 3-D program. Suppose that during the analysis, a velocity-geometry derivative matrix were calculated and stored on a computer file. At any future date, it would be possible to predict the effect of a perturbation in configuration geometry or subsonic Mach number by retrieving the matrix and multiplying it by a new right-hand-side. The additional cost would be insignificant. Applications would include configuration evaluation and optimization, viscous-inviscid interactions, and the calculation of stability derivatives.

The discussion to follow will concentrate on the utility of a precalculated velocity-geometry derivative matrix, not on the method used to establish the matrix. That method has not yet been formulated for the MCAIR 3-D program. However, it is expected to be a straightforward extension of the existing 2-D method incorporated in Program MAAD. In order to simplify the discussion, only zero normal velocity boundary conditions will be considered. It is understood that a general perturbation solution formulation can and indeed should include the option for nonzero normal velocity. Attention will initially focus on simple two-dimensional flow past an airfoil. Then three-dimensional geometry perturbations and Mach number corrections will be discussed.

Consider the airfoil of figure 35. The baseline geometry is perturbed by displacing each panel endpoint j by $\delta\vec{R}_j$. Although the panel indexing remains fixed, the coordinates are translated. Arbitrary perturbations are permitted in airfoil chord, panel length distribution, and airfoil location with respect to any other elements in the flow. The velocity at the midpoint of panel i before and after the geometry perturbation is respectively designated V_i and $(V_i + \delta V_i)$. Assume that the freestream velocity \vec{V}_∞ is parallel to the x -axis and of unit magnitude, i.e. $\vec{V}_\infty = \vec{e}_x$. Then a velocity-geometry derivative matrix \vec{A}_{ij} can be established such that

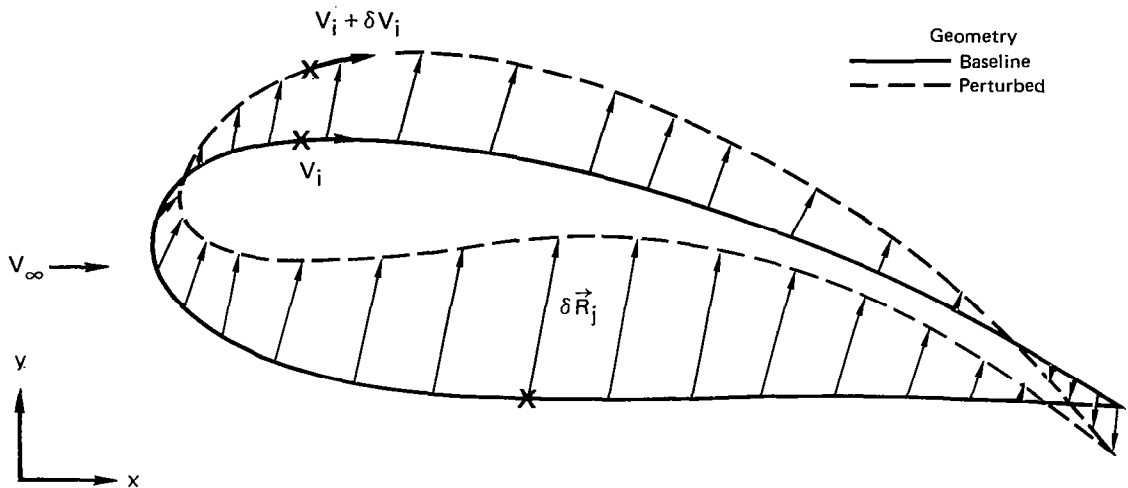


Figure 35. Geometry - Velocity Perturbation for an Airfoil

$$\delta V_i = \sum_j (\vec{A}_{ij} \cdot \delta \vec{R}_j) + O(|\delta \vec{R}_j|^2) \quad (94)$$

The vector nomenclature for matrix \vec{A}_{ij} is intended to indicate that there are two matrix coefficients for each (i,j) , respectively corresponding to the x and y components of $\delta \vec{R}_j$. The derivative matrix \vec{A}_{ij} is calculated as a function of the baseline geometry only. The effect of the geometry perturbation is predicted by multiplying \vec{A}_{ij} and $\delta \vec{R}_j$. This neglects second order and higher terms of $\delta \vec{R}_j$, identified by the nomenclature $O(|\delta R_j|^2)$.

Although only linear terms are included, the prediction accuracy can be good for surprisingly large perturbations. An example is the perturbation from a circular cylinder to a football shape (figure 36). Using Program MAAD, the change in velocity distribution was calculated by three approaches. First, the actual change was calculated by independently solving for the flow about the perturbed and unperturbed geometries. Second, the present approach of multiplying \vec{A}_{ij} by $\delta \vec{R}_j$ was applied. Third, the method of equivalent blowing, also known as the surface transpiration method, was used. The present first-order method provides substantially better agreement with the actual velocity change than the method of equivalent blowing (figure 36). The reason is that only in the present approach are all first-order perturbations included.

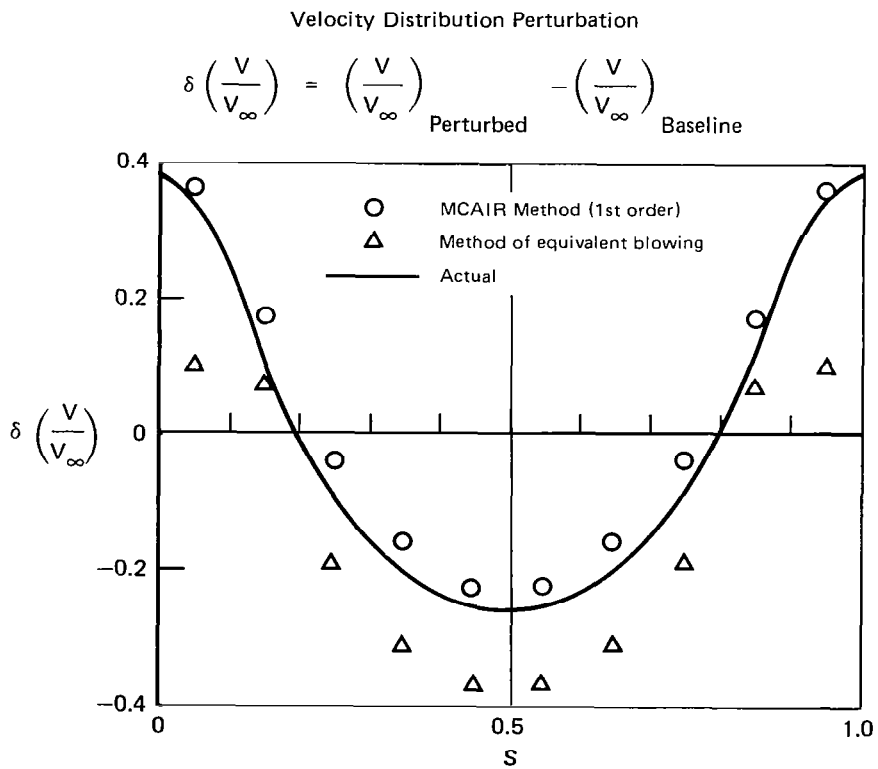
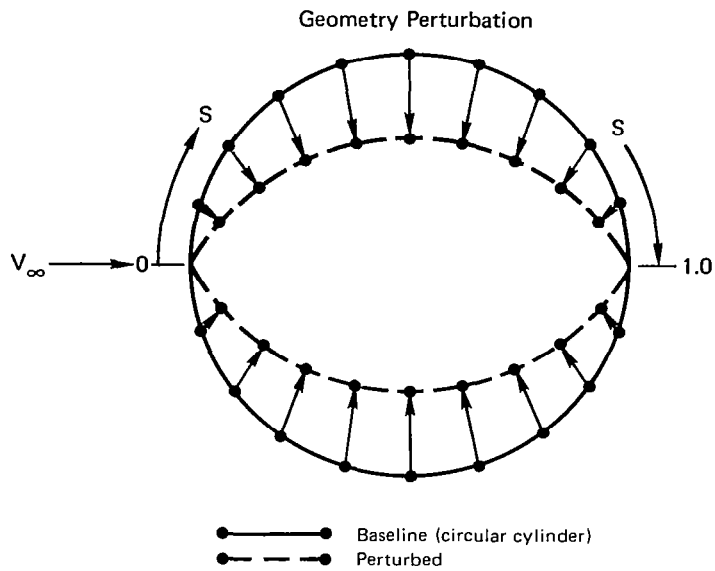


Figure 36. Sample Velocity Perturbation Prediction

Now the procedure for handling arbitrary angles of attack will be described. It is necessary to introduce a second velocity-geometry derivative matrix, corresponding to $\vec{V}_\infty = \vec{e}_y$. Superscripts (1) and (2) are respectively used to denote baseline flow solutions for $\vec{V}_\infty = \vec{e}_x$ and $\vec{V}_\infty = \vec{e}_y$. Suppose that the free-stream velocity \vec{V}_∞ is at an angle of attack α with respect to the x-axis. The baseline solution is

$$V_i = V_\infty [V_i^{(1)} \cos\alpha + V_i^{(2)} \sin\alpha] \quad (95)$$

The first-order velocity change induced by the geometry perturbation at the fixed α is

$$\delta V_i = + V_\infty \cos\alpha \sum_j (\vec{A}_{ij}^{(1)} \cdot \delta \vec{R}_j) + V_\infty \sin\alpha \sum_j (\vec{A}_{ij}^{(2)} \cdot \delta \vec{R}_j) \quad (96)$$

By using equations (95) and (96), it is possible to isolate the effects of geometry perturbation and changes in angle of attack.

For three-dimensional configurations, there are three components to the geometry perturbation vector $\delta \vec{R}_j$ and two components of tangential velocity at each panel center. Consider the velocity in the local (ξ, η, ζ) -coordinate system of any panel. Before the geometry is perturbed, the components are $(V_\xi, V_\eta, 0)$. If the free stream velocity components in the general (x, y, z) system are $(V_{\infty 1}, V_{\infty 2}, V_{\infty 3})$, then

$$\begin{aligned} V_\xi &= V_{\infty 1} V_\xi^{(1)} + V_{\infty 2} V_\xi^{(2)} + V_{\infty 3} V_\xi^{(3)} \\ V_\eta &= V_{\infty 1} V_\eta^{(1)} + V_{\infty 2} V_\eta^{(2)} + V_{\infty 3} V_\eta^{(3)} \end{aligned} \quad (97)$$

where superscripts (1), (2), (3) respectively correspond to baseline flow solutions for $\vec{V}_\infty = \vec{e}_x$, $\vec{V}_\infty = \vec{e}_y$, $\vec{V}_\infty = \vec{e}_z$. Following the geometry perturbation, the velocity components in the updated (ξ, η, ζ) -system will be $(V_\xi + \delta V_\xi, V_\eta + \delta V_\eta, 0)$. The three-dimensional analogue to equation (96) can be expressed in the form

$$\begin{aligned} \delta V_\xi &= \sum_{i=1}^3 V_{\infty i} \{ [\sum_j \vec{a}_{\xi j}^{(i)} \cdot \delta \vec{R}_j] + [\sum_j b_{\xi j} \sum_k \vec{B}_{jk}^{(i)} \cdot \delta \vec{R}_k] \} \\ \delta V_\eta &= \sum_{i=1}^3 V_{\infty i} \{ [\sum_j \vec{a}_{\eta j}^{(i)} \cdot \delta \vec{R}_j] + [\sum_j b_{\eta j} \sum_k \vec{B}_{jk}^{(i)} \cdot \delta \vec{R}_k] \} \end{aligned} \quad (98)$$

where the j-summation will include only a few neighboring corner points and the k-summation will include every corner point of the panelled configuration. The coefficients $\vec{a}_{\xi j}^{(i)}$, $\vec{a}_{\eta j}^{(i)}$, $b_{\xi j}$, $b_{\eta j}$ and $\vec{B}_{jk}^{(i)}$ are functions of only the baseline geometry. The significant computing expense is associated with generating $\vec{B}_{jk}^{(i)}$. Usually, only values for $i = 1$ and 3 will be calculated, with the x-z plane being a plane of flow symmetry. For a configuration modelled by one thousand panels, matrix $\vec{B}_{jk}^{(i)}$ will contain approximately three million values for each of the three values of i . It is anticipated that the calculation of the coefficients of equation (98) will increase the expense of a conventional analysis solution by a factor of five. The payoff is that once the coefficients are generated, equation (98) will provide rapid, inexpensive predictions for arbitrary geometry perturbations. Approximate force and moment perturbations can be calculated by incorporating equation (98) in the Bernoulli equation and then integrating the resulting pressures over the perturbed geometry.

Mach number variations can be simulated by using equation (98) to predict the effect of the geometry stretching associated with Gothert's rule. For example, suppose that at a given baseline subsonic Mach number and angle of attack, the equivalent incompressible coordinates of some body point are (x, y, z) . At some other free stream conditions, the equivalent incompressible coordinates are $(\bar{x}, \bar{y}, \bar{z})$, where

$$\begin{pmatrix} \bar{x} \\ \bar{y} \\ \bar{z} \end{pmatrix} = \begin{bmatrix} b_{11} & b_{12} & b_{13} \\ b_{21} & b_{22} & b_{23} \\ b_{31} & b_{32} & b_{33} \end{bmatrix} \begin{pmatrix} x \\ y \\ z \end{pmatrix} \quad (99)$$

The 3 x 3 matrix b_{ij} is established by Gothert's rule. Equation (99) can be written in the form

$$\begin{aligned} \bar{x} &= x + \delta x \\ \bar{y} &= y + \delta y \\ \bar{z} &= z + \delta z \end{aligned} \quad (100)$$

where δx , δy , and δz are functions of (x, y, z) . Equation (100) is then substituted directly into equation (98) to predict the effect of a change in freestream Mach number.

The benefits of the present perturbation analysis approach will have the greatest impact when used in conjunction with suitable geometry and interactive graphics packages. For example,

suppose the user digitizes a new set of planform coordinates; the geometry package would generate the corresponding values for δR_j , retrieve the velocity-geometry derivative matrix, and perform the required calculations; and the interactive graphics facility would display the desired pressures, forces, and moments. The entire process would require only a few minutes at no appreciable expense.

Finite Wing Design

In an earlier section, an iterative method was presented for calculating the geometry corresponding to a prescribed airfoil pressure distribution. In each iteration cycle, the geometry would be updated and a new analysis solution calculated. This procedure is reasonable for two-dimensional flow because the associated computing cost is usually quite small. However, for three-dimensional configurations, an analogous design method could be prohibitively expensive. Described here is an approach that should provide a more economical method for designing the section geometries of a finite wing.

The approach involves iteration, using a given starting geometry to initialize the calculations. Unlike the two-dimensional design method, the starting geometry will not be updated during every iteration cycle. Significant computing time will be saved because the baseline analysis solution and velocity-geometry derivative matrix can be reused for several iterations. Then the starting geometry can be updated and the process repeated. A flow chart of the design approach is presented in figure 37. Each step is described below.

The objective is to determine the wing streamwise section geometries at fixed spanwise stations corresponding to a prescribed pressure or velocity distribution. The fuselage geometry and wing planform are assumed to be known beforehand and will not change. If a velocity distribution is prescribed, both the streamwise and spanwise components must be specified. If a pressure distribution is prescribed, a wing internal volume constraint should be applied to eliminate the possibility of a nonunique solution. To enhance numerical stability, prescribed values will apply to the centers and edges of the wing panels.

The MCAIR 3-D Program will be used to analyze the starting geometry. The analysis will establish the difference between the initial and the desired distributions of pressure (or velocity). Then the velocity-geometry derivative matrix of equation (98) will be calculated.

Equation (98) will be inverted to calculate the geometry perturbation array δR_j associated with the prescribed pressure distribution. The inversion will be established in the sense of the least-square-error at panel centers, corners, and edge mid-

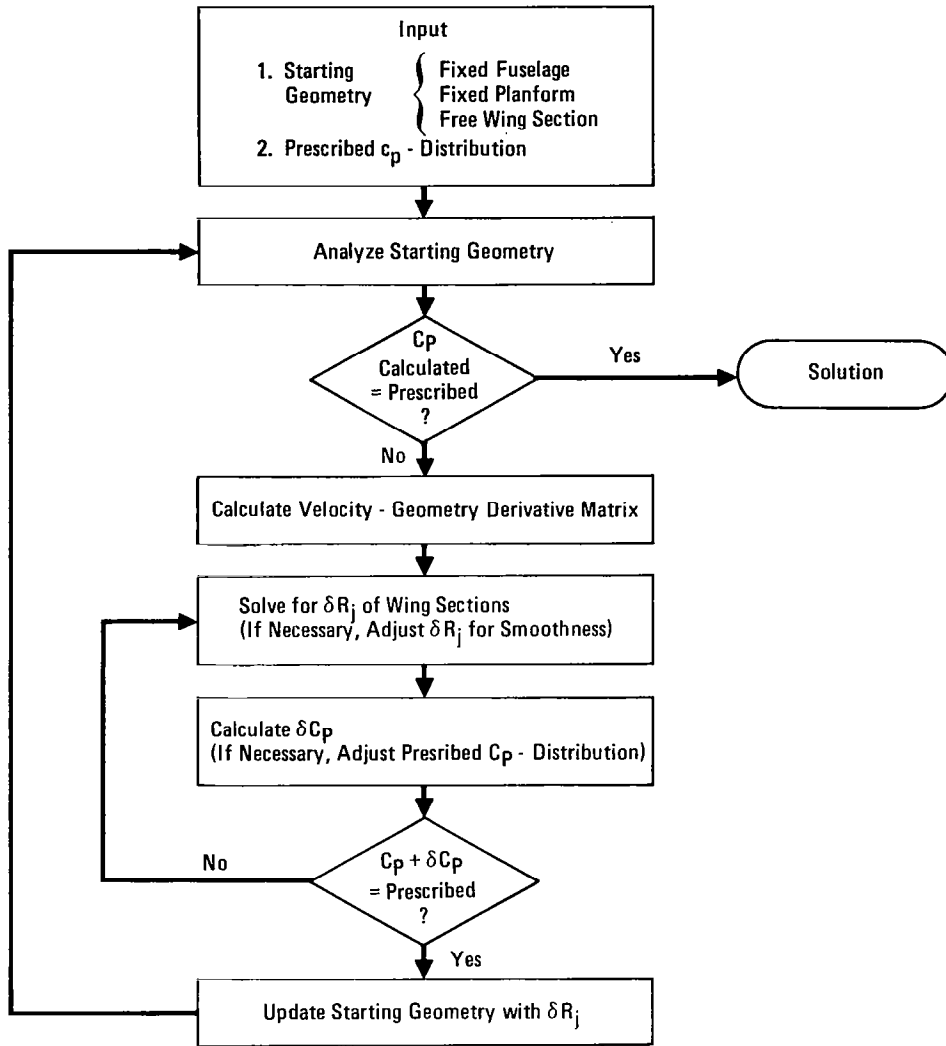


Figure 37. Design Approach for Finite Wings

points. Appropriate linear constraints should be applied for geometric closure and, possibly, prescribed internal volume. Also, the length of the panel streamwise edges should be frozen during the inversion in order to prevent unnecessary disturbance to the surface distance distribution of the panelling. If the calculated array $\delta \vec{R}_j$ is unrealistic or insufficiently smooth, the values can then be modified manually. At that stage, it will not be necessary to maintain the same lengths of panel streamwise edges as in the starting geometry.

By applying equation (98) and Bernoulli's equation, the corrected pressure distribution is calculated, corresponding to the starting geometry perturbed by $\delta \vec{R}_j$. It is noted that the

corrected pressure distribution ($C_p + \delta C_p$) is only accurate to first-order with respect to δR_j . If the difference between the corrected and prescribed pressure distributions is unusually large, it is possible that the prescribed distribution does not exist. In that case, the corrected pressure distribution should guide the user in determining the smallest modification required to create an existing prescribed distribution. If the agreement between the prescribed and corrected pressure distributions is sufficiently good, the array δR_j will be used to update the starting geometry and the entire procedure will be repeated. Otherwise, a new array δR_j should be calculated by again inverting equation (98).

The present finite wing design approach incorporates several features that proved essential to two-dimensional design. Based upon experience with two-dimensional design, it is expected that no more than one or two starting geometry updates will be required to obtain a converged three-dimensional design solution.

CONCLUSIONS

The use of combined source-doublet panels leads to accurate and numerically stable subsonic analysis and design solutions. The prediction accuracy associated with internal perturbation potential boundary conditions and flat panels is competitive with more complex curved panel formulations.

The Multi-Element Airfoil Inviscid Analysis and Design Program can calculate the surface shape and arclength in design regions, corresponding to a prescribed pressure distribution. Converged solutions are usually obtained in fewer than five iteration cycles. The rapid convergence results from the use of all first order velocity-geometry perturbation terms in the inverse step of each iteration cycle. The variable arclength feature can automatically transform a nonexistent prescribed pressure distribution into one of the closest possible distributions, thereby simplifying user input requirements. Applications of the design option include airfoil optimization and viscous-inviscid interactions.

The MCAIR 3-D Subsonic Potential Flow Program predicts the inviscid pressure distribution for arbitrary lifting or non-lifting configurations. The method of least squares minimizes doublet discontinuities at panel edges, which in turn reduces the effect of the selected panelling arrangement on the numerical solution. It is possible to perform a first-order expansion to the solution formulation of the program. This would allow the calculation of a velocity-geometry derivative matrix that could be stored for future use. The analysis of an arbitrary configuration modification would simply require an inexpensive multiplication of the matrix by a new right-hand-side. The matrix would also provide the foundation for a three-dimensional wing design method.

REFERENCES

1. Bristow, D.R. and Grose, G.G.: Modification of the Douglas Neumann Program to Improve the Efficiency of Predicting Component Interference and High Lift Characteristics. NASA CR-3020, August 1978.
2. Bristow, D.R.: Improvements in Surface Singularity Analysis and Design Methods. NASA Advanced Technology Airfoil Research Conference, Langley Research Center, 7-9 March 1978.
3. Kellogg, O.D.: Foundations of Potential Theory. Dover Publications, Inc., 1953.
4. Hess, J.L.: The Use of Higher-Order Surface Singularity Distributions to Obtain Improved Potential Flow Solutions for Two-Dimensional Lifting Airfoils. Computer Methods in Applied Mechanics and Engineering, Vol. 5, 1975, pp. 11-35.
5. Bristow, D.R.: Recent Improvements in Surface Singularity Methods for the Flow Field Analysis About Two-Dimensional Airfoils. AIAA Paper 77-641, June 1977.
6. Morino, Luigi and Kuo, Ching-Chiang: Subsonic Potential Aerodynamics for Complex Configurations: A General Theory. AIAA J., Vol. 12, No. 2, February 1974, pp. 191-197.
7. Bristow, D.R.: A Solution to the Inverse Problem for Incompressible Axisymmetric Potential Flow. AIAA Paper 74-520, June 1974.
8. Williams, B.R.: An Exact Test Case for the Plane Potential Flow About Two Adjacent Lifting Aerofoils. Aeronautical Research Council R. & M. No. 3717, September 1971.
9. Liebeck, R.H.: Design of Subsonic Airfoils for High Lift. Journal of Aircraft, Volume 15, No. 9, September 1978, pp. 547-561.
10. Liebeck, R.H. and Ormsbee, A.I.: Optimization of Airfoils for Maximum Lift. Journal of Aircraft, Vol. 7, No. 5, Sep-Oct 1970, pp. 409-415.
11. Smith, A.M.O.: High-Lift Aerodynamics. Journal of Aircraft, Volume 12, No. 6, p. 501, June 1975.
12. Stratford, B.S.: The Prediction of Separation of the Turbulent Boundary Layer. Journal of Fluid Mechanics, Volume 5, 1959, pp. 1-16.
13. Henderson, M.L.: A Solution to the 2-D Separated Wake Modeling Problem and Its Use to Predict $C_{L_{max}}$ of Arbitrary Airfoil Sections. AIAA Paper 78-156, January 1978.

REFERENCES (Continued)

14. McCullough, G. B. and Gault, D.E.: Examples of Three Representative Types of Airfoil-Section Stall at Low Speed. NACA TN-2502, July 1951.
15. Catherall, D.; Foster, D.N.; and Sells, C.C.L.: Two Dimensional Incompressible Flow Past a Lifting Aerofoil. R.A.E. TR-69118, 1969.
16. Oellers, H.J.: Die Inkompressible Potentialstromung in der Ebener Gitterstufe (The Incompressible Potential Flow in Planar Cascades). Jahrbuch 1962 der Wissenschaftlichen Gesellschaft fur Luft-und Raumfahrt, pp 349-353.
17. Hess, J.L.: Calculation of Potential Flow About Arbitrary Three-Dimensional Lifting Bodies. MDC J5679-01, McDonnell Douglas, October 1972.
18. Johnson, F.T. and Erickson, L.L.: A General Panel Method for the Analysis and Design of Arbitrary Configurations in Incompressible Flows. NASA CR-3079, December 1975.

1. Report No. NASA CR-3234	2. Government Accession No.	3. Recipient's Catalog No.	
4. Title and Subtitle DEVELOPMENT OF PANEL METHODS FOR SUBSONIC ANALYSIS AND DESIGN		5. Report Date February 1980	6. Performing Organization Code
		8. Performing Organization Report No.	
7. Author(s) D. R. Bristow		10. Work Unit No.	
9. Performing Organization Name and Address McDonnell Aircraft Company McDonnell Douglas Corporation St. Louis, Missouri 63166		11. Contract or Grant No. NAS 1-15369	
		13. Type of Report and Period Covered Contractor Report	
12. Sponsoring Agency Name and Address National Aeronautics and Space Administration Washington, D.C. 20546		14. Sponsoring Agency Code	
15. Supplementary Notes Langley Technical Monitor: Harry L. Morgan, Jr. Final Report			
16. Abstract Two computer programs have been developed for subsonic inviscid analysis and design. The first solves arbitrary mixed analysis-design problems for multi-element airfoils in two-dimensional flow. The second calculates the pressure distribution for arbitrary lifting or nonlifting three-dimensional configurations. In each program, inviscid flow is modelled by using distributed source-doublet (or source-vortex) singularities on configuration surface panels. The prescribed normal velocity distribution is satisfied indirectly by applying an internal perturbation potential boundary condition to the center of each panel. The method is numerically stable, and the prediction accuracy is competitive with more complex curved panel formulations. For two-dimensional prescribed pressure design problems, converged geometry solutions are typically obtained in four or five iteration cycles. Numerical formulations and representative solution are presented for the programs.			
17. Key Words (Suggested by Author(s)) Low speed flow Potential flow Wing-body configurations Lifting bodies Green's identity Surface paneling method		18. Distribution Statement Unclassified - Unlimited Subject Category 02	
19. Security Classif (of this report) Unclassified	20. Security Classif (of this page) Unclassified	21. No. of Pages 82	22. Price \$6.00

* For sale by the National Technical Information Service, Springfield, Virginia 22161

NASA-Langley, 1980